

Physiological and Genetic Investigations into Putative Sulfur Oxidation Systems of
Methylococcales

by

Marc Waddingham

A thesis submitted in partial fulfillment of the requirements for the degree of

Master of Science

in

Microbiology & Biotechnology

Department of Biological Sciences

University of Alberta

© Marc Waddingham, 2023

Abstract

Methylotrophic bacteria are ecologically widespread chemotrophs which utilize single carbon compounds as their primary energetic and assimilatory substrate for biomass. Those which utilize methane are commonly referred to as methane oxidizing bacteria (MOB), or methanotrophs. The majority of known MOB are strict aerobes, as they rely on availability of molecular oxygen for the activation of methane via the key enzyme complex particulate methane monooxygenase (pMMO), and for respiration when replete with oxygen. Our understanding of the metabolic diversity of MOB continues to expand, with autotrophy, nitrogen reduction, and most recently sulfur oxidation having been reported across diverse methanotrophic clades. Analysis of MOB genomes from *Gammaproteobacteria*, order *Methylococcales*, have revealed the presence of a putative thiosulfate-oxidizing multienzyme system (TOMES) across multiple species, raising the prospect of dissimilatory catabolic sulfur oxidation in these bacteria. However, the observation of a sulfur/methane mixotrophic growth phenotype or direct sulfur oxidation by *Methylococcales* species has remained elusive. Herein the lack of discernable growth benefit of thiosulfate for *Methylotuvimicrobium buryatense* 5GB1C and *Methylicorpusculum oleiharenae* XLMV4 is confirmed in the conditions tested, verified through growth, substrate gas consumption, and sulfate production measurements. Neither oxygen nor methane limiting conditions resulted in significant change in parameters measured; rather, the growth of *Mp. oleiharenae* XLMV4 was shown to be inhibited by lanthanum and thiosulfate in combination. This effect was replicable, and resulted in slowed doubling rates, lowered final optical density readings, with a commensurate decrease in headspace gas depletion rates for both methane and oxygen for XLMV4 cultures grown in thiosulfate/lanthanum conditions. This effect is hypothesized to be due to competitive inhibition of the lanthanide-dependent methanol dehydrogenase (MDH) XoxF by thiosulfate, inferred through high sequence similarity between XoxF-type MDHs and thiol dehydrotransferase

(ThdT), a novel thiosulfate oxidizing enzyme first identified in the betaproteobacterium *Advenella kashmirensis*. These results indicate that the presence of a conserved sulfur oxidation system across multiple *Methylococcales* species may not be for of energy conservation or carbon fixation, but rather to alleviate competitive inhibition of XoxF-type MDH function by thiosulfate. While this inhibitory interaction between the XoxF MDH and thiosulfate requires validation through targeted enzymatic and metabolomic assays, these data may serve as the basis for future investigations into the role of TOMES in *Methylococcales*. Moreover, the implications of XoxF inhibition may well encompass bacterial clades beyond *Methylococcales*, as XoxF-type MDHs are highly abundant within marine sediment microbial communities and may be similarly affected by thiosulfate.

Acknowledgements

I would like to express my thanks and appreciation to Dr. Dominic Sauvageau, for his informed contributions to all aspects of this research. I am sincerely grateful for your decision to step into the role of lead supervisor partway through my program. Your guidance through the writing process was invaluable in the production of this thesis, which stands stronger as a result.

In addition, I acknowledge Dr. Tariq Siddique and Dr. Casey Fowler for volunteering to adjudicate my defense as committee members, especially given the short notice. Albeit unusual circumstances, you have made it possible to complete my academic program, and I extend my sincere thanks for both of your efforts.

My acknowledgements to Dr. Lisa Stein for your invitation to join the research group a number of years ago, and for your myriad contributions throughout my academic development. Thank you for providing the space, resources, and support across multiple research efforts.

Many thanks to the support personnel of the Department of Biological Sciences, namely the Molecular Biology Services Unit, the Advanced Microscopy Facility, and the departmental storeroom. Through contributions large and small, you provide the means to pursue our research interests, which are gratefully acknowledged.

I would like to express my appreciation to my colleagues, past and present, across campus. Throughout my time at the University of Alberta, I have worked among the finest mentors, peers, and mentees one could ask for, some of which I am fortunate to count as friends. Thank you for the laughs and tears shared along the way, and for being constant lights during our journey.

Most of all, I share my deepest gratitude and love to Valeria Tsviklist. Your reciprocated love, dedication, and strength of will continue to be the source of our shared successes, and I'm

glad to conclude this chapter as another victory. Whatever the future brings, I look forward to meeting it with you. Я люблю тебя, очень.

Marc Waddingham

26 June, 2023

Table of Contents

Abstract	ii
Acknowledgements	iv
Table of Contents.....	vi
List of Tables	ix
List of Figures	x
1. Introduction.....	1
2. Background.....	3
2.1. Methane oxidizing bacteria (MOB).....	3
2.2. Primary methane oxidation pathway.....	5
2.3. Carbon assimilation by gammaproteobacterial methanotrophs	10
2.4. Carbon assimilation by alphaproteobacterial methanotrophs.....	14
2.5. Thiosulfate-oxidizing multienzyme system.....	18
2.6. Reverse dissimilatory sulfate reduction pathway	22
2.7. Sulfite oxidation.....	27
2.8. Sulfur oxidation and methanotrophs.....	28
2.9. Hypothesis and objectives.....	31
3. Materials and Methods	34
3.1. Bioinformatic identification and confirmation of <i>Methylococcales</i> TOMES, including loci cluster mapping.....	34

3.3. Culturing conditions for <i>Methylovimicrobium buryatense</i> 5GB1C.....	35
3.4. Culturing conditions for <i>Methylococcus oleiharenae</i> XLMV4.	36
3.5. Growth assays via optical density and dry cell weight measurement.....	37
3.6. Sulfate precipitation and quantification assay.	38
3.7. Headspace gas chromatography.	38
3.8. Protein alignment of <i>A. kashmirensis</i> thiol dehydrotransferase and <i>Methylococcales</i> XoxF MDH.	39
4. Results.....	40
4.1. BLASTp alignments reveal putative thiosulfate-oxidizing genes in <i>Methylococcales</i>	40
4.2. Confirmation of soxB thiosulfohydrolase in <i>Methylovimicrobium buryatense</i> 5GB1C.	42
4.3. Diversity of SDH enzymes predicted in <i>Methylococcales</i> genetic inventory.....	44
4.4. Thiosulfate has negligible impact on <i>Mt. buryatense</i> 5GB1C growth in a variety of conditions.	45
4.5. <i>Mp. oleiharenae</i> XLMV4 may oxidize thiosulfate as an alternative electron donor...46	
4.6. <i>Methylococcales</i> XoxF-type methanol dehydrogenase is homologous to novel sulfur- oxidizing enzyme thiol dehydrotransferase from <i>A. kashmirensis</i>	47
4.7. Figures.....	49
4.8. Tables.....	68
5. Discussion	73

5.1 Characterization of TOMES genomic inventories of <i>Methylococcales</i> species	73
5.2. Effects of thiosulfate on the physiology of <i>Mt. buryatense</i> 5GB1C and <i>Mp. oleiharenae</i> XLMV4.....	79
6. Conclusion.....	84
7. Bibliography	87

List of Tables

Table 4.1. Summary table on headspace gas depletion rates of *Mt. buryatense* 5GB1C and *Mc. oleiharenae* XLMV4.

Table 4.2. NCBI protein accession ID numbers for TOMES-possessing *Methylococcales* strains reviewed in this manuscript.

Table 4.3. NCBI protein accession ID numbers of proteins co-conserved with TOMES in select *Methylococcales* strains.

Table 4.4. Reference genomes of *Methylococcales* and model SOB utilized in this research.

List of Figures

Introductory Figure 2.1. Primary methane oxidation pathway of gammaproteobacterial methanotrophs.

Introductory Figure 2.2. Ribulose monophosphate pathway diagram.

Introductory Figure 2.3. Simplified H₄MPT/H₄F pathway diagram for formaldehyde assimilation by alpha-MOB.

Introductory Figure 2.4. Thiosulfate-oxidizing multienzyme system diagram based on *P. pantotrophus* GB17 model.

Introductory Figure 2.5. Reverse dissimilatory sulfide reduction pathway diagram, updated to include probable DsrC-trisulfide intermediate as described by Santos et al. 2015¹.

Introductory Figure 2.6. Hypothetical impacts of methane/sulfur mixotrophy on primary methane oxidation pathway of Gammaproteobacterial methanotrophs.

Figure 4.1. Organization of TOMES and co-localized genes in select *Methylococcales* strains.

Figure 4.2. Presence/Absence matrix of TOMES and associated genes from soxB-possessing *Methylococcales*, as determined by BLASTp analysis with *Mt. buryatense* 5GB1C TOMES query.

Figure 4.3. Amino acid sequence alignments of SoxB enzymes from known thiosulfate-oxidizing bacteria and two example methanotrophs.

Figure 4.4. BLASTp results heatmap of *Methylococcales* sulfite dehydrogenase amino acid sequences using *Starkeya novella* DSM 506 SoxC and SorA protein sequence queries.

Figure 4.5. Neighbor-joining phylogenetic tree of *Methylococcales* SDH protein sequences identified through *S. novella* SorA/SoxC BLASTp query.

Figure 4.6. *Methylovimicrobium buryatense* 5GB1C growth and thiosulfate oxidation assay.

Figure 4.7. *Methylovimicrobium buryatense* 5GB1C sulphate production during growth in presence of thiosulfate.

Figure 4.8. *Methylococcus oleiharenae* XLMV4 thiosulfate oxidation assay with or without added lanthanum.

Figure 4.9. Replication experiment of *Methylococcus oleiharenae* XLMV4 thiosulfate oxidation assay with or without added lanthanum.

Figure 4.10. Protein alignment of select *Methylococcales* XoxF MDH and *Advenella kashmirensis* ThdT thiol dehydrotransferase sequences.

Figure 4.11. Hypothetical model of lanthanum-dependent growth inhibition by thiosulfate in *Methylococcales*.

Abbreviations

AcCoA: Acetyl coenzyme A

Alpha-MOB: Alphaproteobacterial methane oxidizing bacteria

APSR: Adenosine-5'-phosphosulfate reductase (pathway)

ATP: Adenosine triphosphate

ATPS: ATP sulfurylase

C1/C2/C3/C4: Single/two/three/four carbon compound(s)

CBB: Calvin-Benson-Bassham (cycle)

CCE: Carbon conversion efficiency

CH₄: Methane

CO₂: Carbon dioxide

DNA: Deoxyribonucleic acid

DO: Dissolved oxygen

E4P: erythrose-4-phosphate

EMC: Ethylmalonyl-CoA (cycle)

ED: Entner-Doudoroff (pathway)

EMP: Emden-Meyerhof-Parnas (pathway)

F1,6BP: fructose-1,6-bisphosphate

F6P: fructose-6-phosphate

FAE: Formaldehyde-activating enzyme

FDH: Formate dehydrogenase

FAD: Flavin adenine dinucleotide

GAP: glyceraldehyde-3-phosphate

Gamma-MOB: Gammaproteobacterial methane oxidizing bacteria

GHG: Greenhouse gas

H₄F: Methylene tetrahydrofolate

H₄MPT: Tetrahydromethanopterin

H6P: D-arabino-3-hexulose-6-phosphate

HPS: 3-hexulose-6-phosphate synthase

ICM: Intracytoplasmic membranes

IM: Inner membrane

KDPG: 2-keto-3-deoxy-6-phosphogluconate

MDH: Methanol dehydrogenase

MFR: Methanofuran

MMO: Methane monooxygenase

MOB: Methane oxidizing bacteria

MoCo: Molybdopterin cofactor

MQ/MQL: Menaquinone/menaquinol

NAD/NADH: Nicotinamide adenine dinucleotide

NADP/NADPH: Nicotinamide adenine dinucleotide phosphate

PDB: Protein Database

PDH: Pyruvate dehydrogenase

PHI: 6-phospho-3-hexuloisomerase

PLFA: Phospholipid fatty acid

pMMO: Particulate methane monooxygenase

ppb: Parts per billion

PP_i: Pyrophosphate

PP_i-PFK: Pyrophosphate-dependent phosphofructokinase

PQQ: Pyrroloquinoline quinone

PSB Purple sulfur bacteria

R5P: Ribose-5-phosphate

rDSR: Reverse dissimilatory sulphate reduction (pathway)

REE: Rare earth element

RISC: Reduced inorganic sulfur compound

RNA: Ribonucleic acid

rRNA: Ribosomal ribonucleic acid

Ru6P: ribulose-5-phosphate

RuBisCo: Ribulose-bisphosphate carboxylase

RuMP: Ribulose monophosphate (pathway)

S₀: Elemental sulfur

SO₃²⁻: Sulfite

SO₄²⁻: Sulfate

S₂O₃²⁻: Thiosulfate

sMMO: Soluble methane monooxygenase

SDH: Sulfite dehydrogenase

SO: Sulfite oxidase

SOB: Sulfur-oxidizing bacteria

SRP: Sulfur-reducing prokaryote

TA: transaldolase

TCA: Tricarboxylic acid (cycle)

TEA: Terminal electron acceptor

TK: transketolase

TOMES: Thiosulfate-oxidizing multienzyme system

UQ/UQH: Ubiquinone/ubiquinol

1. Introduction

Methane (CH_4) gas is a core component of the global biogeochemical carbon cycle and is emitted from a variety of natural sources, including geological processes, wetlands, aquatic sediments, soils, animal guts, and melting permafrost^{2,3}. Anthropogenic methane is produced via agriculture, the petrochemical industry, and waste management (among others), and now exceeds natural global emissions, accounting for ~64% of total annual emissions ($352 \text{ Tg y}^{-1} \pm 45$)⁴⁻⁶. These emissions have resulted in a 2.5-fold increase in atmospheric CH_4 concentrations over the last three centuries, with globally averaged atmospheric CH_4 concentrations increasing from 1550 ppb to 1800 ppb since 1980^{3,7}. Now, combined global emissions of CH_4 have been estimated at $550 \text{ Tg}\cdot\text{yr}^{-1}$, equivalent to 4% of total combined CO_2 emissions in terms of mass. While comparatively minor in mass terms, CH_4 is responsible for 20% of the increase in radiative forcing potential of the lower atmosphere since 1970, making it an important greenhouse gas (GHG)^{3,4,8}. Radiative forcing estimates of CH_4 vary given its short lifespan in the atmosphere (ca. 9 years⁶) and the need to account for its breakdown products (i.e. ozone, water vapor, and CO_2). Despite this ambiguity, it is generally accepted that CH_4 has a radiative efficiency 25-fold greater than that of CO_2 on a per mass basis over 100 years, and that CH_4 is the second most impactful GHG in terms of overall global radiative forcing^{3,9}.

While the immediate effects of anthropogenic emissions on global climate are cause for concern, CH_4 emissions are predicted to continue their upward trajectory not only due to human activity, but also due to disproportionate effects of increased annual temperatures in high-latitude ecosystems¹⁰. Frozen lakes and permafrost soils are immense natural carbon sequestration reservoirs which are susceptible to positive feedback events, where increased thaw rates and melt duration allow for the release of methane, which contributes to increased radiative forcing levels, and thereby to climate change^{11,12}. Carbon sequestered in perennial permafrost systems is

estimated at ~1,466 gigatonnes, approximately 50% of global soil carbon balance. This large methane emission potential is deeply concerning given that permafrost melt provides ideal anoxic conditions for methanogenesis to occur^{10,11,13-15}.

The abundance and environmental impact of methane has spurred research on its mitigation and utilization as a low-value feedstock for biomanufacturing, specifically through use of methylotrophic bacteria. Methylotrophs are defined by their utilization of single carbon (C1) compounds for biomass and energetic needs, particularly methanol; the subset of methylotrophs which utilize methane gas are known collectively as methane oxidizing bacteria (MOB; methanotrophs)¹⁶⁻¹⁸. Currently, known MOB taxa belong to *Gammaproteobacteria*, *Alphaproteobacteria*, *Verrucomicrobia*, and Phylum NC10 classifications, and are globally distributed in a variety of aquatic, sediment, and soil ecosystems^{19,20}. Insofar, gammaproteobacterial and alphaproteobacterial MOB have garnered the most interest for potential industrial applications, as their long tenure in pure laboratory cultures has produced a sound knowledge base required for their employment in bioindustry^{21,22}.

MOB are known to employ a variety of catabolic strategies which benefit their ecological fitness, with the most recent addition being catabolic sulfur oxidation for autotrophic growth by the alphaproteobacterial MOB *Methylovirgula thiovorans* HY1²³. Additionally, this discovery is bolstered by the accompanying data demonstrating the range of gamma-MOB which possess putative thiosulfate oxidizing systems²³⁻²⁵. Taken together, these findings have renewed interest in the possibility of sulfur oxidation by other MOB taxa, given its significance for niche establishment and the potential use of reduced sulfur compounds as a feedstock alternative in bio-industrial applications. Encouragingly, these lines of inquiry would be supported by the pre-existing literature on sulfur oxidizing bacteria (SOB), which have been the subject of extensive study for a number of decades²⁶⁻³⁰.

2. Background

2.1. Methane oxidizing bacteria (MOB)

MOB belong to a polyphyletic grouping united by the ability to utilize methane as their sole carbon and energy source. They are globally distributed across terrestrial, marine, freshwater, agricultural, and anthropogenic ecosystems with simultaneous access to methane and oxidants^{31,32}.

The majority of ecological methane production is biogenic, resulting from the action of anaerobic methanogenic archaea, or methanogens -- microbes highly specialized in the anaerobic respiration of by-products produced by other organisms as electron donors, including hydrogen gas and simple acids, alcohols, and similar short-chain carbon compounds, commonly using carbon dioxide as electron acceptor³³. Methanogens are highly prevalent in anaerobic climes and soil microenvironments, largely due to competition by aerobic heterotrophs in oxic environments as well as the methanogen-specific enzymes/cofactors are susceptible to irreversible inactivation by oxygen^{34,35}. As a result, methanotrophic ecology generally straddles aerobic/anaerobic interfaces, between zones of methanogenic activity and accessible oxygen³⁶. Through these interactions, methanotrophs serve as the largest known terrestrial methane sink, mitigating the release of an estimated 100 megatonnes of biogenic methane per annum^{8,19,37}.

Methane conversion into more complex organic compounds by MOB can serve as an alternative primary production pathway to autotrophy, particularly when concentrations of methane approach or surpass that of carbon dioxide. A prominent example is Movile Cave in Romania, a subterranean ecosystem in which diverse MOB genera contribute to carbon cycling within floating microbial mats, supplementing chemoautotrophic activity by sulfur- and ammonium-oxidizing bacteria^{38,39}. This supplemental carbon-cycling role is also observed within

surface aquatic ecosystems including bogs and shallow lakes, where methanotrophic biomass enters into the broader food supply via pelagic and benthic consumers, especially zooplankton, arthropod larvae, and other grazing invertebrates^{40,41}. Aside from grazing interactions, some methanotrophs excrete organic acids and hydrogen gas as by-products of fermentative growth in oxygen-limiting conditions, which is hypothesized to be an important contribution of MOB to their local ecosystem⁴²⁻⁴⁴. For example, mutualistic interactions have been observed by methanotrophic endosymbionts within gill tissue of Bathymodiolinae mussels living in proximity to deep sea hydrothermal vents and cold seeps. These organisms form delicately-balanced consortia alongside SOB to provide their host with nutrients, depending on carbon and reductant sources available⁴⁵.

The modern era of methanotroph research began with the seminal work of Whittenbury and colleagues, who isolated and characterized an extensive array of obligate methanotrophic cultures⁴⁶. Morphology, substrate utilization/sensitivity, intracytoplasmic membrane (ICM) structures, and resting stages were used to construct a preliminary phylogeny which established the Group I/II classification of MOB. These basal phylogenies would be confirmed and amended through the work of Bowman and colleagues by validation of established phospholipid fatty acid (PLFA) profiling, 16s rRNA gene sequence alignments, DNA-DNA hybridization, and numerical taxonomies, resulting in the placement of Group I MOB into the class of *Gammaproteobacteria* as the family *Methylococcaceae*⁴⁷⁻⁴⁹. Group II MOB were assigned to *Alphaproteobacteria* through similar methodologies, and found to align within the methylotrophic families of *Methylocystaceae* and *Beijerinckiaceae*, referred to as Group IIA and IIB methanotrophs^{16,19,50}. By the mid-1990s, the consensus for Group I characteristics were established as 1) utilizing the ribulose monophosphate (RuMP) pathway for C1 assimilation, 2) having PLFA chain lengths of 14 and 16 carbons, and 3) possessing bundled vesicular disks of ICM extending within the cell; whereas Group 2 were found

to 1) employ the serine cycle for C1 assimilation, 2) have PLFA chain lengths of 18 carbons, and 3) contain lamellar ICM fold-structures organized along the inner membrane boundary^{51,52}. In addition, the “Type X” classification was previously used to describe members of *Methylococcaceae*, for example *Methylococcus capsulatus*, that possess partial serine cycles and the Calvin-Benson-Bassham (CBB) cycle enzyme ribulose-bisphosphate carboxylase (RuBisCo), in addition to possessing a higher genomic GC content, owing to higher optimal growth temperatures. In this document the distinct proteobacterial MOB phyla will be referred to as gamma-MOB and alpha-MOB instead of the Group I/II nomenclature, to better delineate specific physiological capabilities in relation to phylogenetic distinctions.

2.2. Primary methane oxidation pathway

The highly conserved primary methane oxidation pathway proceeds through the intermediates of methanol, formaldehyde, and formate, with the latter two compounds feeding into bioassimilatory pathways (Fig. 2.1)^{44,51,53,54}. This process begins with the energy-requiring conversion of CH₄ to methanol, performed by methane monooxygenase (MMO) enzymes, of which there are two main isoforms: the inner membrane localized, copper-dependent, highly specific particulate MMO (pMMO), and the cytosolic, promiscuous, iron-dependent soluble MMO (sMMO)^{52,55,56}. All obligate methanotrophs possess pMMO – some additionally possess sMMO – and it is now known that alphaproteobacterial and some gammaproteobacterial methanotrophs utilize both isoforms^{57–59}. In species with both MMO enzymes, their regulation is tightly controlled by copper ion availability, a mechanism known as the “copper switch.” Micromolar quantities of copper trigger the upregulation of pMMO and associated inner membrane complexes with simultaneous downregulation of sMMO gene expression^{58,60}. Inversely, sMMO – a promiscuous enzyme with a broader substrate range than pMMO – is expressed under conditions of copper deprivation and does not benefit from the proposed direct redox coupling mechanisms with other

inner membrane electron transport components observed with pMMO^{59,61-63}. Moreover, the copper switch has been shown to regulate genes beyond the MMO enzymes, including ICM fold production, copper storage proteins, transporters, ribosomal proteins, and proteins of unknown functions^{64,65}.

The importance of copper for methanotrophs is reflected in other adaptations, particularly the mechanisms employed to acquire, transport, and store copper ions. Perhaps of most interest are the chalkophores, termed methanobactins, which are employed by alphaproteobacterial methanotrophs to scavenge copper from the environment^{60,66,67}. Methanobactins are genome-encoded, post-translationally modified polypeptides which have been shown to bind copper ions with extremely high affinities ($>10^{21} \text{ M}^{-1}$)^{68,69}. This activity is the result of two interspaced ring structures of 5- to 6-members in length, specifically imidazole, oxazolone, or pyrazinedione rings, which are associated with enethiol groups that interact to coordinate a single copper (II) ion^{60,70,71}. Beyond copper-scavenging activity, methanobactins are implicated in regulatory mechanisms including the copper switch and interference with nitrous oxide reduction by denitrifiers. Methanobactins have also garnered interest in remediation of toxic metals due to their ability to bind other cations, particularly mercury^{60,67,72,73}.

After methane is oxidized into methanol by pMMO or sMMO, methanol is oxidized into formaldehyde in the periplasm by methanol dehydrogenases (MDHs), yielding two electrons. This reducing potential is believed to re-reduce pMMO via reverse electron flow, which becomes oxidized through activation of CH₄, either via direct coupling of MDH to pMMO or through a reducing species like NADH⁶². Much like the MMO enzymes, the MDH enzymes occur in two isoforms whose activity and regulation are dependent on the availability of metal cofactors, representing another enzymatic redundancy in the methanotrophic primary oxidation pathway⁵². First identified was MxaFI, a pyrroloquinoline quinone (PQQ)-linked calcium-dependent MDH,

which has been extensively studied and was long regarded as the primary MDH operating in methanotrophs and methylotrophs⁷⁴⁻⁷⁶. However, it was later discovered that methanotrophs of all known phyla – *Proteobacteria*, Phylum NC10, and *Verrucomicrobia* – possess XoxF, an alternative MDH dependent on rare earth elements (REEs)^{75,77-79}. Experimentation on *Methylotuvimicrobium* and *Methylosinus* species have revealed that sub-micromolar amounts of La³⁺ and Ce³⁺ result in a strong upregulation of XoxF and complete repression of MxaFI, including when Ca²⁺ is supplied in excess^{75,78,80,81}. Moreover, other lanthanides including Nd³⁺, Pr³⁺, and Sm³⁺, may be biochemically relevant for XoxF-type MDHs, although this has not yet been demonstrated in methanotrophs⁸².

The robust REE regulatory switch indicates that lanthanide/actinide-containing MDHs are preferred to calcium-dependent variants in methanotrophs, and are ecologically significant based on their presence in metagenomic datasets encompassing organisms beyond MOB, particularly methylotrophs^{77,83,84}. The reasons why REE-dependent MDHs are preferred over Ca²⁺-MDHs remain to be elucidated, although it has been postulated that REEs are stronger electrophiles owing to their relatively large atomic masses and common oxidation state of 3+, and therefore able to extract electrons more efficiently from the methanol C-H bond^{75,77}. It has also been demonstrated that REE-MDHs can result in faster growth rates and CH₄ consumption in some methanotrophs, and potentially catalyze the two-step oxidation process of methanol through formaldehyde to formate^{81,85}. This would theoretically accelerate complete CH₄ oxidation, increasing NADH production rates and therefore the overall growth rate, but this remains to be experimentally validated *in vivo*.

The final metal-dependent diversity of the methane oxidizing pathway coincides with the final step of formate oxidation into CO₂ by metal-dependent, NAD⁺-linked formate dehydrogenases (FDHs). FDH isoforms utilizing different metal cofactors have been long-established in methylotrophs, with FDH diversity being recently recognized as an important element of obligate

MOB catabolism^{17,61}. The primary difference between FDH isoforms is the employment of either a molybdenum- or tungsten-containing pterin cofactor within the active site; metal-independent FDHs exist as well, but are not involved in C1 metabolisms⁸⁶. The effects of different FDHs for C1 microbes differ depending on the organism in question. The facultative methylotroph *Methylobacterium extorquens* AM1 possesses one tungsten- and two molybdenum-containing FDHs, which are all redundant and dispensable for growth on methanol¹⁷. This is in stark contrast to *Mt. alcaliphilum* 20Z^R grown with methane, which exhibits a significant reduction in formate production when supplemented with tungsten as opposed to molybdenum⁶¹. The authors confirmed that only the tungsten-dependent FDH cluster was expressed under methane conditions, implicating its selection over the molybdenum counterpart and its possible importance for *Methylococcales* species beyond *Mt. alcaliphilum* 20Z.

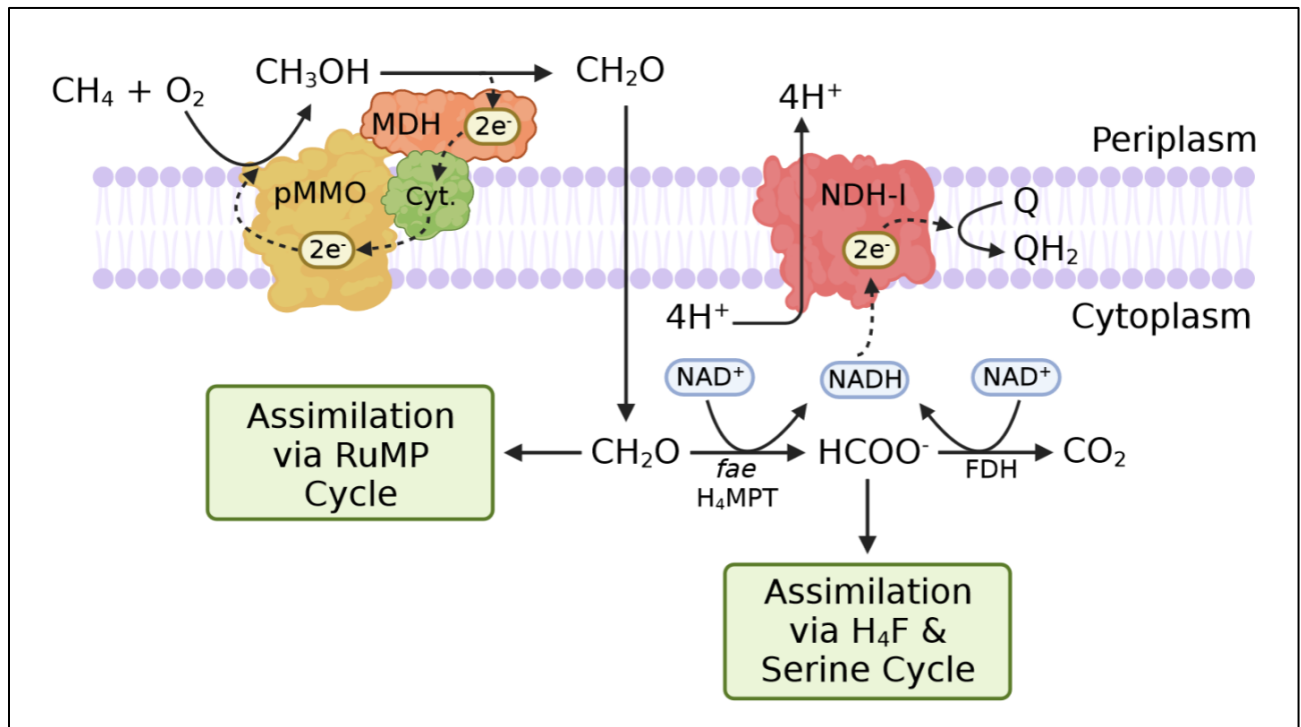


Figure 2.1. Primary methane oxidation pathway of gammaproteobacterial methanotrophs. Note that diagram includes canonical *Methylococcales* formaldehyde assimilation pathway via RuMP cycle in addition to updated model of formate salvage via serine cycle as observed in *Mt. alcaliphilum* 20Z^{44,51,53,54}. pMMO – particulate methane monooxygenase; MDH – methanol dehydrogenase; Cyt. – accessory cytochrome; RuMP – ribulose monophosphate; *fae* – formaldehyde activating enzyme; H₄MPT – tetrahydromethanopterin; FDH – formate dehydrogenase; H₄F – tetrahydrofolate; NDH-I – NADH dehydrogenase complex I; Q/QH₂ – quinone/quinol.

2.3. Carbon assimilation by gammaproteobacterial methanotrophs

Gamma-MOB predominantly utilize the RuMP pathway to incorporate formaldehyde derived from methane oxidation into biomass (Fig. 2.2)^{51,81,87-89}. The process is initiated by 3-hexulose-6-phosphate synthase (HPS), which combines ribulose-5-phosphate (Ru6P) with formaldehyde yielding D-arabino-3-hexulose-6-phosphate (H6P). As an unstable product, H6P is rapidly isomerized into fructose-6-phosphate (F6P) by 6-phospho-3-hexuloisomerase (PHI). The F6P intermediate is a key branching point in the RuMP process, either being activated by pyrophosphate-dependent phosphofructokinase (PP_i-PFK) into fructose-1,6-bisphosphate (F1,6BP) or entering a complex series of transformation reactions by transaldolase (TA) and transketolase (TK) enzymes. The branched flux of F6P is critical in the additive assimilation of C1 carbon into intermediates suitable for downstream glycolytic pathways, specifically F1,6BP and glyceraldehyde-3-phosphate (GAP) for the Emden-Meyerhof-Parnas (EMP) pathway or glucose-6-phosphate (G6P) for the Entner-Doudoroff (ED) pathway. Alternatively, the RuMP cycle can generate anabolic intermediates, namely ribose-5-phosphate (R5P) and erythrose-4-phosphate (E4P), precursors for nucleic acids and aromatic amino acids, respectively. Like F6P, GAP may also branch into the aforementioned TA/TK transformation reactions or into the EMP pathway resulting in substrate-level ATP generation and pyruvate production⁸⁷.

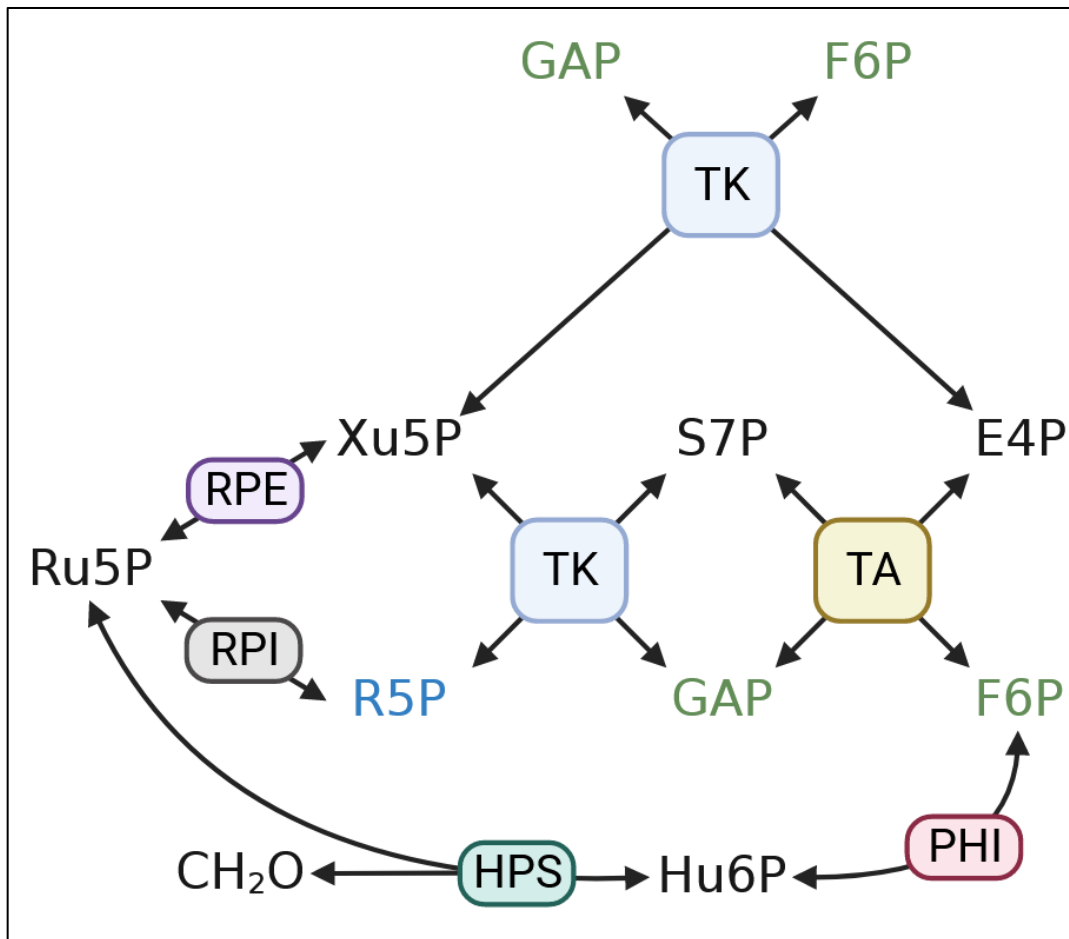


Figure 2.2. Ribulose monophosphate pathway diagram. Pathway enzymes denoted with rounded boxes. Substrates for downstream glycolytic reactions are denoted in green; substrates for nucleic acid synthesis are denoted in blue. Enzymes: 3-hexulose-6-phosphate synthase (HPS), 6-phospho-3-hexuloisomerase (PHI), ribulose-5-phosphate-3-epimerase (RPE), ribose 5-phosphate isomerase (RPI), transaldolase (TA), and transketolase (TK). Intermediates: ribulose 5-phosphate (Ru5P), xylulose 5-phosphate (Xu5P), ribose 5-phosphate (R5P), sedoheptulose 7-phosphate (S7P), glyceraldehyde 3-phosphate (GAP); erythrose 4-phosphate (E4P), fructose 6-phosphate (F6P). Adapted with permission from Orita et al., 2006.

For decades, the Entner-Doudoroff pathway was regarded as the major glycolytic route in gamma-MOB, as early efforts could not confirm the activity of key EMP pathway enzymes, most notably pyruvate kinase⁴⁴. Despite these apparent lesions in the EMP pathway, metabolic models involving the ED pathway could not account for the higher-than-predicted carbon conversion efficiencies observed in *Methylococcales* species. This discrepancy was resolved when *Methylovivimicrobium alcaliphilum* 20Z was shown to possess a functional pyruvate kinase (*pfk2*). The inclusion of C₁₃ metabolite tracing data helped demonstrate high levels of flux through EMP intermediates, indicating that *Mt. alcaliphilum* 20Z specifically utilizes the PP_i-dependent phosphofruktokinase (PP_i-PFK) variant of the EMP pathway⁴⁴. Moreover, the increased yield of two ATP from the PP_i-dependent EMP pathway versus the ATP-dependent variant partly explains the faster growth rates of gamma-MOB versus other MOB clades. The difference in reducing equivalent yield is more pronounced between the PP_i-EMP and ED pathways, given that the ED variant requires the investment of six ATP and generates three NADH in molar equivalents. The increased methane carbon flux through the RuMP-EMP rather than the RuMP-ED variant has also been confirmed in *Mt. buryatense* 5GB1, *Methylomonas* sp. DH-1, and *Methylomicrobium album* BG8, implicating the EMP pathway as the dominant glycolytic route in gamma-MOB^{54,88,90,91}.

Despite the importance of carbon flux via the EMP pathway in gamma-MOB, the ED pathway has been confirmed as essential for *Mt. buryatense* 5GB1⁹². Previous attempts to knockout the ED pathway of *Mt. buryatense* 5GB1C were unsuccessful, requiring the development of chromosomal constructs with inducible promoters. Lack of induction of the ED locus caused a null growth phenotype while minute amounts restored specific growth rate near wild type levels, corroborating the unviability of ED knockout mutants. Increasing the induction of the ED locus in *Mt. buryatense* 5GB1 led to a commensurate decrease in growth rate, attributable to shifting methane carbon flux away from the EMP pathway into the ED pathway. The specifics regarding

the essential nature of the ED pathway for *Mt. buryatense* 5GB1 are currently unknown. Recent investigations into methanol-grown *Mt. buryatense* 5GB1 showed increased flux through the ED pathway versus growth on methane, in addition to increased formate excretion and higher serine cycle activity^{88,90}. Intriguingly, production of acetyl coenzyme A (AcCoA) in methanol-grown *Mt. buryatense* 5GB1 was primarily due to malyl-CoA lyase rather than pyruvate dehydrogenase (PDH), implicating the ED pathway's involvement in a broader metabolic response to C1 substrate changes⁹⁰. The methanol-induced shift towards the ED pathway has also been demonstrated in *Mm. album* BG8, lending further credence to the substrate response role of the ED pathway in gamma-MOB beyond *Mt. buryatense* 5GB1⁵⁴.

However, the specific role of the ED pathway remains cryptic in other gamma-MOB, as *Mt. alcaliphilum* 20Z and *Methylomonas* sp. DH-1 utilize the EMP pathway as the primary glycolytic route when grown on either methane or methanol^{91,93}. To date, the necessity of the ED pathway has not been confirmed in either *Mt. alcaliphilum* 20Z or *Methylomonas* sp. DH-1. *Mt. buryatense* 5GB1 demonstrates similar growth rates when grown on methanol or methane, explainable by the additional reducing potential of methanol offsetting the decreased energy yield of the ED pathway, while the higher-efficiency EMP process operating in methane conditions compensates for reducing potential lost to pMMO reduction²². Whereas, *Mt. alcaliphilum* 20Z exhibits a higher growth rate in methanol conditions owing to the increased energy yield from this substrate, as its utilization does not require re-reduction of pMMO by MDH⁹³.

Assimilated carbon is subject to further transformations and catabolic reactions via well-described pathways. Carbon compounds exiting the RuMP pathway via associated glycolytic routes, particularly 2-keto-3-deoxy-6-phosphogluconate (KDPG) and G3P, are converted to pyruvate and fed into the oxidative tricarboxylic acid cycle for production of biosynthetic precursors and respiration^{54,87,90,94}. In addition, gamma-MOB operate a reductive pentose

phosphate pathway generally believed to promote Ru5P regeneration, given the key role of Ru5P as the acceptor for formaldehyde entering the RuMP pathway^{18,87}. Finally, many gamma-MOB also utilize the serine cycle to salvage formate produced by either the H₄MTP pathway or activity of XoxF-type MDHs, although carbon flux through this route is considered minor for methane-grown cultures^{18,87,93,95}. There are numerous examples of gamma-MOB that when grown on methanol rely on the serine cycle to maintain optimal growth rate, reinforcing its role in assimilating formate produced from the rapid oxidation of formaldehyde^{53,90}.

2.4. Carbon assimilation by alphaproteobacterial methanotrophs

Unlike the gamma-MOB, alpha-MOB cannot solely rely on the incorporation of formaldehyde into multi-carbon intermediates and instead must generate methylene tetrahydrofolate (H₄F) from formate for C1 incorporation via the serine cycle (Fig. 2.3)⁹⁶. While formaldehyde can spontaneously react with H₄F to yield methylene H₄F, the reaction rate is insufficient to support carbon flux into the serine cycle. This may be beneficial during transient periods of increased methanol oxidation and therefore high formaldehyde concentrations for methylotrophs specifically, and is generally associated with cycles of methanol release from host plant stomata⁹⁶. Hence, this inefficient direct assimilation mechanism of formaldehyde is preserved among the obligate alpha-MOB, given their relatively recent descent from ancestral methylotrophs⁹⁷.

First, the dissimilatory tetrahydromethanopterin (H₄MTP) pathway oxidizes formaldehyde to formate, initiated by formaldehyde-activating enzyme (FAE), which catalyzes the condensation of formaldehyde with H₄MTP to generate methylene H₄MPT, generating a N-C-N cyclic structure through covalent binding between the N⁵ and N¹⁰ atoms^{98,99}. Methylene H₄MPT is a substrate for two related methylene H₄MPT dehydrogenases (MtdA/MtdB), respectively performing NADP⁺ or NAD⁺/NADP⁺ dependent oxidation reactions to yield methenyl H₄MPT^{100–102}. Despite the ability of MtdA and MtdB to catalyze the reversible methylene/methenyl H₄MPT conversion, methylotrophic

strains deficient in either enzyme are unable to grow on C1 compounds, save for $\Delta mtdB$ strains growing on methylamine^{102,103}. MtdA has dual roles in both the H₄MTP and H₄F pathways, with substrate specificities towards methylene/methenyl H₄MPT and methylene/methenyl H₄F, whereas MtdB is limited to the former reaction^{100,101}. However, MtdA is insufficient to save $\Delta mtdB$ mutants due to accumulation of methenyl-H₄MPT which competitively inhibits MtdA-mediated reduction of methenyl H₄F to methylene H₄F and therefore carbon assimilation¹⁰². Taken together, these findings demonstrate the role of MtdB as an essential methylene H₄MPT dehydrogenase for the sufficient production of methenyl H₄MPT. The methenyl-N⁵,N¹⁰ H₄MPT ring is then hydrolyzed by methenyl tetrahydromethanopterin cyclohydrolase (*mch*) yielding formyl H₄MPT⁹⁹. The formyltransferase/hydrolase complex (Fhc) then performs a two-step catalysis by transferring the formyl group to methanofuran (MFR) from H₄MTP, and sequentially hydrolyzes the formyl-MFR adduct to release formate^{104,105}.

Formate is the key branching node between dissimilation to carbon dioxide by formate dehydrogenases (FDHs) to produce reducing equivalents or towards carbon assimilation via the H₄F pathway, which begins through combination of formate to H₄F by formyl H₄F ligase¹⁰⁶. Methenyl H₄F is produced through introduction of another N⁵,N¹⁰ ring structure into formyl H₄F by methenyl tetrahydrofolate cyclohydrolase (FchA); notably, FchA does not share significant identity with *mch* cyclohydrolase of the H₄MPT pathway despite its analogous function^{96,99}. As previously described, MtdA reduces methenyl H₄F to methylene H₄F, completing the final step of the H₄F pathway and generating C-substrate for assimilation into the serine cycle^{78,100,102}. This convoluted assimilation strategy likely descended from an ancestral methanol/formaldehyde detoxification system, which would have proceeded linearly from methanol dehydrogenase through the H₄MTP pathway, with the resultant formate oxidized to carbon dioxide by FDHs as the terminal reaction¹⁰⁷.

The serine cycle initiates through transfer of the methylene group of methylene H₄F serine to glycine by serine hydroxymethyltransferase (*glyA*), yielding serine^{78,80}. Serine-glyoxylate aminotransferase (*sga*) then converts the serine to hydroxypyruvate through transfer of the amine group to glyoxylate, regenerating glycine for subsequent reactions by *glyA* and conserving the amine group. Metabolites downstream of hydroxypyruvate may then be directed to a range of fates, owing to the intersection of the serine cycle with both the TCA cycle and the ethylmalonyl-CoA (EMC) cycle, sharing the oxaloacetic acid and malate metabolite nodes with the former, and malyl-CoA and glyoxylate nodes with the latter. The EMC cycle is of particular relevance for alpha-MOB such as *Ms. trichosporium* OB3b, as it is key for glyoxylate and glycine pools to accept additional carbon entering from the upstream H₄MPT pathway. Moreover, it has been demonstrated that the EMC pathway of *Ms. trichosporium* OB3b significantly contributes to biomass directly via EMC, pyruvate, and phosphoenolpyruvate carboxylases; ≥60% of assimilated carbon is derived from CO₂⁷⁸.

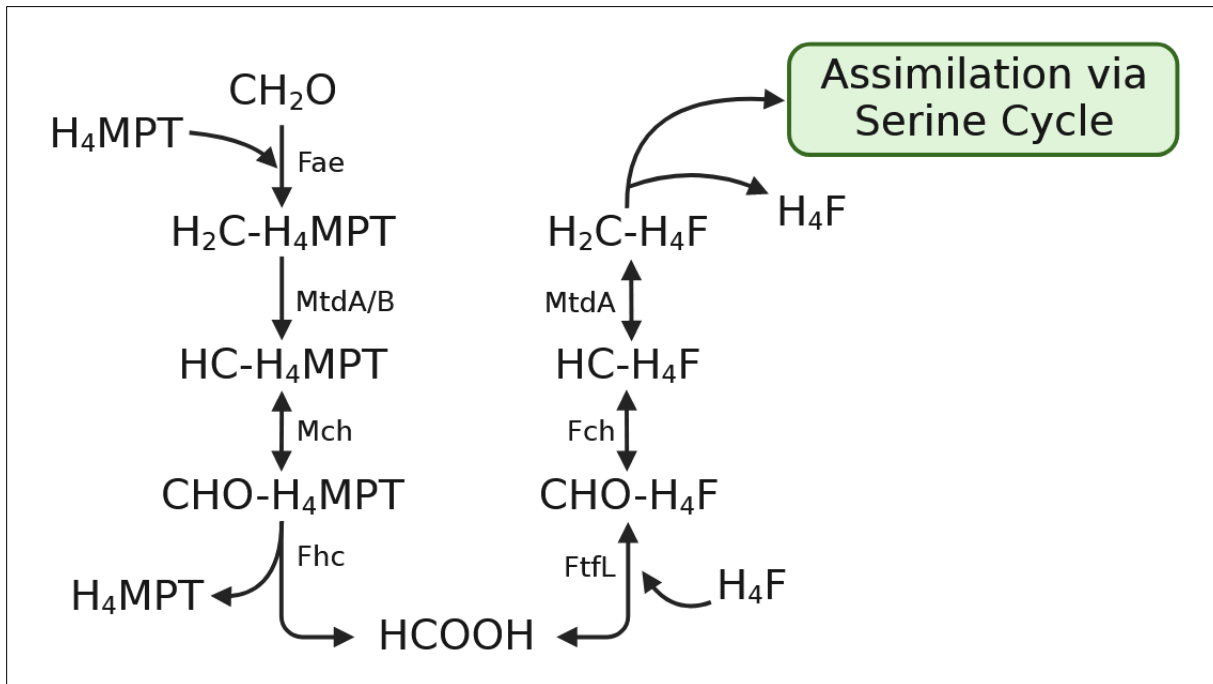


Figure 2.3. Simplified H₄MPT/H₄F pathway diagram for formaldehyde assimilation by alpha-MOB. Enzymes: NADP-dependent methylene-H₄F/methylene-H₄MPT dehydrogenase (MtdA); methenyl-H₄F cyclohydrolase (Fch); formate-H₄F ligase (FtfL); formaldehyde-activating enzyme (Fae); NAD(P)-dependent methylene-H₄MPT dehydrogenase (MtdB); methenyl-H₄MPT cyclohydrolase (Mch); formyltransferase/hydrolase complex (Fhc). Intermediates: CH₂O, formaldehyde; H₄MPT, tetrahydromethanopterin; HCOOH, formic acid; H₄F, tetrahydrofolate. Reproduced from Marx et al., 2003¹⁰⁷ with permission.

2.5. Thiosulfate-oxidizing multienzyme system

The sulfur cycle is a key biogeochemical process as sulfur is an essential nutrient for all life, and the various sulfur species serve critical roles in dissimilatory oxidation and reduction, as electron donors and receptors, respectively. Sulfur chemistry is defined by a range of redox states ranging from sulfide (S^{2-}) to sulphate (SO_4^{2-}), representing an eight-electron traverse from fully reduced to complete oxidation. Microorganisms performing dissimilatory catabolic reduction (i.e., sulfur-reducing prokaryotes, SRP), or oxidation (i.e., sulfur-oxidizing bacteria, SOB) of inorganic sulfur compounds are ecologically important and abundant across the globe, comprising the biotic component of global sulfur cycling²⁷.

Paracoccus pantotrophus GB17, an alphaproteobacterial facultative chemoautotroph, has been the model subject of extensive study into the thiosulfate-oxidizing multi-enzyme system (TOMES) (Fig 2.2.). In *P. pantotrophus*, TOMES is organized between three operons within a single locus of chromosome 2, comprised of the divergently encoded *soxRS*, followed by *soxVW*, with the main sulfur oxidizing complex *soxXYZABCDEFGH* proceeding in the relative sense direction downstream of the first two operons¹⁰⁸⁻¹¹⁰. The dissimilatory oxidation of reduced inorganic sulfur compounds (RISCs) by TOMES begins with SoxXA, a heterodimeric cytochrome comprised of the monoheme SoxX and diheme SoxA, catalyzing the covalent attachment of a suitable RISC (S^{2-} , $S_2O_3^{2-}$, SO_3^{2-}) to the heterodimeric sulfur carrier SoxYZ complex, yielding two electrons¹¹¹. SoxA contains the catalytic reactive center, whereas SoxX performs the restorative oxidation of SoxA into the active state and transfers the two electrons to an associated electron acceptor, generally a small c-type cytochrome¹¹². RISCs are covalently bound to SoxY via the thiol group of the invariant cysteine-110 residue within a conserved C-terminal GGCGG motif, and part of a “swinging-arm” mechanism allowing for modular interaction with other TOMES enzymes¹¹³⁻

¹¹⁵. The dimanganese-containing thiosulfohydrolase SoxB interacts directly with the SoxYZ-sulfuryl-sulfone adduct to hydrolytically cleave the terminal sulfone group yielding SO_4^{2-} and a newly exposed sulfane moiety as part of the SoxYZ-adduct^{114,116}. The molybdo-hemo sulfane dehydrogenase SoxCD oxidizes the exposed sulfane to sulfone in the most significant energy-generating step of the process, yielding six electrons, and this mechanism is considered characteristic of the alphaproteobacterial sulfur oxidizers^{114,117}. Finally, SoxYZ is reverted to its original state by hydrolysis of the remaining sulfone group by SoxB, allowing for the cycle to continue.

The functional SoxY-Cys110 residue poses quality control challenges, as SoxY forms inter-protein disulfide bridges with other proteins possessing exposed thiol groups, especially other SoxYZ complexes^{118,119}. The resulting SoxZY-YZ dimers are inactive but can be remedied by the action of thiol-disulfide oxidoreductase SoxS, an essential thioredoxin for thiosulfate oxidation in *P. pantotrophus*^{109,120}. Site-directed mutagenesis of the conserved thioredoxin-motif cysteine residues showed that SoxS specifically binds to SoxY *in vivo*, indicating that SoxYZ is a specific target of SoxS¹²⁰. This involves the reduction of SoxY by SoxS, given that resolution of the SoxZY-YZ disulfide bridges requires re-reduction of one sulfur atom involved in the bond, the ability to chemically complement SoxS-deficient strains with reductants such as dithiothreitol, and the action of the essential SoxV inter-cytoplasmic membrane protein which transfers reducing potential from inner membrane electron donors to periplasmic proteins, particularly SoxS¹²¹. The most fascinating result is that this essential role of the SoxSV reductive quality control proteins is only present *in vivo*, as early studies of the reconstituted TOMES *in vitro* proceeded with only the core enzymes (SoxXYZABCD) with horse cytochrome c as the electron acceptor, indicating that the oxidizing environment of the periplasm requires this additional level of quality control¹²².

It has been observed that the SoxXA-mediated sulfuryl-sulfane attachment mechanism of thiosulfate or sulfide to SoxY may proceed even if the sulfane moiety is not the integral R-group of the conserved Cys110 residue¹¹⁵. This indicates that the outer sulfane group exposed by SoxB hydrolysis is a suitable substrate for SoxAX up to a certain sulfuryl chain length, and may explain the production of sulfur globule chains by organisms which lack SoxCD¹²³. The cycle of SoxAX attachment and SoxB hydrolysis results in the addition of one sulfur atom per round, hence the polysulfide chain formation. This phenomenon is observed in SOB with functional sulfane dehydrogenases, as SoxYZ isolated from *P. pantotrophus* exhibits a pattern of mass multiples consistent with sulfur adducts which can be removed via reduction of the protein^{113,115}.

It was initially thought SoxS was involved in the regulation of the other Sox operons in *P. pantotrophus* as a partner to SoxR, a transcriptional repressor of the ArsR-family which binds upstream to *soxVW* and *soxXYZA-H*; however, no impact on *sox* operon expression has been observed in Δ *soxS* mutants^{109,124}. SoxR is the only known transcriptional regulator of TOMES in *P. pantotrophus*, cooperatively binding to conserved sites in the *sox* intergenic regions via a helix-turn-helix DNA-binding motif. While thiosulfate is an evident signal for *sox* operon up-regulation, DNA-binding by SoxR has not been demonstrated to be alleviated by direct interaction with thiosulfate, and the direct mechanism of SoxR de-repression is not known¹²⁴. Another form of *sox* genetic regulation occurs as a canonical two-component system (TCS) comprising of a sensor histidine kinase and a partner response regulator. The extremely acidophilic chemolithoautotroph *Acidithiobacillus caldus* possesses *tspSR*, a σ^{54} -dependent TCS encoded directly upstream of the *A. caldus* Sox-I operon¹²⁵. TspR response regulator binds activator sequences upstream of the Sox-I operon with indirect evidence to recruit σ^{54} -RNA polymerase, thereby upregulating TOMES, although it has not been confirmed that TspS senses thiosulfate directly.

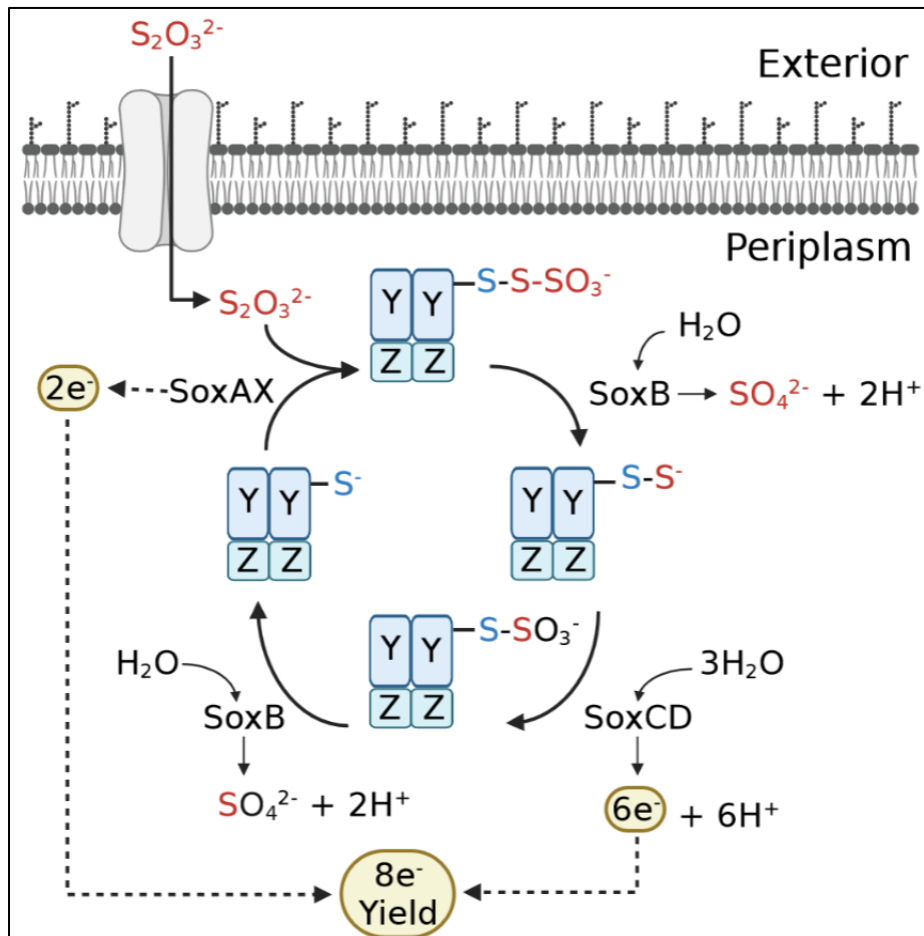


Figure 2.4. Thiosulfate-oxidizing multienzyme system diagram based on *P. pantotrophus* GB17 model^{113,122,126,127}. Note that the SoxYZ heterodimer is theoretically capable of carrying two RISC moieties between both SoxY subunits, however one bonded RISC is shown for ease of presentation. Furthermore, complications including SoxY-dimerization are omitted for clarity. SoxB – thiosulfohydrolase; SoxCD – sulfane dehydrogenase; SoxYZ – sulfur carrier complex; SoxAX – sulfur-attachment cytochrome.

2.6. Reverse dissimilatory sulfate reduction pathway

For sulfur chemolithotrophs lacking SoxCD, an alternative pathway is required to oxidize RISCs. As an example, the nonoxygenic phototrophic purple sulfur bacterium (PSB) *Allochromatium vinosum* utilizes a truncated TOMES (*soxYZAXB*) in combination with the reverse dissimilatory sulfate reduction (rDSR) pathway (*dsrABEFHCMKLJOPNRS*; Fig. 2.5)^{128,129}. As the name suggests, the rDSR pathway is a variant of the dissimilatory sulfate reduction pathway employed by anaerobic SRPs which can utilize thiosulfate, sulfite, and sulfate as terminal electron acceptors¹³⁰. Indeed, many of the reactions of the two DSR pathways are reversible with the redox direction dictated by the form of dissimilatory sulfite reductase (DsrAB/rDsrAB) utilized^{130,131}.

The process begins with the initial oxidation of thiosulfate or sulfide to zero-valent sulfur by SoxBAXYZ, leading to the development of sulfur globules as characteristic periplasmic inclusions while sulfide is non-limiting¹³². This activity is dependent on sulfur globule proteins, which are essential for sulfur oxidation in *A. vinosum*¹³³. While the exact mechanisms of sulfur transfer across the inner membrane are not fully understood, homologs of other sulfur transporters have been implicated, for example the thiosulfate transporters PmpAB and YedE/YeeE^{134,135}. Current models present small molecule sulfur carriers including persulfidic variants of glutathione, glutathione amide, or thiosulfate as candidates to facilitate the transfer of sulfur from periplasmic sulfur globules across the cytoplasmic membrane¹³⁶⁻¹³⁸. Following transport into the cytoplasm, the sulfane moiety is interchanged between a sequence of sulfuryl transferases belonging to the *rhd-tusA-dsrE2* cluster, highly conserved among sulfur oxidizers belonging to the Chromatiaceae, Chlorobiaceae, and Acidithiobacillaceae families¹³⁹. Initial lines of evidence towards the *rhd-tusA-dsrE2* cluster involvement included genomic co-localization with other sulfur-oxidizing genes including rDSR, *hdr*, and *soeABC* operons. This is supported by transcriptomic data from *Acidithiobacillus ferrooxidans* demonstrating *tusA* and *dsrE2* are highly upregulated in sulfur-

oxidizing versus iron-oxidizing conditions¹³⁹⁻¹⁴¹. Similarly, *Ac. vinosum rhd-tusA-dsrE2* expression is also triggered by the presence of RISCs¹³⁸. Patterns of sulfuryl transfer between TusA/Rhd and DsrC/DsrEFH have been identified, with the order of sequential sulfane transfers proposed as Rhd-TusA-DsrEFH¹³⁸. The specific role of DsrE2 remains unclear despite its necessity for rDSR-utilizing sulfur-oxidizing microbes, as experimental conditions were unable to confirm sulfur transfer between DsrE2 and TusA, Rhd, or persulfidic donors.

DsrEFH is a heterohexameric sulfuryl transferase complex which accepts sulfane from TusA via a conserved Cys78 residue, and is a defining feature of rDSR versus DSR pathways as SRPs utilizing the reductive pathway do not possess DsrEFH^{129,142}. DsrEFH transfers the sulfane group to the sulfur carrier protein DsrC through formation of stabilized protein complex interaction, and the sulfane group is bonded to the DsrC-Cys111 residue. In an interesting case of convergent evolution, the two functional cysteine residues of DsrC are located on a mobile C-terminal domain to facilitate protein-protein interactions with DsrMKJOP and DsrAB in an analogous fashion to the C-terminal swinging-arm of SoxY, despite DsrC and SoxY sharing no homology^{114,142}. Before the identification of the Rhd-TusA-DsrEFH sulfur relay, persulfidic small molecule sulfur carriers were thought to be potential substrates for DsrEFH and/or DsrC, however neither sulfur carrier protein can utilize these persulfidic molecular carriers as substrates¹⁴².

The rDSR pathway beyond formation of the DsrC-SH adduct is not fully resolved. The current model proposes that the sulfane group on DsrC is oxidized through another tight protein-protein interaction with the key siroheme-[4Fe-4S] reverse sulfite reductase rDsrAB, which in turn transfers four electrons via the iron-sulfur flavoprotein DsrL to reduce NAD⁺ to NADH^{131,142-144}. The sulfone of DsrC is presumed to dissociate as free sulfite following spontaneous disulfide bridge formation between the Cys111 (CysA) and Cys100 (CysB) residues of DsrC, with the CysA-B disulfide bridge hypothetically resolved through reduction by the catalytically active cytoplasmic

DsrK subunit of the inner membrane-localized DsrMKJOP complex^{139,142,145}. Once the two thiol groups of DsrC have been restored, DsrC can accept another sulfane from DsrEFH allowing the cycle to proceed. However, this model rests on the assumption that the DsrC disulfide bridge reaction can proceed at pH >7, which has not been experimentally validated and is complicated by model neutrophilic SOB like *A. vinosum* whose cytoplasmic pH ranges from 7.0 to 7.3^{139,146}.

Furthermore, the redox potential (E°) of the DsrC disulfide bond is hypothesized to pose a challenge for the current model of resolution by DsrK, although the exact E° value of the DsrC disulfide bridge is not known¹³⁹. Some insight can be gleaned through comparison to the methanogenic archaeal intermediate CoM-S-S-CoB, whose disulfide bond ($E^{\circ} = -143$ mV) is reduced by methanophenazine ($E^{\circ} = -165$ mV)¹⁴⁷. In addition, measured catalytically functional protein disulfide redox potentials have an upper redox potential boundary around -95 mV^{148,149}. Hence, the fact that *A. vinosum* and a variety of related PSB utilize ubiquinone/ubiquinol (UQ/UQL) as the primary components of their phototrophic electron carrier pools, and that UQ has a positive E° value ($\sim +65$ mV), it is unlikely that DsrMKJOP can reduce the DsrC disulfide bridge with UQL as electron donor¹⁵⁰. Menaquinone/menaquinol (MQ/MQL) is the other major constituent of PSB quinone pools associated with IM-bound rDSR complex electron transfer and they possess a redox potential of -75 mV, and are therefore similarly insufficient to reduce the DsrC disulfide bridge¹⁵¹. Furthermore, the lack of relevant electron-transporting flavoenzymes capable of electron bifurcation in PSB species including *A. vinosum*, for example the QmoABC complex, rules out the mechanism in this reaction^{151,152}. While it has been postulated that the periplasm-facing triheme c-type cytochrome DsrJ subunit could perform oxidative catalysis to collect higher energy electrons from periplasmic electron donors including RISCs for transfer to DsrK, such activity has not been demonstrated and the function of DsrJ remains cryptic despite its essentiality for rDSR sulfur oxidation^{139,153}.

The solution for the rDSR model may lie within recent developments in SRP DSR metabolisms. *In vitro* experimentation with purified reductive DsrC and DsrAB isolated from the thermophilic archaeon *Archaeoglobus fulgidis* demonstrated that sulfite reduction by DsrAB/C relies on the formation of a trisulfide bridge between the catalytically active DsrC C-terminal cysteine residues¹. In addition, decreased growth rates were observed for $\Delta dsrC$ *Desulfovibrio vulgaris* strains growing with sulfite and DsrC Cys_BAla expressed *in trans*; Cys_AAla mutants were unviable. While the DsrC trisulfide adduct is yet to be confirmed in rDSR-utilizing SOB, its inclusion in the pathway would solve the complications posed by the reduction of the DsrC disulfide bridge by DsrK. Consequently, this finding re-contextualizes the conserved nature of both C-terminal DsrC cysteines residues as catalytically functional in the transport and oxidation of the sulfane moiety in the cytoplasm.

These findings have profound consequences for the rDSR pathway, as it calls for rearrangement of the pathway order with implications for energy conservation. Following the upstream sulfuryl transfer relay, the updated rDSR pathway would begin with oxidation of the DsrC-sulfane adduct by DsrK, producing DsrC-trisulfide and transferring 2 electrons through DsrM/P to reduce ubiquinone. DsrC-trisulfide would then be oxidized by DsrAB, transferring 2 electrons to NAD⁺ via DsrL, thereby releasing sulfite. This updated model suggests the collection of all four electrons from the oxidation of elemental sulfur to sulfite, as opposed to requiring the transfer of two electrons from the UQ pool to resolve the DsrC disulfide bridge. For the entire pathway from sulfide to sulfate, the updated model permits an additional mole of reducing equivalents (four versus three NADH), a 33% increase which is evidently advantageous for photochemoautotrophic SOB, given the high demand for NADH and ATP by the CBB cycle.

2.7. Sulfite oxidation

The fate of sulfite released into the cytoplasm is well defined and proceeds via indirect or direct pathways. The indirect route proceeds through the adenosine-5'-phosphosulfate reductase (APSR) pathway. The first occurs as a total inversion of the reductive DSR process, centered on translational products of the *sat-aprAB-qmoABC* gene cluster found in a wide variety of SOB and SRP genomes^{27,154-156}. The process initiates through the cytoplasmic heterodimeric iron-sulfur flavoenzyme adenylylsulfate reductase (AprAB; APS reductase), which catalyzes the reversible oxidative coupling of sulfite and AMP to produce adenosine-5'-phosphosulfate^{151,157}. Electrons are transferred from AprA-bound flavin adenine dinucleotide (FAD) through AprB iron-sulfur centers to the IM-bound QmoABC complex via AprB-QmoA interaction, after which the reduced QmoA-bound FAD releases the reducing potential to tandem iron-sulfur centers of QmoC and subsequently reduces MQ¹⁵¹. Another APSR pathway variant occurs in SOB lineages which lack *qmoABC*, whose function is replaced by the membrane-bound AprM with correlated alterations in the AprB structure presumed to promote docking between AprAB/M^{154,158-160}. The APSR pathway resolves by the transfer of PP_i onto APS by ATP sulfurylase (ATPS; *sat*) to form sulfate and ATP, in addition to providing an important recycling route for PP_i generated through biosynthetic reactions¹⁶¹. Notably, the APSR pathway is not obligatory to complete rDSR sulfur oxidation given its absence in multiple rDSR-utilizing PSB species, a finding accentuated by the sulfite-oxidation capabilities of APSR-deficient *A. vinosum* mutants^{140,152,158}. In these taxa, direct sulfite oxidation proceeds via the inner-membrane-bound polysulfide reductase-like iron-sulfur molybdoprotein SoeABC, and is likely the predominant route of sulfide oxidation for PSB¹⁴⁰. The cytoplasmically-oriented SoeA subunit catalyzes the oxidation of sulfite through to sulfate, and transfers the reducing potential through SoeB to the transmembrane SoeC subunit to reduce MQ^{152,162}. SoeABC is universally encoded in PSB genomes and widespread in chemotrophic taxa

across *Gamma*-, *Alpha*-, and *Betaproteobacteria*, further cementing its importance in sulfite oxidation among SOB¹⁴⁰.

Sulfite oxidases (SO), a molybdoenzyme subclass alongside nitrate reductases whose active sites contain a molybdopterin cofactor (MoCo), facilitate the conversion of sulfite to sulfate in the periplasm¹⁶³. SOs serve an essential role in mitigating sulfite toxicity within eukaryotic mitochondria, plant peroxisomes, and bacterial periplasms, with three forms of SOs identified, each corresponding to animal, plant, or bacterial classifications^{164–166}. Bacterial SOs (BSOs) are heterodimeric enzymes with an A subunit containing MoCo and the B subunit utilizing heme *c*, and specifically categorized as sulfite dehydrogenases (SDH; sulfite:cytochrome *c* oxidoreductase, SorAB), as BSOs do not utilize molecular oxygen as substrate unlike their eukaryotic counterparts^{163,166,167}. Instead, the BSO subunit B heme transfers electrons from sulfite to accessory *C_{55N}*-type cytochromes, and therefore presumably able to contribute to energy conservation through reduction of *cbb₃/aa₃* cytochrome oxidases^{163,166,168}. While primarily involved in periplasmic sulfite detoxification, BSOs have also been proposed as alternative terminal enzymes of cytoplasmic sulfur oxidation for organisms that utilize the rDSR pathway but lack the APSR or SoeABC components²³. In these cases, sulfite released into the cytoplasm by rDsrAB would be transported to the periplasm via a TauE-like exporter, allowing for BSO oxidation to proceed in an interesting example of cross-compartment catabolic coordination¹⁶⁹.

2.8. Sulfur oxidation and methanotrophs

Sulfur oxidation genes have been observed in well-characterized strains of the alpha- and gamma-MOB taxa, with some gamma-MOB found to contain complete putative TOMES. To date, complete *sox* inventories have been predicted in *Mt. buryatense* 5GB1, *Mt. alcaliphilum* 20Z, *Methylobacter marinus* A45, *Methylobacter whittenburyi* ACM 3310, *Methylobacter* sp. BBA5.1, and *Mb. luteus* IMV-B-3098²³. This interest has been bolstered by the introduction of novel

gamma-MOB isolates with predicted *sox* gene inventories, with a complete set found within the *Methylicorpusculum oleiharenae* XLMV4 genome, and a partial *soxYZCD* set within *Methylospirillum oryzae* Strain C50C1^{24,170}. The presence of partial TOMES gene sets has been noted in *Methylococcus capsulatus* Bath (*soxYZC*) and *Mm. methanica* MC09 (*SoxYZ*). The function of partial *sox* gene sets, save for *soxBAXYZ*, is unknown and may indicate the progressive selection-driven loss of TOMES in these lineages. For alpha-MOB, the *Ms. trichosporium* OB3b genome encodes *soxBYZCD* with *soxB* localized on one large plasmid, while *Methylosinus* sp. 3S-1 possesses a single putative *soxB* gene¹³⁵. Many MOB across all lineages also possess sulfide:quinone oxidoreductases, but these are suspected to be for sulfide detoxification, as is the case for many bacteria in proximity to anaerobic clines where SRPs are active¹⁷¹.

Despite the number of isolates with TOMES inventories, experimental evidence of MOB sulfur oxidation remained elusive until the recent isolation of '*Methylovirgula thiovorans*' strain HY1, an alpha-MOB of the family Beijerinckiaceae¹³⁵. This strain demonstrates the ability to oxidize methane and RISCs concurrently; the first reported case of methane/sulfur mixotrophy observed in methanotrophs. *Mv. thiovorans* HY1 can utilize thiosulfate, tetrathionate, and elemental sulfur for growth when supplemented with 5% carbon dioxide; growth on sulfide could not be assessed due to the auto-oxidizing growth conditions. *Mv. thiovorans* HY1 can grow on a variety of C2-4 substrates as well, a trait shared by other Beijerinckiaceae, such as the model example of *Methylocella silvestris* BL2. Intriguingly, *Mv. thiovorans* HY1 has an even broader carbon substrate range compared to *Ma. silvestris* BL2, including butane and its primary alcohol, aldehyde, and ketone derivatives, although concentrations of 20 mM proved inhibitory.

Genomic and proteomic analyses demonstrated that *Mv. thiovorans* HY1 utilizes SoxBAXYZ in conjunction with a partial rDSR pathway for the complete oxidation of RISCs to sulphate, akin to nonoxygenic phototrophic sulfur bacteria^{27,135,152}. In this study, the authors were able to account

for all required transport and oxidation steps of the rDSR pathway except for the terminal oxidation of sulfite to sulfate by either the APSR pathway or SoeABC; instead, an inner membrane-localized sulfite transporter and periplasmic sulfite:cytochrome c oxidoreductase (SorAB) are predicted to replace this lesion. *Mv. thiovorans* HY1 is capable of autotrophic carbon assimilation through the CBB cycle during sulfur oxidation, evidenced by the upregulation of the large RuBisCO subunit CbbL when thiosulfate and carbon dioxide are present. The use of the CBB cycle in conjunction with RISC electron donors is common in chemolithoautotrophs, and is also employed in methanotrophic carbon assimilation by other MOB clades, for example *Verrucomicrobia*²⁰. It remains to be seen if carbon dioxide assimilation via the EMC cycle is essential for biomass production by *Mv. thiovorans* HY1 as for other alpha-MOB, for example *Ms. trichosporium* OB3b, although the presence of the CBB cycle counteracts this notion. Indeed, the authors speculate that the involvement of the CBB cycle may partially explain why *Mv. thiovorans* HY1 can utilize RISCs for growth, while the same has not been demonstrated in gamma-MOB with complete TOMES but lacking the CBB cycle¹³⁵.

The possibility of a dissimilatory sulfur oxidation pathway alongside methane oxidation raises questions regarding the interaction of these systems based on substrate combinations. The authors measured substrate-specific oxygen consumption rates with a range of RISCs and C1-3 compounds on *Mv. thiovorans* HY1 cells grown on methane, thiosulfate, or the two substrates in combination¹³⁵. The results were intriguing; *Mv. thiovorans* HY1 does not constitutively express either methane or sulfur oxidation systems; cells grown solely with methane are unable to immediately oxidize RISCs, and thiosulfate-grown cells could not oxidize methane. Cells grown with methane and thiosulfate could oxidize both substrates, demonstrating concurrent operation of the SOX/MOX systems, although the mixotrophic cells displayed lower rates of oxygen consumption on a per-substrate basis when compared to their respective sole-substrate

counterparts. Oxygen consumption rates of the thiosulfate-grown *Mv. thiovorans* HY1 cells treated with RISCs were 1.8 to 2.7-fold higher than the methane-grown cells treated with methane, except for elemental sulfur which exhibited a 1.6-fold decrease¹³⁵. While it may be expected that a MOB strain would demonstrate higher oxygen consumption with methane, the mass transfer of methane in aqueous solution is limited compared to the readily water-soluble sulfur anions. Interestingly, all three groups demonstrated similar oxygen uptake rates in the methanol, ethanol, and 1-propanol conditions, highlighting the importance of the MDH and H₄MTP/H₄F pathways in *Mv. thiovorans* HY1¹³⁵.

2.9. Hypothesis and objectives

The presence of conserved, complete TOMES systems across *Methylococcales* genera, combined with the recent discovery of *Mv. thiovorans* HY1, raises the possibility of a similar mixotrophic strategy by members of the gamma-MOB. However, methane/sulfur mixotrophy has not been demonstrated for any gamma-MOB species, resulting in a discrepancy between the predicted genomic inventories and metabolic capabilities for these bacteria. It is hypothesized that *Methylococcales* may employ sulfur compounds as alternative electron donors, particularly under methane-limiting growth conditions. Sulfur/methane mixotrophy by gamma-MOB could spare a greater fraction of methane from complete oxidation while supporting energy production, ultimately improving carbon conversion efficiency (CCE) under carbon starvation conditions (Fig. 2.6). As mentioned previously, this would be especially beneficial for obligate methanotrophs which depend on a single substrate as both carbon and energy source. Moreover, CCE improvement would be highly beneficial for industrial application of these strains, as it would lead to an increased fraction of assimilated carbon towards desired end-products while considerably reducing the CO₂ emissions of the process.

As such, the first goal of this work was to collect, collate, and document the presence of TOMES in genomic data of methanotrophic bacteria of the order *Methylococcales*, particularly the presence/absence of specific genes and their relative organization within genomes of interest. Then preliminary validation of the TOMES genes were completed, through review of conserved domains, functional residues, and utilization of cross-comparative alignments with validated sox genes of model SOB, specifically *P. pantotrophus*, *A. vinosum*, and *Starkeya novella*. Finally, physiological investigations into potential sulfur-oxidizing phenotypes of select *Methylococcales* genera were performed, including addition of thiosulfate and relevant co-factors, while testing both carbon/oxygen limiting conditions. Cultures were assayed via a combination of headspace gas chromatography, optical density spectroscopy, cell mass production, and sulfate production measurement.

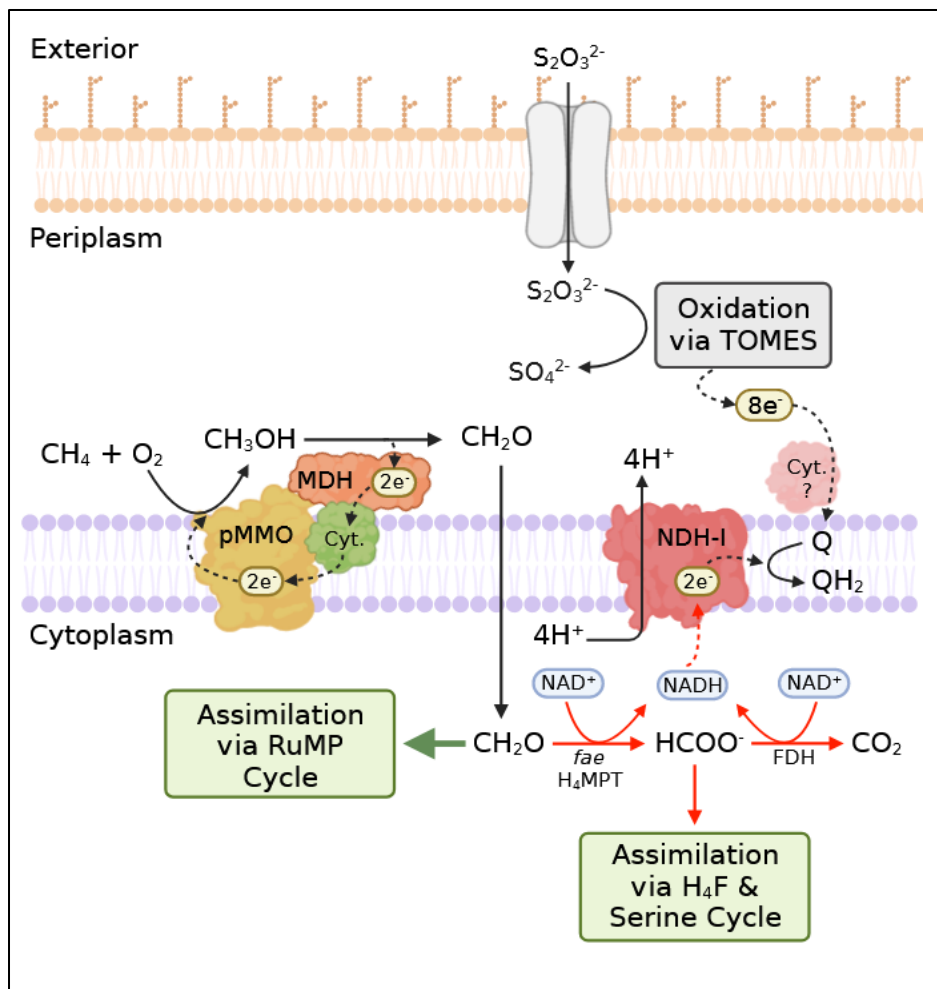


Figure 2.6. Hypothetical impacts of methane/sulfur mixotrophy on primary methane oxidation pathway of Gammaproteobacterial methanotrophs. Green/red arrows denote increased/reduced carbon flux, respectively.

3. Materials and Methods

3.1. Bioinformatic identification and confirmation of *Methylococcales* TOMES, including loci cluster mapping.

Protein alignment of SoxB thiosulfohydrolase from *T. thermophilus* HB8 (AP008226.1), *P. pantotrophus* GB17 (QFG35248.1), *Mb. luteus* (WP_027159286.1), *Mt. buryatense* 5GB1C (WP_017842264.1), and *A. vinosum* DSM 180 (ADC63088.1) was produced via ESPript 3.0, including *T. thermophilus* HB8 SoxB protein database (PDB) file to provide secondary structure features identified in SoxB crystal structure¹⁷²⁻¹⁷⁴. Alignment was replicated in Jalview 2.11, with the *T. thermophilus* HB8 SoxB sequence subtracted, with BLOSUM62 matrix coloring to illustrate functional conservation of amino acid replacements between SoxB proteins¹⁷⁵. Following *Mt. buryatense* 5GB1C SoxB confirmation Targeted NCBI BLASTp alignment of *P. pantotrophus* SoxBC and *A. vinosum* SoxXYZ protein sequences was utilized to identify putative TOMES genes *Mt. buryatense* 5GB1C^{176,177}. Cutoffs of 90% for query coverage and 40% for identity were applied, with a corresponding significant E-value of <1E-6. The *Mt. buryatense* 5GB1C TOMES genes were then used to query *Methylococcales* via NCBI BLASTp using the same cutoffs as described, with SoxB presence used as an additional criterion for selection. Batch DNA sequences were processed through clinker cluster visualization pipeline, using global crosswise alignments of translated amino acid sequences and calculating pairwise percent identities between adjacent sets¹⁷⁸.

3.2. Protein alignment and phylogenetic comparison of *Methylococcales* sulfite dehydrogenases.

Protein sequences of putative *Methylococcales* sulfite dehydrogenases identified via *Mt. buryatense* 5GB1C SoxC BLASTp alignment were compared against sulfite dehydrogenase subunit A (SorA; AAF64400.1) and sulfane dehydrogenase (SoxC; AAF61449.1) protein sequences from *Starkeya novella* DSM 506 (NC_014217.1). Alignment was performed via the NCBI BLASTp suite, and the resultant table of percent identity and query coverage values were converted into a heatmap with Prism 9 (GraphPad). Percent identity values of $\geq 40\%$, combined with query coverages of $\geq 85\%$ and an E-value $< 1E-6$ were considered significant, and metagenomic/environmental sequences were omitted¹⁷⁹. BLASTp search of homologs of *S. novella* SoxC/SorA and *P. pantotrophus* SoxC within *Methylococcales* were performed with protein sequences of *Methylococcales* SDHs downloaded via NCBI Batch Entrez service. The neighbor-joining phylogenetic tree was produced via the “One Click” phylogeny service by Methods and Algorithms for Bioinformatics (Computer Science, Robotics, and Microelectronics Unit, University of Montpellier, France)^{180,181}. Output was subsequently amended through FigTree v.1.4.4 for final visualization.

3.3. Culturing conditions for *Methylovivimicrobium buryatense* 5GB1C.

M. buryatense 5GB1C was cultured in modified nitrate mineral salt (NMS2) medium, containing 1.7 mM $MgSO_4 \cdot 7H_2O$, 0.1 mM $CaCl_2 \cdot 2H_2O$, 10 mM KNO_3 , 0.1 M NaCl, 1.5 μM $CuSO_4$, and trace elements solution. The concentration of trace elements in the media was 15 μM Na_2EDTA , 7 μM $FeSO_4 \cdot 7H_2O$, 1 μM $ZnSO_4 \cdot 7H_2O$, 0.2 μM $MnCl_2 \cdot 4H_2O$, 0.8 μM $CoCl_2 \cdot 6H_2O$, 0.9 μM $Na_2WO_4 \cdot 2H_2O$,

0.2 μM $\text{NiCl}_2 \cdot 6\text{H}_2\text{O}$, 0.2 μM $\text{Na}_2\text{MoO}_4 \cdot 2\text{H}_2\text{O}$, and 0.5 μM H_3BO_3 . 100 mL of medium was subsequently buffered with 4.0 mL of carbonate buffer (1.1 M NaHCO_3 , 0.1 M Na_2CO_3); and 1.0 mL phosphate buffer, (0.2 mM Na_2HPO_4 , 0.1 KH_2PO_4). Cultures were prepared with a 1% (v/v) inoculum in 100 mL NMS2 medium, contained within 250-mL Wheaton bottles (DWK Life Sciences) fitted with butyl-rubber septum inlaid screw caps. Unless otherwise noted, 40 mL of air was removed and 50 mL of 99.9% methane gas (Linde Canada) was added to the headspace through a 0.5-micron syringe filter (Millipore). Cultures were incubated at 30°C and ~130 rpm in a controlled environment incubator/shaker (New Brunswick Scientific Co., Inc., NJ, USA), and were mature within 48 h. Inoculum was sourced from culture stored in dark conditions at room temperature for no longer than 1 week, produced via same method.

3.4. Culturing conditions for *Methylicorpusculum oleiharenae* XLMV4.

M. oleiharenae XLMV4 was cultured in 10X copper and iron (M10XCF) mineral salts medium, containing 0.8 mM $\text{MgSO}_4 \cdot 7\text{H}_2\text{O}$, 45.5 μM $\text{CaCl}_2 \cdot 2\text{H}_2\text{O}$, 9 mM NH_4Cl , 0.15mM Ferric EDTA, 1.25 μM CuSO_4 , and trace elements solution²⁴. Trace elements concentration of the media was 1.5 μM $\text{ZnSO}_4 \cdot 7\text{H}_2\text{O}$, 1.4 μM $\text{MnCl}_2 \cdot 4\text{H}_2\text{O}$, 0.3 μM $\text{CoCl}_2 \cdot 6\text{H}_2\text{O}$, 0.25 μM $\text{Na}_2\text{MoO}_4 \cdot 2\text{H}_2\text{O}$, and 1.6 μM H_3BO_3 . 100 mL of medium was subsequently buffered with 4.0 mL of carbonate buffer, (1.1 M NaHCO_3 , 0.1 M Na_2CO_3); and 1.0 mL phosphate buffer (0.2 mM Na_2HPO_4 , 0.1 M KH_2PO_4). Cultures were prepared with a 1% (v/v) inoculum in 100 mL NMS2 medium, contained within 250-mL Wheaton bottles (DWK Life Sciences) fitted with butyl-rubber septum inlaid screw caps. Unless otherwise noted, 40 mL of air was removed and 50 mL of 99.9% methane gas (Linde Canada) was added to the headspace, sterilized through a 0.5-micron syringe filter (Millipore). Cultures were incubated at 20°C and ~130 rpm on a controlled environment incubator/shaker (New Brunswick Scientific Co., Inc., NJ, USA), and matured in ~120 h. Inoculum was sourced from

culture stored in dark conditions at room temperature for no longer than 1 week, produced via same method.

3.5. Growth assays via optical density and dry cell weight measurement.

Each growth assay followed a similar protocol, with certain species-specific amendments made depending on inoculum concentration and temperature. Cultures were prepared in media as described above and amended with 2.1 mM Na_2MoO_4 and 10 mM MnCl . Filter-sterilized solutions of $\text{Na}_2\text{S}_2\text{O}_3$ (2 – 20 mM) or LaCl_3 (5 μM) were added depending on the experimental conditions being tested. Generally, all assays followed a similar format; optical density readings were performed every 12 hours through 100- μL sample collections. These samples were deposited into 96-well plates (Falcon) and their optical density at a wavelength of 540 nm was measured using a Multiskan Spectrum plate reader (Thermo Scientific, USA) via SkanIt RE 2.4.2 software. For dry cell weight, 100 mL of stationary phase cultures were harvested on pre-weighed 0.5-micron filter paper (MilliporeSigma) placed on glass mesh vacuum filtration assembly (Cole-Parmer), vacuum filtered via electric pneumatic vacuum pump, measured for wet weight, then dried at 70°C in a ventilated oven. Samples were weighed every 24 h to track desiccation and weighed once mass had stabilized; ~92 h after samples were collected. Dry cell weight values were reported as dry mass per mL of culture. Each experimental group included three biological replicates and one cell-free control to ensure instrument consistency. The data reported is the mean of triplicates plus/minus one standard deviation.

3.6. Sulfate precipitation and quantification assay.

1 mL of stationary-phase cell culture was collected at the end of experiment via syringe, placed inside 1.5-mL centrifuge tube, and centrifuged in a tabletop Centrifuge 5424 (Eppendorf) at 9,000 RCF for 10 minutes. 500 μ L of supernatant was then collected and deposited into another 1.5-mL tube containing 500 μ L conditioning reagent comprising 2.6 M NaCl, 1.4 M glycerol, 3.3 M ethanol, and 0.2 M HCl. The supernatant and conditioning reagent were mixed thoroughly via vortexing, after which 85 μ L of 1.7 M BaCl₂ was added and mixed by inversion. 500 μ L of the completed mixture was pipetted into a 48-well plate (Falcon), and absorbance was measured at 420 nm using a *Citation 5* microplate reader (BioTek) via accompanying workspace software.

3.7. Headspace gas chromatography.

Wheaton bottle butyl-rubber septa were sterilized with 95% ethanol solution, and 100 μ L of headspace gas was extracted with a gas tight syringe assembly equipped with a Luer lock connection (SGE Analytical Science, Australia) and injected into a gas chromatograph equipped with a thermal conductivity detector (GC-TCD; Shimadzu GC-8A, Shimadzu Corporation). Data was recorded via the N2000 Chromatostation program (Zhejiang University, China), and converted into molar concentration units through development of standard curves using known amounts of pure analytical grade gases (Linde, Canada). Helium (Linde, Canada) was utilized as carrier gas with an injector/detector temperature of 120°C for all samples. Molsieve 5A packed column (Restek) at 90°C was used for CH₄ and O₂ measurements, whereas a HayeSep Q 80/100 mesh packed column (Restek) at 80°C was utilized for CO₂ measurements.

3.8. Protein alignment of *A. kashmirensis* thiol dehydrotransferase and *Methylococcales* XoxF MDH.

A. kashmirensis ThdT thiol dehydrotransferase amino acid sequence (WP_014751259.1) was used to query *Mt. buryatense* 5GB1C and *Mb. Luteus* protein datasets via NCBI BLASTp platform^{176,182}. XoxF MDH sequences for *Mt. buryatense* 5GB1C (WP_017842117.1) and *Mb. Luteus* (WP_027156973.1) were aligned with *A. kashmirensis* ThdT using the NCBI Multiple Sequence Alignment Viewer, with the resultant ALN file processed through ESPript 3.0 using the included Equivalent% physiochemical similarity scoring matrix^{172,173}. The RCSB Protein Data Bank file (ID: 6DAM) for *Mt. buryatense* 5G XoxF crystal structure was included to provide secondary structure information to the alignment¹⁸³⁻¹⁸⁵.

4. Results

4.1. BLASTp alignments reveal putative thiosulfate-oxidizing genes in Methylococcales.

Sox genes were initially noticed through review of annotated genomic data of *Methylovium buriatense* 5GB1C (NZ_CP035467), a well-characterized alkaliphilic gamma-MOB regarded as a model organism with extensive omic/physiological data and validated genetic manipulation techniques available^{22,87,88,186,187}. First, the suspected TOMES homologs of *Mt. buriatense* 5GB1C were cross compared to those of *P. pantotrophus* DSM 2944 and *A. vinosum* DSM 180 using BLASTp (Fig. 4.1A). All core TOMES proteins were identified in *Mt. buriatense* 5GB1C through this approach; SoxBYZAX homologs were present based on NCBI SPARCLE functional assignment, whereas the SoxC homolog was identified as a generic sulfite dehydrogenase (Fig. 4.1A). SoxD was not observed in the BLASTp alignment using *P. pantotrophus* DSM 2944 protein sequence queries, however the *Mt. buriatense* SDH/SoxC homolog is accompanied by an accessory cytochrome encoded directly downstream in an operonic configuration (Fig. 4.1A). These data indicate that *Mt. buriatense* 5GB1C encodes all necessary components of TOMES and therefore may plausibly conduct reduced inorganic sulfur compound (RISC) oxidation. *Mt. buriatense* 5GB1C TOMES protein sequences were then utilized to query *Methylococcales*, with species possessing soxB selected for further analysis; accordingly, genetic maps from eight additional strains were developed (Fig. 4.1B). Species of the genera *Methylovium*, *Methylomicrobium*, *Methylobacter*, and *Methylicorpusculum* were identified as having complete TOMES, with *Methylosarcina*, *Mm. lacus* LW14, and *Mm. agile* ATCC 35068 possessing incomplete sets, lacking soxCD. These data are summarized as a presence/absence matrix for ease of review (Fig 4.2).

The genetic organization of the *Methylococcales* *sox* loci varied but with definite localization patterns throughout the taxon (Fig. 4.1B). First, the general organization of the *sox* genes relative to each other was preserved across all species surveyed. The thiosulfohydrolase *soxB* was localized separately from the other genes: in isolation (e.g., *Methylotheobacterium* spp.), alongside an MBL-fold metallohydrolase-coding sequence (e.g., *Mb. Marinus* LW14), or as part of an operon with various hypothetical proteins and membrane transport-associated sequences, for example in *Mm. lacus* LW14. The *soxYZA* operon is established as a single transcriptional unit accompanied by a molybdopterin molybdotransferase *moeA* homolog and is invariant across the *soxB*-possessing *Methylococcales* strains. The *soxX* loci feature homologs for thiamine biosynthesis (*thiDE*), TlpA-family thioredoxin, and *hemJ*-type protoporphyrinogen IX oxidase upstream of the *soxX* gene. The *tlpA-hemJ-thiDE-soxX* operon was broadly conserved across the *Methylococcales* strains analyzed, save for *Mm. agile*, *Mm. lacus* LW14, and *Ms. Fibrata* AML-C10 which lacked the TlpA and HemJ coding sequences (Fig. 4.1B). The *soxX* loci occurred either separated from their enzymatic partner *soxA* (e.g., *Methylotheobacterium* spp.) or associated upstream of the *soxYZA-moeA* operon (e.g., *Methylobacter* spp.).

For the SDH-encoding genes, the *soxCD*-type sulfane dehydrogenases were found to be isolated in the *Methylobacter* spp. genomes (Fig. 4.1B). For the *Methylotheobacterium* spp. and *Methylomicrobium* sp. Wino1 genomes, *soxCD* was found to be located alongside putative sensory histidine kinase response regulator at the 3'-end in addition to two YedE/YeeE sulfur transport protein family coding sequences at the 5'-end¹³⁴. As for *Mp. Oleiharenae* XLMV4, the response regulator was similarly co-localized with *soxCD* but with YedE/YeeE absent, although YedE/YeeE homologs are present elsewhere in the XLMV4 genome (Fig. 4.1B). The SDH genes encoded within *Mm. lacus* LW14 and *Ms. Fibrata* AML-C10 genomes were identified as SorAB-type sulfite dehydrogenases, and do not localize with any other conserved protein sequences.

4.2. Confirmation of *soxB* thiosulfohydrolase in *Methylovimicrobium buryatense* 5GB1C.

Following the identification of putative TOMES genes across *Methylococcales* genera, further bioinformatic confirmation was required to justify physiological experimentation. To this end, the putative thiosulfohydrolase gene *soxB* was selected for in-depth identity validation given its central role in RISC oxidation and utility as a validated functional marker for SOB phylogenetic analysis¹⁸⁸. The 5GB1C SoxB protein sequence was independently verified through BLASTp searches of the 5GB1C genome using well-characterized SoxB amino acid (AA) sequences from *Paracoccus pantotrophus* DSM 2944 and *Allochromatium vinosum* DSM 180 as representatives of alphaproteobacterial and gammaproteobacterial thiosulfohydrolase enzymes^{110,123,189}. The *Mt. buryatense* 5GB1C SoxB amino acid sequence was aligned with these protein sequences, in addition to SoxB genes from *Thermus thermophilus* HB8 and *Methylobacter luteus* IMV-B-2098. *Thermus thermophilus* HB8 was included due to the availability of a confirmed crystal structure with an accompanying Protein Database (PDB) file (2WDC), while *Mb. Luteus* was chosen as another representative *soxB* gene from *Methylococcales*¹⁷⁴.

The sequences were aligned by the NCBI BLASTp suite, processed via the ESPript 3.0 server with the corresponding PDB file, with features highlighted based on *T. thermophilus* HB8 as the reference sequence (Fig. 4.3A)¹⁷²⁻¹⁷⁴. The residues for manganese cofactor coordination of two metal sites were conserved between the SoxB sequences analyzed: metal site A ligands consist of Asp-47, His-49, Asp-143, His-299, and site B metal ligands Asp-143, His-174, His-274, and His-297 (Fig. 4.3A). Second sphere metal coordination ligands Gly-141, Trp-175, His-297, Trp-417, and Gln-473 were also found to be conserved across all lineages. Furthermore, residues predicted to interact directly or indirectly with the thiosulfate substrate are preserved in the *Methylococcales*

SoxB amino acid sequences, namely Glu-59, Trp-175, Arg-385, Arg-416, Trp-417 and Asp-476 (Fig. 4.3A).

As expected, there were some divergences in conserved residues between the *T. thermophilus* HB8 and queried SoxB amino acid sequences, as *T. thermophilus* HB8 SoxB possesses additional tertiary structure elements to promote stability under elevated temperatures¹⁷⁴. Thiosulfate-interacting ligands feature a V415F replacement in the *Methylococcales* and *A. vinosum* SoxB proteins, indicating a conserved structural change in the gammaproteobacterial lineage. The second sphere metal coordination ligands were subject to three instances of amino acid replacement from HB8 SoxB, namely S46T, N147G, and H237N; interestingly, the alphaproteobacterial and gammaproteobacterial SoxB sequences agreed on all second-sphere replacements, making the *T. thermophilus* HB8 SoxB enzyme unique in this regard.

As the ESPript 3.0 results only highlighted exact amino acid identity, the SoxB amino acid sequences were re-aligned via Clustal Omega and subjected to BLOSUM62 matrix scoring in Jalview (Fig. 4.3B)^{175,190–193}. As the BLOSUM matrix scores amino acid replacements based on biochemical similarity, it allows for further inferences on the significance of a given amino acid replacement. From visual assessment of Fig. 4.3B it is evident that despite differences in exact amino acid identity, the overall biochemical profile of the amino acid replacements is relatively minimal. 82.8% of residues aligned have a positive BLOSUM score for *P. pantotrophus* GB17 SoxB, compared to 86% of *A. vinosum* SoxB residues. This independent verification confirms the Hidden Markov Model assignment by the NCBI annotation pipeline, demonstrating that the *soxB* gene is present within *Methylococcales* strains.

4.3. Diversity of SDH enzymes predicted in *Methylococcales* genetic inventory.

Initial BLASTp alignment of *Mt. buryatense* 5BG1C SoxC to *Methylococcales* resulted in the identification of several enzymes with non-specific functional labels, denoted as generic sulfite dehydrogenases, molybdopterin-dependent oxidoreductases, or sulfite oxidases. This was somewhat expected, as sulfane/sulfite dehydrogenases are paralogs through a common ancestral SO gene, with SoxCD originally being termed “sulfite dehydrogenase” before the terminology was corrected to sulfane dehydrogenase^{114,194}. To resolve SDH identities, sulfite and sulfane dehydrogenase (SorA/SoxC) amino acid sequences from *Starkeya novella* were used to query the collective *methylococcales* protein database. Given that *S. novella* possesses both *sorA* and *soxC*, these sequences were expected to be differentiated based on their distinct catalytic activities and useful for differentiating SDH homologs when used in conjunction^{195,196}. The resultant BLASTp alignment demonstrated an intriguing pattern, namely that the *Methylococcales* strains investigated possessed homologs of significant similarity to either SoxC or SorA, but no individual *Methylococcales* SDH simultaneously corresponded to both (Fig. 4.4). For example, genomes of *Methylotetracoccus oryzae* and *Methylocaldum szegediense* were found to encode SDH enzymes with notable homology to both *soxC* and *sorA*-like SDHs, a trait shared with *S. novella*.

To better understand the phylogenetic relationships between the *Methylococcales* SDH enzymes, the sequences were assembled into a neighbor-joining tree alongside SorA/SoxC from *S. novella* and SoxC from *P. pantotrophus* (Fig. 4.5). As was initially determined from the BLASTp data, three distinct clusters were apparent: SoxC-like sulfite dehydrogenases, SorA-like molybdopterin-dependent oxidoreductases, and sulfite oxidase enzymes. While the annotations were broad and non-specific, protein sequences clustered alongside identically labeled sequences, i.e., all sulfite dehydrogenase sequences associated in the SoxC cluster, whereas the

molybdopterin-dependent oxidoreductases all clustered alongside SorA from *S. novella*. This pattern was also observed with the protein sequences labelled as sulfite oxidases, which formed a third distinct cluster primarily composed of *Methylobacter* spp. SO sequences with one additional SO belonging to *Methylohalobius crimeensis*. In addition, *Mb. Luteus*, *Mb. Marinus A45*, and *Methylobacter* sp. BIB1 possess SoxC-associated SDHs in addition to the SO enzymes observed, reflecting a similar pattern of multiple sulfite oxidoreductase molybdoenzymes in a single genome, analogous to the aforementioned *Methylococcales* strains with SoxC/SorA-homolog inventories and again to *S. novella*.

4.4. Thiosulfate has negligible impact on *Mt. buryatense* 5GB1C growth in a variety of conditions.

Following the preliminary bioinformatic work confirming the presence of a complete TOMES encoded within the *Mt. buryatense* 5GB1C chromosome, experiments were performed to determine if the strain exhibited a thiosulfate oxidation phenotype (Fig. 4.6). The growth of *Mt. buryatense* 5GB1C did not exhibit significant differences between conditions based on the parameters measured, including change in optical density, O₂/CH₄ consumption, CO₂ production, and final dry cell weight (DCW). The initial oxygen-limited conditions of the experiment were conducted at a [O₂]:[CH₄] ratio of 1:1.2, which was sufficient for complete oxygen depletion in the headspace within 48 h (Fig. 4.6B). As no detectable differences in growth were noticed by 96 h, pure O₂ was added at this time to an average concentration of 12.4 mmol/L (denoted by the black arrows in Fig 6). The resultant [O₂]:[CH₄] ratio of approximately 3:1 was deemed sufficient to allow for the oxidation of the remaining CH₄ in addition to the respiration of up to 0.9 mmol of thiosulfate reducing equivalents. However, no difference in oxygen consumption, DCW, or CO₂ production was noticed in the thiosulfate-attenuated cultures post-oxygenation.

Sulphate measurements of the media were also recorded, and culture supernatant was collected both before the addition of the additional O₂ (at 96 h) and after growth following the addition of additional O₂ (at 144 h) (Fig. 4.7). Cultures grown with 20 mM thiosulfate produced significantly higher sulphate concentrations relative to the other experimental groups and control. This is an intriguing development, as there were no other observed effects in the thiosulfate attenuated strains, and the development of thiosulfate was only significant at the higher thiosulfate concentration of 20 mM. For the 2 mM thiosulfate-amended cultures, sulfate production did not significantly differ from that of the control group. It is important to note that some potential sulfate production was observed in the thiosulfate-free control group (Fig. 4.7). However, owing to the non-specific nature of the barium precipitation assay, this finding can also be attributed to the production of non-soluble barium salts with mineral salts media components, such as Ba₃(PO₄)₂¹⁹⁷.

4.5. *Mp. oleiharenae* XLMV4 may oxidize thiosulfate as an alternative electron donor.

Mp. oleiharenae XLMV4 is a recent gamma-MOB isolate sourced from Canadian oil sands tailing pond sediment¹⁹⁸. It was selected for experimentation owing to its niche coinciding with RISC availability, relative novelty in laboratory culture, and availability to our research group^{24,199}. Initial data from experimentation with *Mc. oleiharenae* XLMV4 demonstrated a pronounced growth rate increase in the presence of 2 mM thiosulfate, 10 µM manganese, and 2 µM molybdate (Fig. 4.8). The thiosulfate-attenuated group completed logarithmic growth by 72 h, as opposed to 120 h for the control, but then underwent a drastic drop in optical density after 96 h (Fig. 4.8A). The presence of lanthanum had no impact on growth rate or final optical density relative to the control, but lanthanum in combination with thiosulfate significantly decreased final OD and growth rate. Similar patterns were also noted in gas consumption rates, where the thiosulfate-amended cultures demonstrated CH₄ and O₂ depletion rates which exceeded those of the control group by

notable margins (Table 2, Fig. 4.8B-E). In these samples, CH₄ was consumed at a rate of 114.5 nmol/h (+19.6% over control), whereas O₂ featured a more dramatic consumption rate of 143 nmol/h (+79.2 % over control). As with optical density, the lanthanum-amended group displayed no notable difference from the control, and the lanthanum/thiosulfate group had a slower rate of CH₄ depletion.

The *Mp. oleiharenae* XLMV4 experiment was repeated with an archival stock culture to test the replicability of the phenotype (Fig. 4.9). While the lanthanum/thiosulfate growth inhibition effect was replicated, the pronounced increase in growth in conjunction with rapid rates of headspace gas depletion previously observed were not apparent in the thiosulfate-amended group (Fig. 4.9ABC). Furthermore, the cells only reached a maximum OD₅₄₀ of ~0.075 as opposed to ~0.2, representing a 2.7-fold decrease. This growth impairment was suspected to be the result of using the archival stock culture in non-alkaliphilic NMS media, whereas the previous *Mp. oleiharenae* XLMV4 had been passaged many times through standard NMS media and had likely adapted to the new parameters.

4.6. Methylococcales XoxF-type methanol dehydrogenase is homologous to novel sulfur-oxidizing enzyme thiol dehydrotransferase from *A. kashmirensis*.

BLASTp search utilizing thiol dehydrotransferase (ThdT) from *A. kashmirensis* was able to effectively query Methylococcales XoxF-type MDHs, owing to high percentages of amino acid sequence identity, as illustrated in Fig. 4.10. ThdT from *A. kashmirensis* shared all conserved cofactor coordination residues with XoxF MDHs from *Mt. buryatense* 5GB1C, *Mp. oleiharenae* XLMV4, and *Mb. luteus* IMV-B-3098. Specifically, PQQ-coordinating residues Cys-129, Cys-130, and Trp-267, alongside lanthanum-coordinating residues Glu-197, Asn-285, Asp-327, and Asp-

329; numbering is reflective of *Mt. buryatense* 5GB1C XoxF amino acid sequence (Fig. 4.10)¹⁸⁵. Despite high overall sequence similarity, ThdT structure deviates from XoxF in specific regions, most notably between residues 580-589, which correlates with the negatively-charged region of disordered residues proximal to the XoxF active site¹⁸⁵.

4.7. Figures

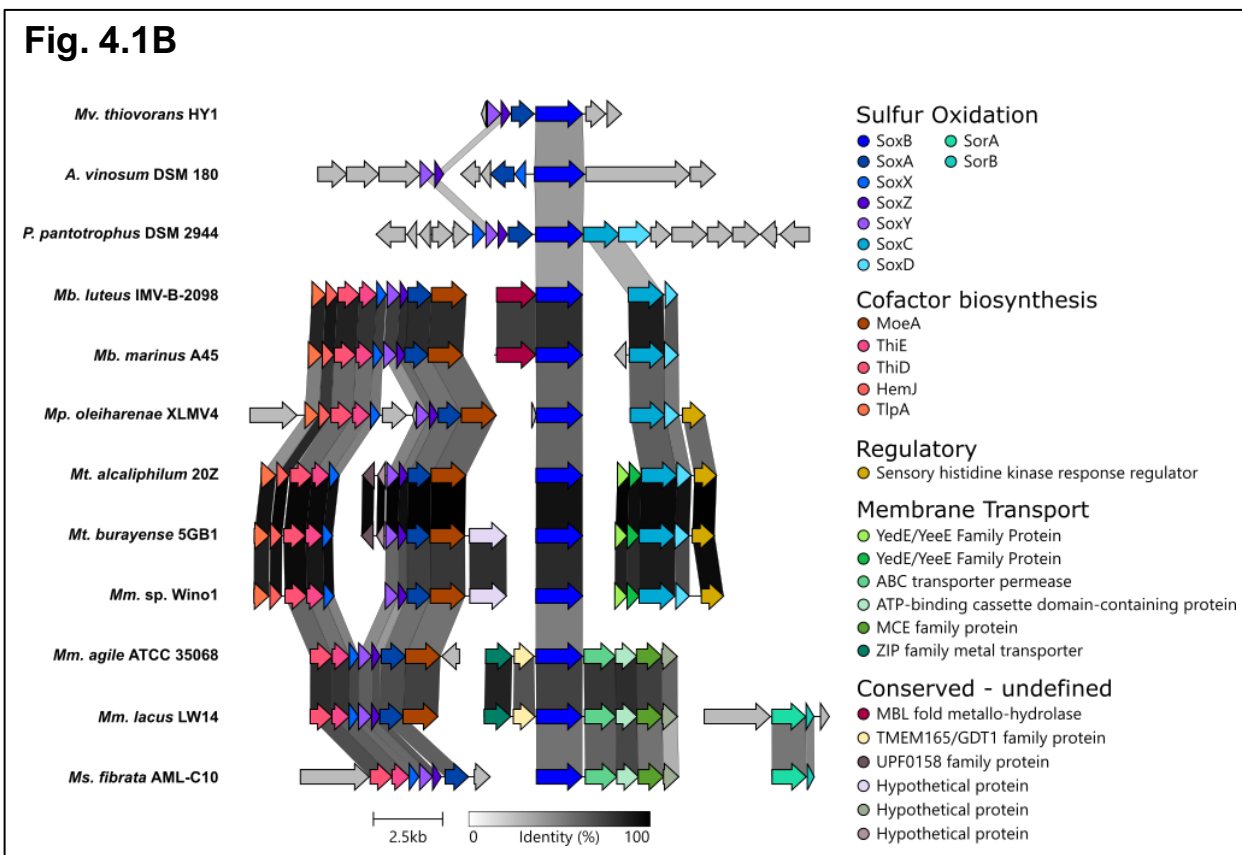
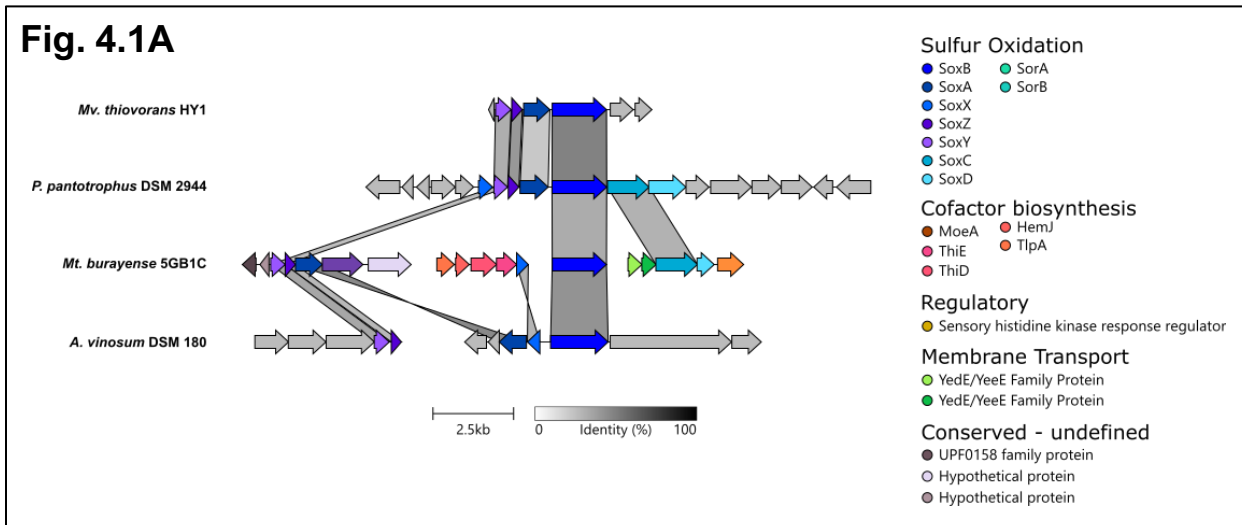


Figure 4.1. Organization of TOMES and co-localized genes in select *Methylococcales* strains. **A)** Visualization of BLASTp results of *P. pantotrophus* 2944 and *A. vinosum* DSM 180 TOMES protein sequences to respective homologs of *Mt. buryatense* 5GB1C using the clinker bioinformatic tool¹⁷⁸. *Mv. thiovorans* HY1 is included as reference MOB sulfur/methane mixotroph. **B)** TOMES components and organization among select *Methylococcales* species, identified via BLASTp alignment using *Mt. buryatense* TOMES as query and visualized via clinker. See Table 3 for description of predicted functions of conserved genes. Genus abbreviations: *Mb.*, *Methylobacter*; *Mp.*, *Methylicorpusculum*; *Mt.*, *Methylotuvimicrobium*; *Mm.*, *Methylomicrobium*; *Ms.*, *Methylosarcina*.

Fig. 4.2.

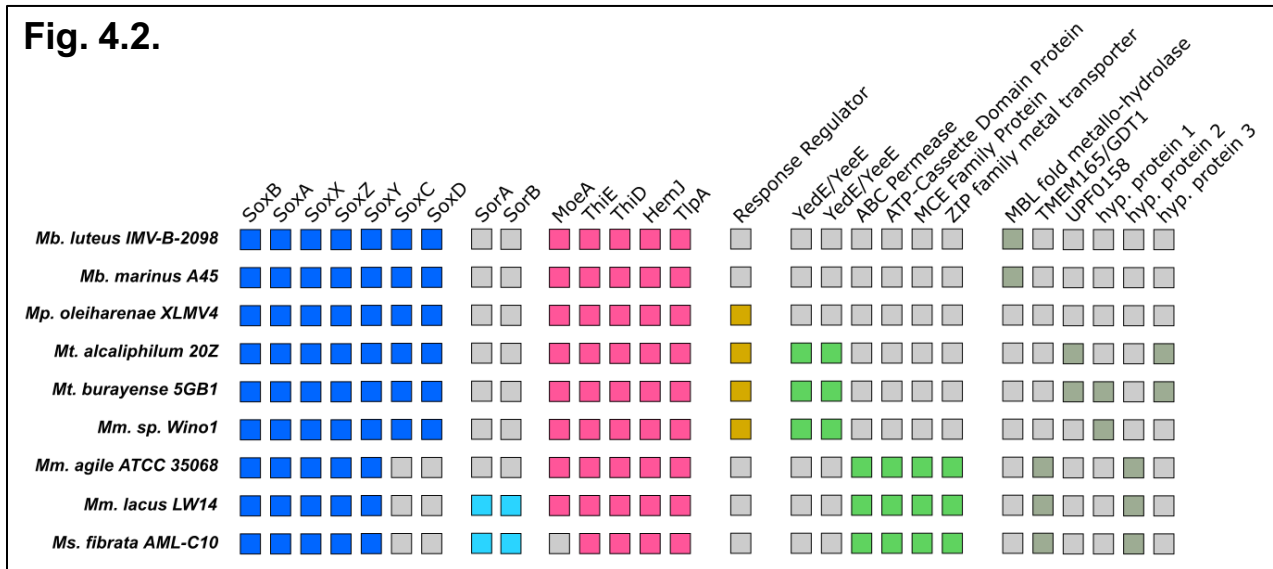


Figure 4.2. Presence/Absence matrix of TOMES and associated genes from soxB-possessing *Methylococcales*, as determined by BLASTp analysis with *Mt. buryatense* 5GB1C TOMES query. Genes/proteins of interest included TOMES (SoxBXYZCD - blue), sulfite dehydrogenase (SorAB – light blue), cofactor biosynthesis enzymes (pink), histidine kinase-activated response regulator (yellow), assorted membrane-associated transporters (green), and proteins of unknown/hypothetical function (olive green). Gene product identity/function based on NCBI annotations, either by direct evidence or functional domain assignment via SPARCLE²⁰⁰.

Fig. 4.3A

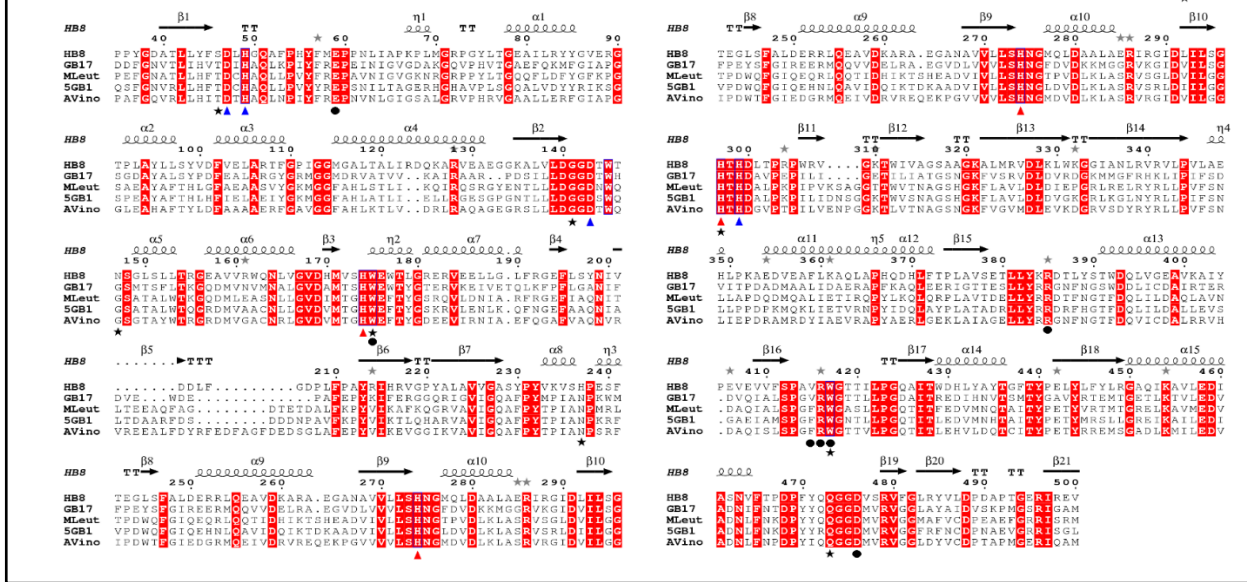


Fig. 4.3B

GB17	18	ITTRREF	19	IQVAMASSALVGSAGF	20	---GWRVAAQQALTDQQLDF	21	QDFGNVTL	22	IHWTD	23	IH	58								
AVino	1	MSLSRREF	2	VRLM---	3	ALGAGA	4	LEPVTGR	5	AAERPSDP	6	---VEIPAF	7	QVRLI	8	ITDTH	53				
MLeut	1	---MNR	2	HFLQCL	3	---ALLGL	4	SSRALPG	5	GRSA	6	-----GLY	7	LDPEFG	8	NATLL	9	HFTDCH	48		
5GB1	1	MNLSRREF	2	LQAL	3	---TITL	4	SSN---	5	CSTQRR	6	FGDFD	7	IEGLYS	8	QSFGNVRL	9	HFTDCH	53		
GB17	59	AQLK	60	PIYFREPE	61	INIGVGD	62	KAGQVPHV	63	TGAE	64	QKMF	65	GIAPGSD	66	AYALSY	67	PDFE	68	ALARYG	119
AVino	54	AQLNP	55	IYREPNVNL	56	IGSALGR	57	VPVHVA	58	ALLLFG	59	IAPGL	60	EAHAFTY	61	LDFAAA	62	AEERF	63	---	114
MLeut	49	AQLP	50	PVYFREPA	51	VMIGVGN	52	RGRFPYL	53	TGQF	54	LDYF	55	QKPSA	56	EAYATHL	57	FGA	58	EAASYG	109
5GB1	54	AQLP	55	VYREPNL	56	TAGERH	57	GHAVPL	58	LSQALVD	59	YRIK	60	SGSPEA	61	YAFHL	62	HEIAE	63	IYG	114
GB17	120	RGGMDR	121	VATVKA	122	IRAA	123	---PDS	124	ILLDGG	125	TWIG	126	MS	127	SFLTK	128	QDMVNV	129	NMLG	178
AVino	115	AVGG	116	FAHLK	117	TVDR	118	LRQA	119	QEGERS	120	LLDGG	121	TWQSG	122	TATW	123	GRDMV	124	AGN	175
MLeut	110	KMG	111	FHLSTL	112	IKIQ	113	RSRQY	114	ENTLL	115	DDGG	116	NQGS	117	ATALW	118	KQDML	119	EA	170
5GB1	115	KMG	116	FHLATL	117	IELLR	118	GES	119	SPNTLL	120	DDGG	121	SWG	122	SATALW	123	QGRDM	124	VACNL	175
GB17	179	HWE	180	TYGTRV	181	KEIV	182	ETQL	183	RFPFL	184	GANT	185	FOVE	186	---WDE	187	-----PA	188	FEPY	223
AVino	176	HWE	177	TYG	178	DEYIR	179	RIA	180	---EFG	181	SA	182	VAQNV	183	VRVEE	184	ALFD	185	YFED	235
MLeut	171	HWE	172	TYG	173	SRQV	174	LDN	175	IA	176	---BFR	177	GAQ	178	ITL	179	TEA	180	QAF	222
5GB1	176	HWE	177	TYG	178	SKRV	179	LDN	180	IK	181	---QNG	182	EAQ	183	IAL	184	DAAR	185	FDS	227
GB17	224	RGG	225	QIGV	226	IQGAF	227	PYMP	228	IANP	229	RM	230	PF	231	FEYS	232	FG	233	IREER	283
AVino	236	VGG	237	IKVAV	238	IQGAF	239	PYTP	240	IANP	241	SR	242	IPDW	243	FG	244	IEGR	245	ME	286
MLeut	223	F	224	KQGR	225	VAV	226	IQGAF	227	PYTP	228	IANP	229	SR	230	IPDW	231	FG	232	IEGR	283
5GB1	228	L	229	QAR	230	VAV	231	IQGAF	232	PYTP	233	IANP	234	SR	235	IPDW	236	FG	237	IEGR	288
GB17	284	D	285	V	286	K	287	M	288	G	289	M	290	G	291	G	292	293	294	295	340
AVino	297	V	298	D	299	L	300	K	301	L	302	A	303	S	304	R	305	V	306	307	357
MLeut	284	P	285	W	286	D	287	L	288	K	289	L	290	A	291	S	292	R	293	294	344
5GB1	289	V	290	D	291	L	292	K	293	L	294	A	295	S	296	R	297	L	298	299	349
GB17	341	M	342	M	343	M	344	F	345	R	346	H	347	K	348	L	349	350	351	352	401
AVino	358	V	359	S	360	D	361	V	362	R	363	R	364	L	365	L	366	367	368	369	418
MLeut	345	L	346	R	347	L	348	R	349	L	350	L	351	P	352	V	353	354	355	356	410
5GB1	350	L	351	K	352	L	353	N	354	L	355	L	356	P	357	P	358	359	360	361	410
GB17	402	I	403	C	404	D	405	A	406	L	407	I	408	R	409	T	410	411	412	413	462
AVino	419	I	420	C	421	A	422	L	423	R	424	V	425	H	426	D	427	428	429	430	479
MLeut	406	I	407	L	408	D	409	A	410	V	411	N	412	D	413	A	414	415	416	417	469
5GB1	411	I	412	L	413	D	414	L	415	E	416	V	417	S	418	G	419	420	421	422	471
GB17	463	E	464	D	465	V	466	A	467	D	468	N	469	I	470	F	471	472	473	474	523
AVino	480	E	481	D	482	V	483	A	484	D	485	N	486	I	487	F	488	489	490	491	539
MLeut	467	E	468	D	469	V	470	A	471	D	472	N	473	F	474	K	475	476	477	478	526
5GB1	472	E	473	D	474	A	475	D	476	N	477	F	478	K	479	P	480	481	482	483	531
GB17	524	G	525	W	526	A	527	S	528	V	529	N	530	E	531	G	532	533	534	535	594
AVino	540	G	541	W	542	A	543	S	544	V	545	N	546	E	547	G	548	549	550	551	594
MLeut	527	G	528	W	529	A	530	S	531	V	532	N	533	E	534	G	535	536	537	538	594
5GB1	532	G	533	W	534	A	535	S	536	V	537	N	538	E	539	G	540	541	542	543	594

Figure 4.3. Amino acid sequence alignments of SoxB enzymes from known thiosulfate-oxidizing bacteria and two example methanotrophs. **A)** ESPript 3.0 output of SoxB Clustal Omega amino acid sequence alignment comparing SoxB enzyme sequence between *T. thermophilus* HB8, *P. pantotrophus* GB17, *Mb. luteus*, *Mt. buryatense* 5GB1C, and *A. vinosum*. Strains were selected to include two example *Methylococcales* species and three canonical SOB species. *T. thermophilus* HB8 Protein Database file included to outline secondary structure features. Residues with exact identity between all sequences are highlighted in red; blue triangles indicate ligands of metal site A; red triangles indicate ligands of metal site B; black star indicates second sphere metal ligands; black circles indicate residues involved in substrate coordination. **B)** BLOSUM62 matrix scoring of SoxB protein alignment between *P. pantotrophus* GB17, *A. vinosum*, *Mb. luteus*, and *Mt. buryatense* 5GB1C; proportion of positive scoring residues per the BLOSUM62 matrix are 83%, 86%, 92%, 91%, respectively.

Fig. 4.4

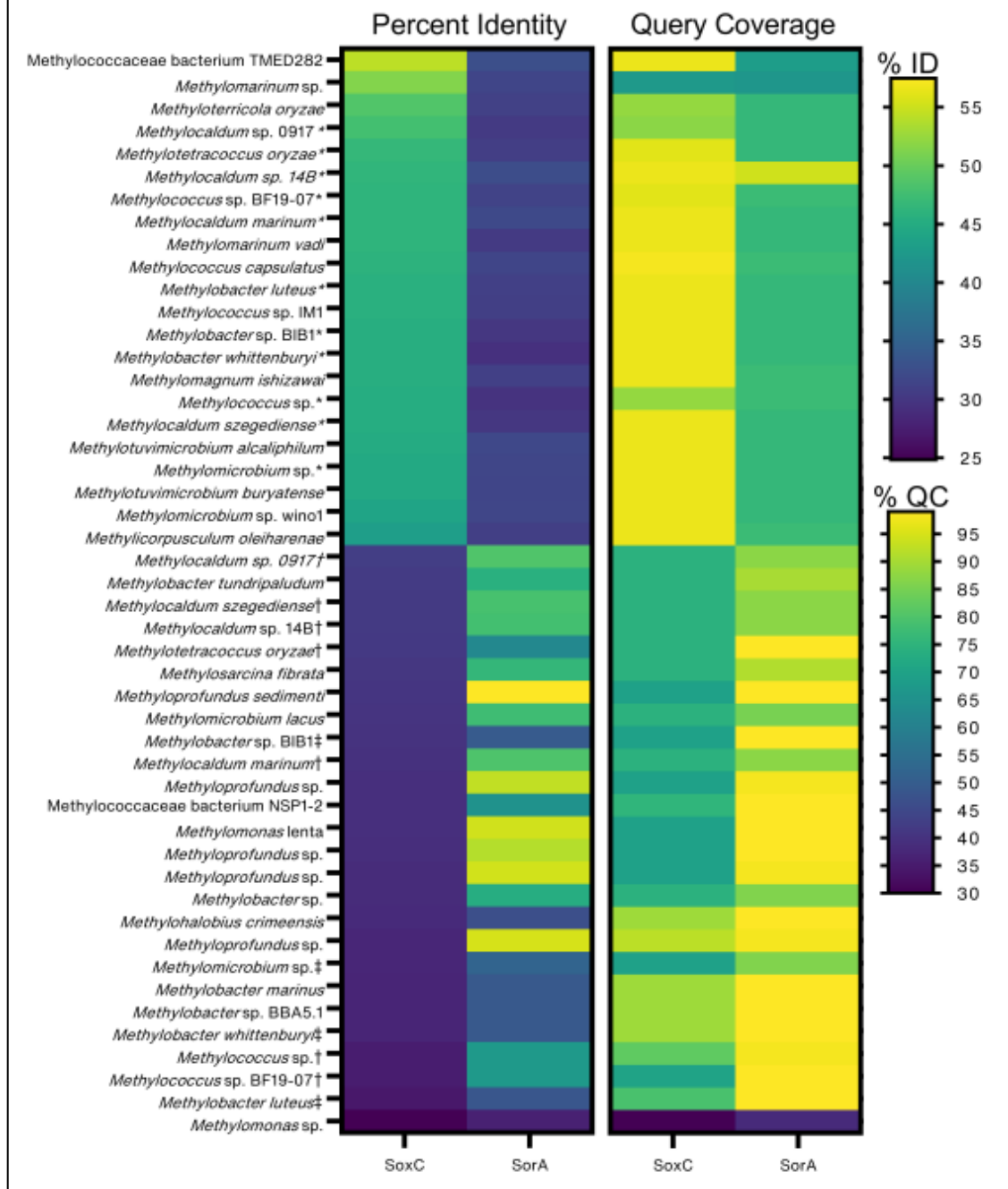


Figure 4.4. BLASTp results heatmap of *Methylococcales* sulfite dehydrogenase amino acid sequences using *Starkeya novella* DSM 506 SoxC and SorA protein sequence queries^{176,177,180}. Percent ID values of $\geq 40\%$ query, coverages $\geq 85\%$, and E-values $<1E-6$ were considered significant. SoxC-like, SorA-like, and non-similar sequences are denoted with *, †, and ‡, respectively. Note that some species possess multiple homologs.

Fig. 4.5

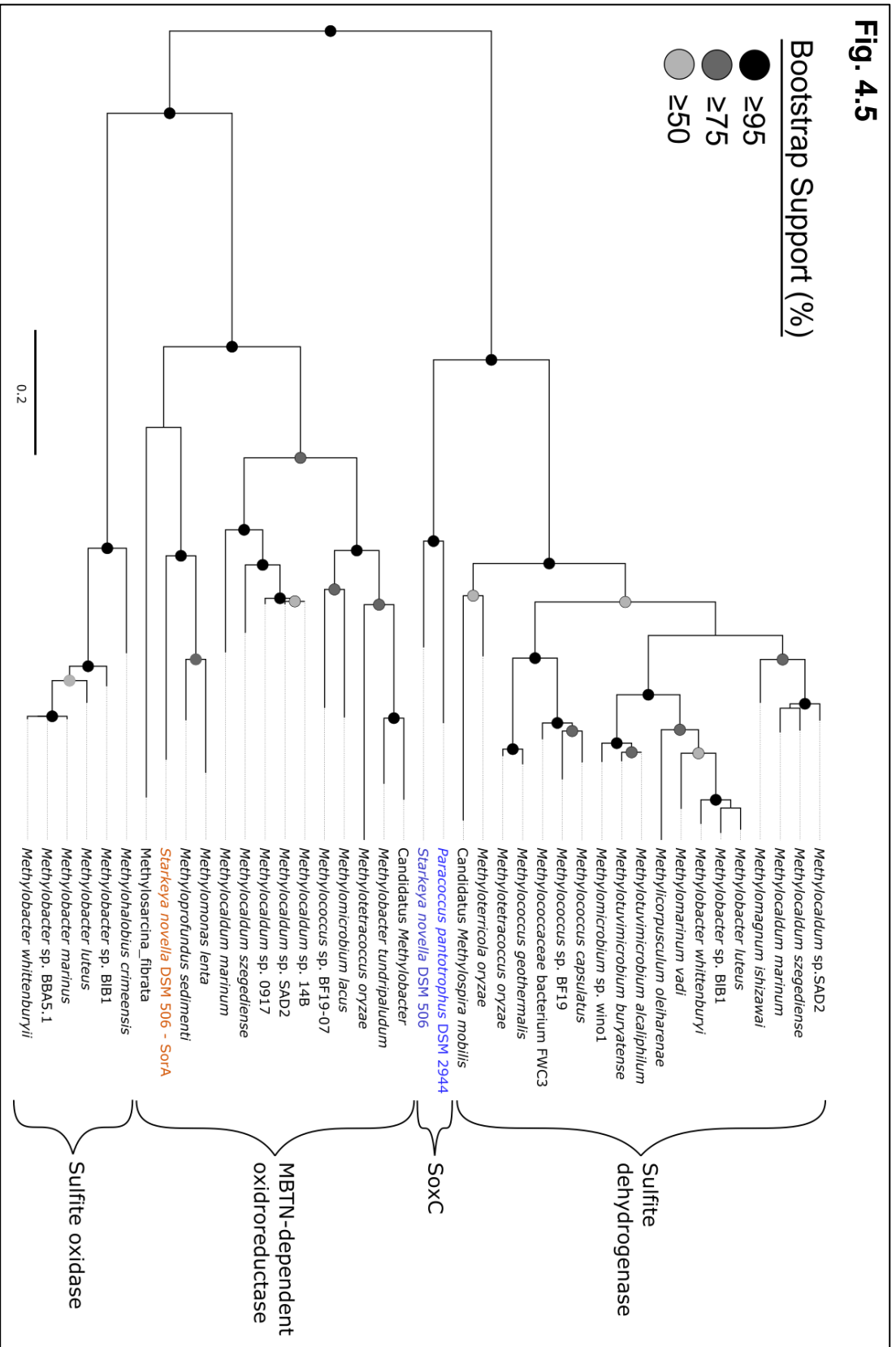


Figure 4.5. Neighbor-joining phylogenetic tree of *Methylococcales* SDH protein sequences identified through *S. novella* SorA/SoxC BLASTp query. The phylogenetic tree was constructed using the phylogeny.fr pipeline provided through University of Montpellier^{180,181}. Distinct clusters are denoted with bracket labels; note that sulfite dehydrogenase and SoxC labels represent a shared cluster. Nodes with shaded circles to the corresponding bootstrap values; nodes with bootstrap values below 50% are unlabeled.

Fig. 4.6

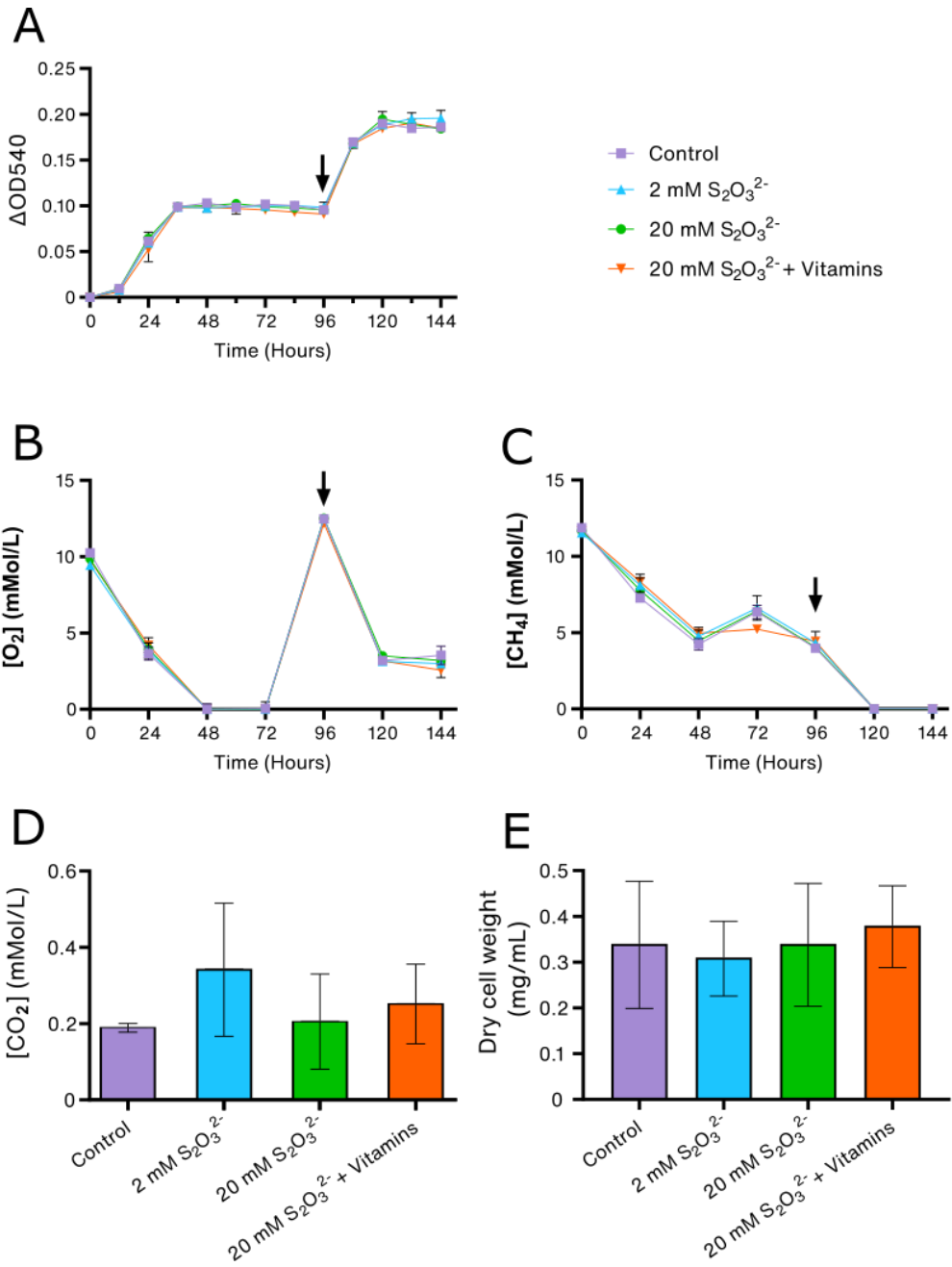


Figure 4.6. *Methylovimicrobium buryatense* 5GB1C growth and thiosulfate oxidation assay. A) Growth as monitored by optical density measured at 540 nm. B, C) Headspace gas concentration as a function of time for oxygen and methane, respectively, determined by gas chromatography. D) Final carbon dioxide concentration in headspace, taken at 144 h. E) Final dry cell weight after 144 h. All experimental were conducted in triplicate plus one cell-free control; error bars represent one standard deviation. Cultures were incubated at 30°C, 130 rotations per minute. Initial [O₂]:[CH₄] ratio was 1:1.2, which was then adjusted to 3:1 upon addition of 12.4 mmol/L of pure oxygen at the 96-h mark, as denoted by the black arrows.

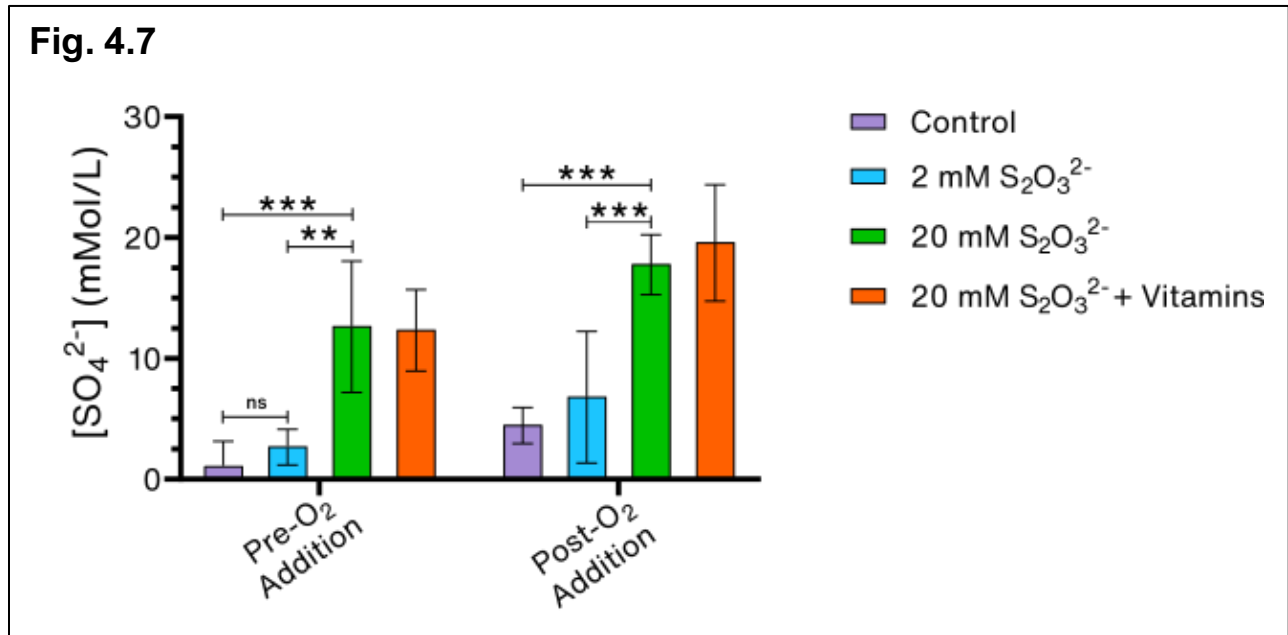
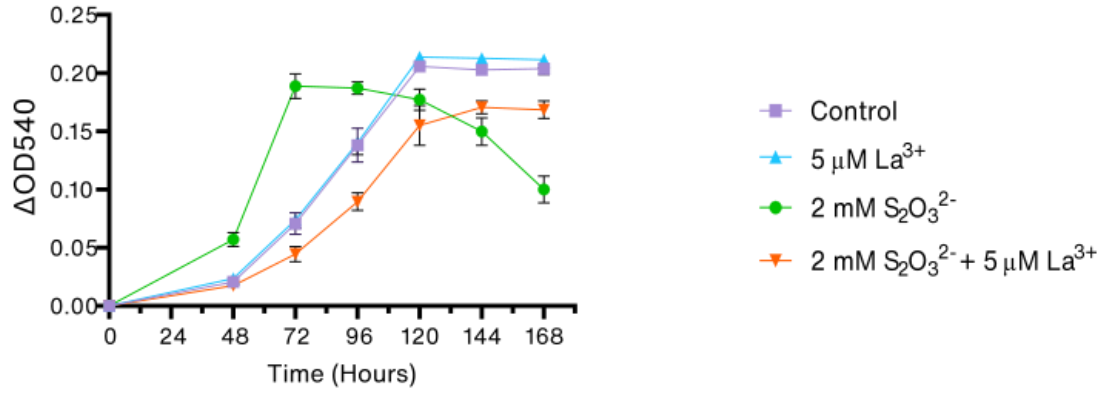


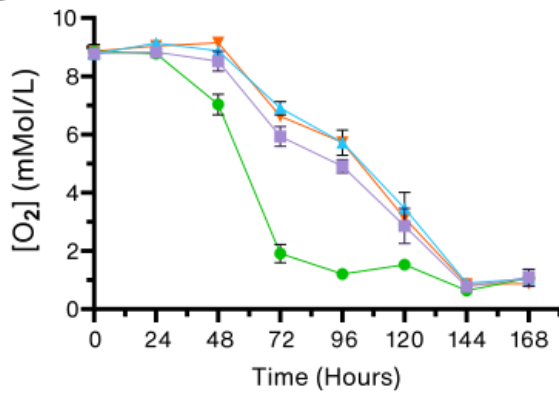
Figure 4.7. *Methylotheobacterium buryatense* 5GB1C sulphate production during growth in presence of thiosulfate. Concentration of sulphate in spent media at 96 h (Pre-O₂) and 144 h (Post-O₂), as determined by barium chloride precipitation with absorbance measured at 420 nm. Experiments were performed in triplicates plus one cell-free control; error bars represent one standard deviation. Cultures were incubated at 30°C, 130 rotations per minute. Asterisks represent P-value scores as determined by Student's T-test; double and triple asterisks indicate P-values of < 0.05 and < 0.005, respectively.

Fig. 4.8

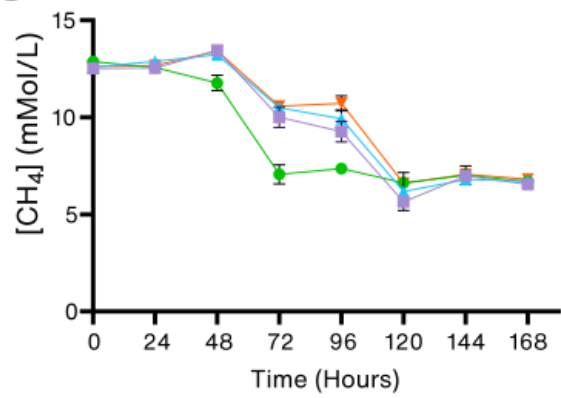
A



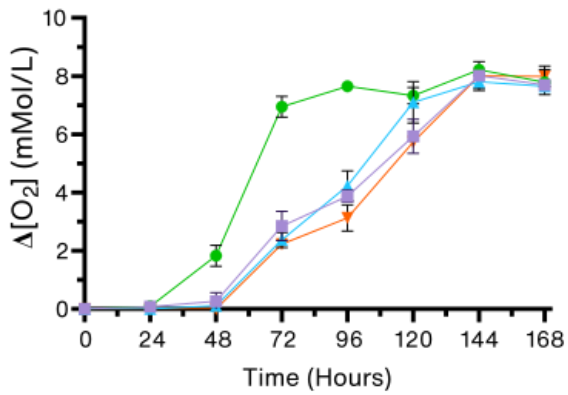
B



C



D



E

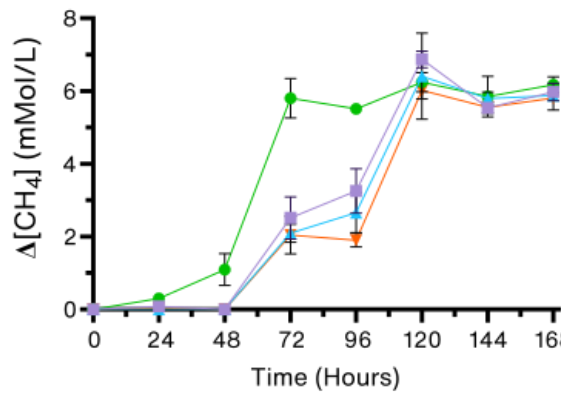
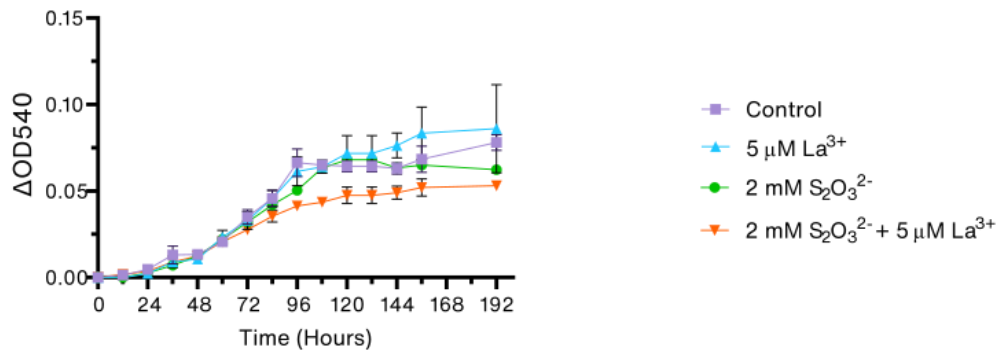


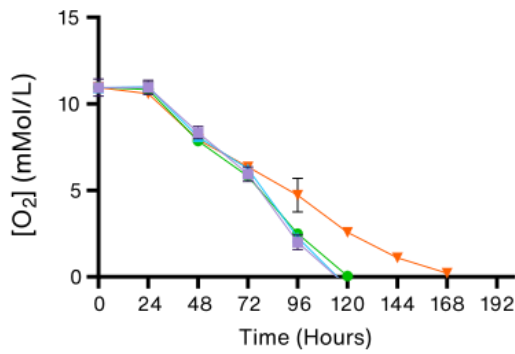
Figure 4.8. *Methylicorpusculum oleiharenae* XLMV4 thiosulfate oxidation assay with or without added lanthanum. A) Change in optical density measured at 540 nm utilizing 0.5 mL of culture, every 12 hours. B) Headspace oxygen concentration over time, measured every 24 hours. C) Headspace methane molar concentration over time, measured every 24 hours. D) & E) Change in headspace molar concentrations of oxygen and methane respectively. All experimental groups included 3 biological replicates plus one cell-free control, error bars represent one standard deviation. Cultures were incubated at 21°C, 100 rotations per minute.

Fig. 4.9

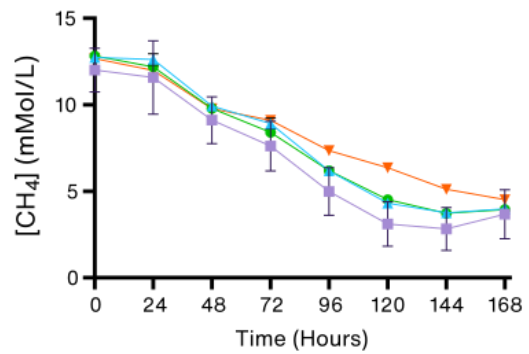
A



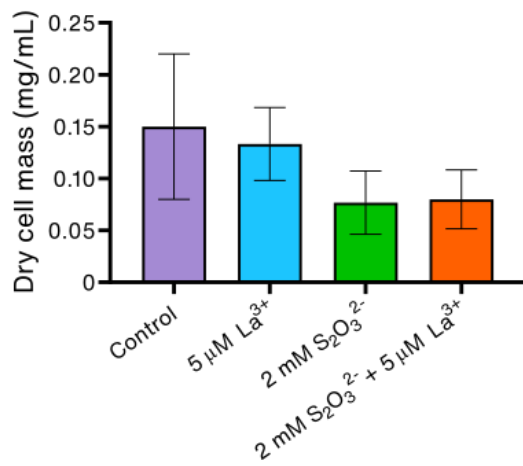
B



C



D



E

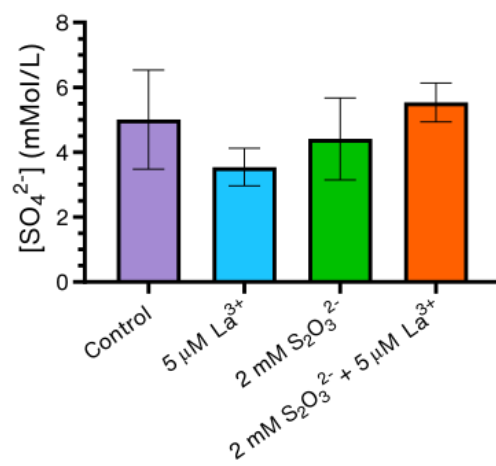


Figure 4.9. Replication experiment of *Methylicorpusculum oleiharenae* XLMV4 thiosulfate oxidation assay with or without added lanthanum. A) Change in optical density measured at 540 nm utilizing 0.1 mL of culture, every 12 hours. B) Headspace oxygen concentration over time, measured every 24 hours. C) Headspace methane concentration over time, measured every 24 hours. D) Final dry cell weight as of 144 hours, samples dried for 120 hours at 80°C. E) Concentration of sulphate in spent media at 240 hours, as determined by barium chloride precipitation with absorbance measured at 420 nm. All experimental groups included 3 biological replicates plus one cell-free control, error bars represent one standard deviation. Cultures were incubated at 21°C, 100 rotations per minute.

Fig. 4.10

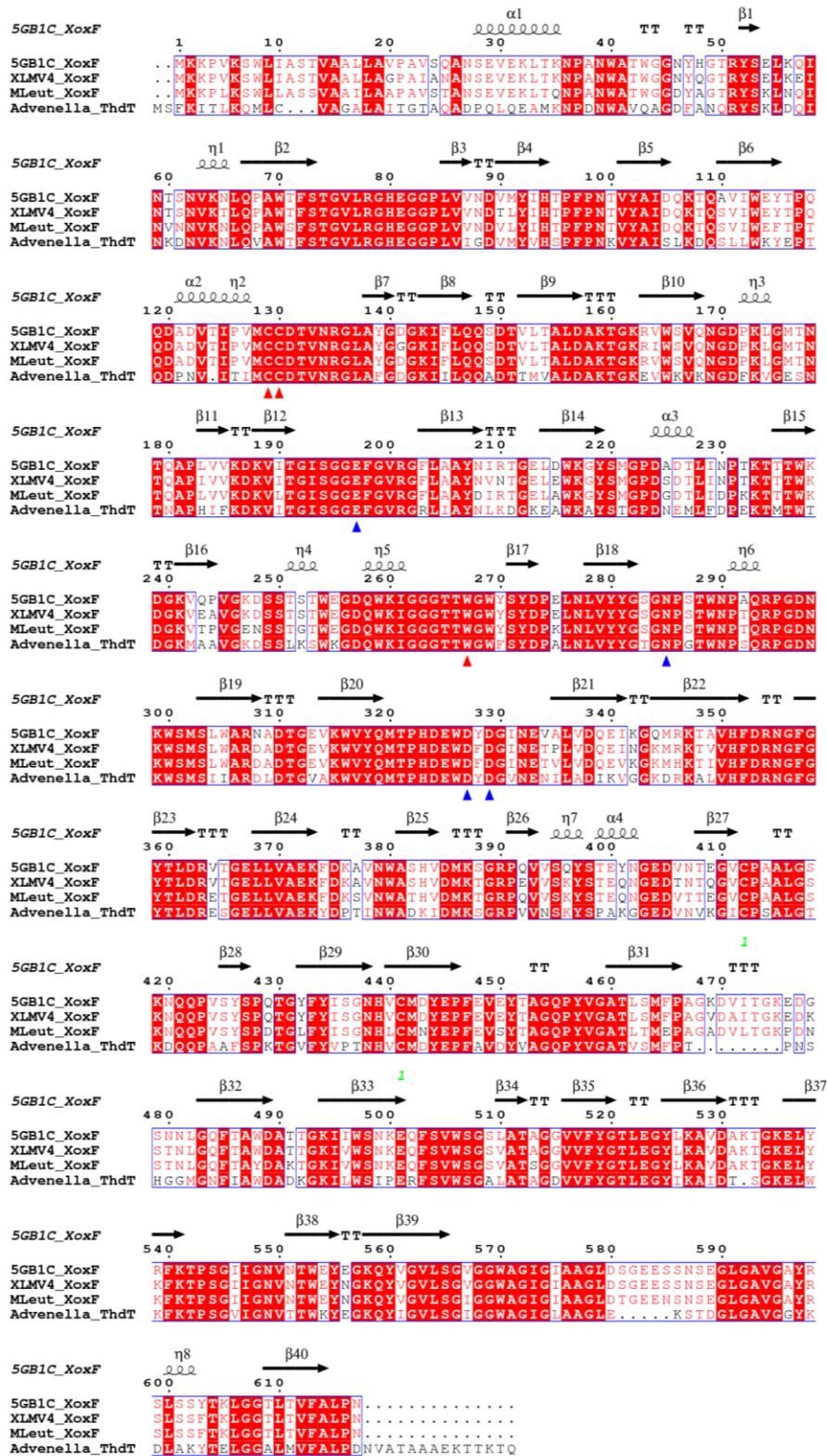


Figure 4.10. Protein alignment of select *Methylococcales* XoxF MDH and *Advenella kashmirensis* ThdT thiol dehydrotransferase sequences. Coloring based on ESPript 3.0 Equivalent% similarity scoring matrix; red blocks indicate identical conservation between aligned sequences, whereas red letters indicate physiochemically similar amino acid residues¹⁷³. Red arrows denote PQQ-coordinating ligands; blue arrows denote lanthanum-coordinating ligands. Black horizontal arrows above sequence denoted with β indicate β -sheet placement, with bolded T symbols indicating turns between β -strands. Loop symbols designated with α indicate presence of α -helices. Alignment sourced from NCBI BLASTp multiple sequence alignment viewer, using *A. kashmirensis* ThdT to query SoxB-possessing *Methylococcales* strains. *Mt. buryatense* 5GB1C XoxF secondary structure features included above aligned sequences, as determined from crystal structure (PDB Entry: 6DAM)¹⁸⁵. Strains/proteins used: XoxF MDH protein sequences of *Mt. buryatense* 5GB1C (WP_017842117.1), *Mp. oleiharenae* XLMV4 (WP_159658741.1), and *Mb. luteus* (WP_027156973.1); ThdT thiol dehydrotransferase protein sequence from *A. kashmirensis* (WP_014751259.1)¹⁸².

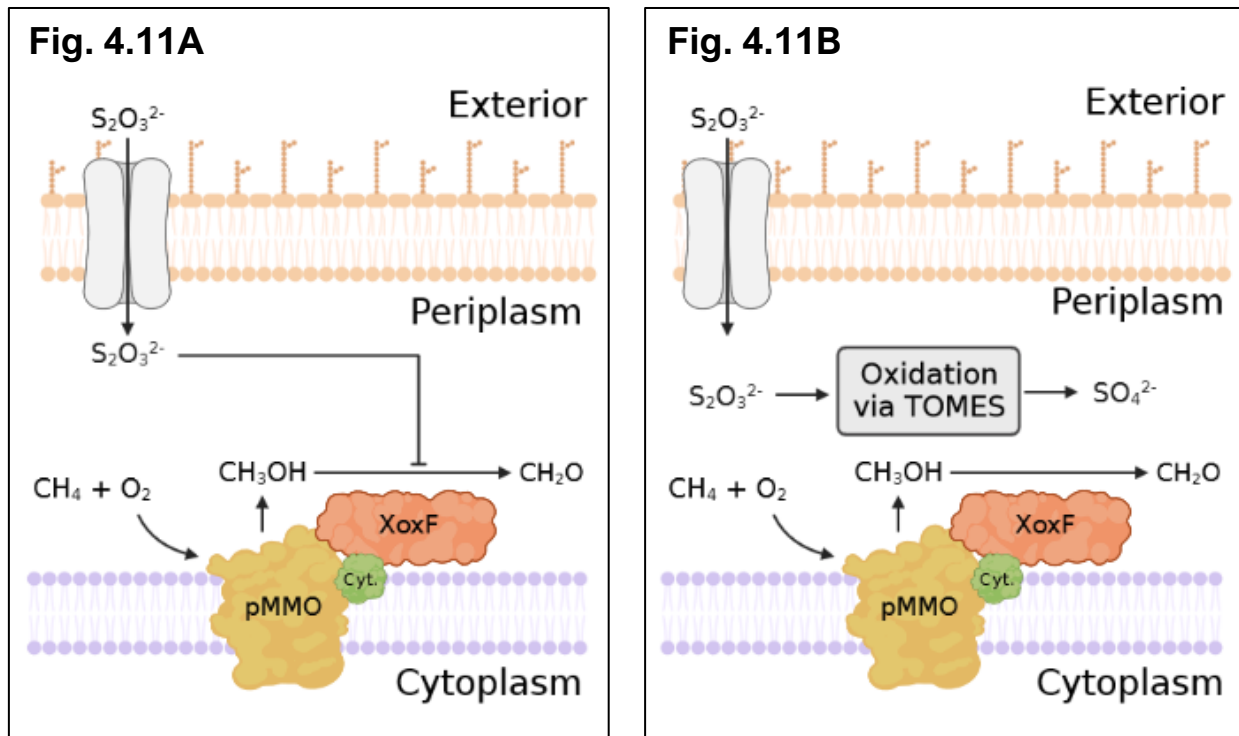


Figure 4.11. Proposed model of lanthanum-dependent growth inhibition by thiosulfate in *Methylococcales*. **A)** Hypothetical interaction of XoxF and thiosulfate as a competitive inhibitor of methanol oxidation by lanthanide-dependent MDH enzymes based on physiological assays and high degree of homology between XoxF and thiol dehydrotransferase (ThdT) of *A. kashmirensis*¹⁸². **B)** Alleviation of growth inhibition through oxidation of thiosulfate by TOMES allowing for unimpeded function of XoxF MDH in conversion of methanol to formaldehyde. pMMO – particulate methane monooxygenase; XoxF – lanthanum-dependent methanol dehydrogenase; Cyt. – accessory cytochrome; TOMES – thiosulfate-oxidizing multienzyme system.

4.8. Tables

Experiment/Groups	Depletion Rate (nMol L ⁻¹ hr ⁻¹)		Difference to Control (%)	
	[CH ₄]	[O ₂]	[CH ₄]	[O ₂]
5GB1C				
Control	159.0	213.4	-	-
2 mM S ₂ O ₃ ²⁻	141.4	196.7	- 11.0%	- 7.8%
20 mM S ₂ O ₃ ²⁻	150.4	205.2	- 5.4%	- 3.9%
20 mM S ₂ O ₃ ²⁻ + Vitamins	139.1	203.4	- 12.5%	- 4.7%
XLMV4 No. 1				
Control	57.3	49.4	-	-
5 μM La ³⁺	53.4	44.1	- 6.8%	- 10.7%
2 mM S ₂ O ₃ ²⁻	80.6	96.5	+ 40.8%	+ 95.4%
5 μM La ³⁺ + 2 mM S ₂ O ₃ ²⁻	38.6	55.6	- 32.6%	+ 12.5%
XLMV4 No. 2				
Control	73.1	93.2	-	-
5 μM La ³⁺	70.2	96.1	- 4.0%	+ 3.1%
2 mM S ₂ O ₃ ²⁻	69.2	90.9	- 5.4%	- 2.4%
5 μM La ³⁺ + 2 mM S ₂ O ₃ ²⁻	52.6	69.7	- 28.1%	- 25.2%

Table 4.1. Summary table on headspace gas depletion rates of *Mt. buryatense* 5GB1C and *Mc. oleiharenae* XLMV4. Rates calculated based on logarithmic phase consumption, with differences reflecting changes to relative control group. Figure references for data presented are as follows: 5GB1C, Fig. 4.6; XLMV4 No. 1, Fig. 4.8; XLMV4 No. 2, Fig. 4.9.

Species	Thiosulfate-oxidizing multi-enzyme system			
	SoxB	SoxYZ	SDH ¹	SoxAX
<i>Methylovimicrobium</i>				
<i>Mt. alcaliphilum</i> 20Z	WP_014149815	WP_014147805 WP_014147804	WP_014147936.1 WP_046061037	WP_014147803 WP_014147519
<i>Mt. buryatense</i> 5GB1C	WP_017842264	WP_017839849 WP_017839850	WP_017839024 WP_017839025	WP_017839851 WP_017842492
<i>Methylomicrobium</i>				
<i>Mm. agile</i> ATCC 35068	WP_005373449	WP_031431641 WP_005371943		WP_084675377 WP_031431642
<i>Mm. sp.</i> Wino1	WP_125218314	WP_125219131 WP_125219130	WP_164515662.1 WP_125220778	WP_125219129 WP_125220533
<i>Mm. lacus</i> LW14	WP_024300273	WP_024297054 WP_024297053	WP_024299774 WP_024299775.1	WP_024297052 WP_024297055
<i>Methylicorpusculum</i>				
<i>Mc. oleiharenae</i> XLMV4	WP_159652427.1	WP_159655193.1 WP_159655191.1	WP_159654519.1 WP_159654645.1	WP_159655189.1 WP_159655199.1
<i>Methylobacter</i>				
<i>Mb. marinus</i> A45	WP_020157973	WP_027158561 WP_027158562	WP_020157237.1 WP_156830665.1	WP_156830654 WP_020159976.1
<i>Mb. luteus</i> IMV-B-3098	WP_027159286	WP_027158561 WP_027158562	WP_027158229 WP_156830665.1	WP_081679097 WP_027158560.1
<i>Methylosarcina</i>				
<i>Ms. fibrata</i> AML-C10	WP_020562900	WP_020565864 WP_020565863	WP_020561950 WP_033411968.1	WP_020565862 WP_026223888

Table 4.2. NCBI protein accession ID numbers for TOMES-possessing *Methylococcales* strains reviewed in this manuscript. Strains of interest were identified through blastp alignment of sox genes from *Methylovium buriatense* 5GB1, which were in turn identified through blastp alignment of homologous genes of *Paracoccus pantotrophus* GB17 and *Allochromatium vinosum*. Only those strains with available genome sequences and with a confirmed *soxB* gene were included. 1. SDH: sulfite dehydrogenase; category inclusive of SorAB and SoxCD-type SDHs, see Figs. 4 and 5 for strain-specific presence/absence.

Species	Associated biosynthetic proteins			
	ThiDE	HemJ	TlpA-like thioredoxin	MoeA
<i>Methylovimicrobium</i>				
<i>Mt. alcaliphilum</i> 20Z	WP_014147521.1 WP_014147520.1	WP_014147522.1	WP_014147523.1	WP_014147802.1
<i>Mt. buryatense</i> 5G(B1)	WP_017842494.1 WP_017842493.1	WP_017842495.1	WP_017842496.1	WP_017839852.1
<i>Methylomicrobium</i>				
<i>Mm. agile</i> ATCC 35068	WP_031431644.1 WP_031431643.1	-	-	WP_005371939.1
<i>Mm. sp.</i> Wino1				
<i>Mm. lacus</i> LW14	WP_024297057.1 WP_024297056.1	WP_027158557.1	WP_027158556.1	WP_024297051.1
<i>Methylicorpusculum</i>				
<i>Mc. oleiharenae</i> XLMV4				
<i>Methylobacter</i>				
<i>Mb. marinus</i> A45	WP_020159978.1 WP_020159977.1	WP_020159979.1	WP_020159980.1	WP_020159972.1
<i>Mb. luteus</i> IMV-B-3098	WP_027158558.1 WP_036243093.1			WP_027158564.1
<i>Methylosarcina</i>				
<i>Ms. fibrata</i> AML-C10	WP_020565867.1 WP_020565866.1			

Table 4.3. NCBI protein accession ID numbers of proteins co-conserved with TOMES in select *Methylococcales* strains. Strains of interest were identified through blastp alignment of *sox* amino acid sequences from *Methylovimicrobium buryatense* 5GB1, which were in turn identified through blastp alignment of homologous genes of *Paracoccus pantotrophus* GB17 and *Allochromatium vinosum*. Only those strains with available genome sequences and with a confirmed *soxB* gene were included.

Scientific Name	Reference Genome Identifiers		
	Assembly	RefSeq	GenBank
<u><i>Methylococcales</i></u>			
<i>Methylovimicrobium alcaliphilum</i> 20Z	ASM96853v1	GCF_000968535.2	GCA_000968535.1
<i>Methylovimicrobium buryatense</i> 5GB1C	ASM593109v1	GCF_005931095.1	GCA_005931095.1
<i>Methylomicrobium agile</i> ATCC 35068	ASM73385v1	GCF_000733855.1	GCA_000733855.1
<i>Methylomicrobium</i> sp. Wino1	ASM393275v1	GCF_003932755.1	GCA_003932755.1
<i>Methylomicrobium lacus</i> LW14	ASM52709v1	GCF_000527095.1	GCA_000527095.1
<i>Methylomicrobium oleiharenae</i> XLMV4	ASM982892v2	GCF_009828925.2	GCA_009828925.2
<i>Methylobacter marinus</i> A45	ASM38385v1	GCF_000383855.1	GCA_000383855.1
<i>Methylobacter luteus</i> IMV-B-3098	ASM42762v1	GCF_000427625.1	GCA_000427625.1
<i>Methylosarcina fibrata</i> AML-C10	ASM37286v1	GCF_000372865.1	GCA_000372865.1
<u>Model sulfur oxidizing bacteria</u>			
<i>Allochromatium vinosum</i> DSM 180	ASM2548v1	GCF_000025485.1	GCA_000025485.1
<i>Paracoccus pantotrophus</i> DSM 2944	ASM882418v1	GCF_008824185.1	GCA_008824185.1
<i>Thermus thermophilus</i> HB8	ASM9154v1	GCF_000091545.1	GCA_000091545.1
<i>Starkeya novella</i> DSM 506	ASM9292v1	GCF_000092925.1	GCA_000092925.1

Table 4.4. Reference genomes identifiers of *Methylococcales* and model SOB utilized in this research. Reference genome sequences were selected and retrieved from the NCBI nucleotide database¹⁷⁶.

5. Discussion

5.1 Characterization of TOMES genomic inventories of *Methylococcales* species

The presence of TOMES genes within methanotrophic genomes has raised the prospect of their potential catabolic function for MOB. Until recently, only a few examples of novel MOB isolates with accompanying whole-genome sequences had been reported to possess TOMES genetic inventories^{24,170}. Recent work on sulfur oxidation by the alpha-MOB *Methylovirgula thiovorans* HY1 expanded on the presence of TOMES within the *Methylococcales*, identifying 10 species across 6 genera with complete *sox* gene sets^{23,24,170}. Prior to the work of Gwak et al., 2022, strains of interest among the *Methylococcales* were determined by the presence of SoxB thiosulfohydrolase, given its central role in bacterial sulfur oxidation and as a proven phylogenetic molecular marker for proteobacterial sulfur oxidizers (Fig. 4.1, Fig. 4.3)^{188,201}. Despite the newly available presence/absence data of a variety of sulfur oxidizing genes in MOB, little else is known regarding the genomic organization and co-conserved genes/operons of TOMES in these organisms. Moreover, no sulfur-oxidation activity has been reported for any member of the *Methylococcales*. As such, the identification, characterization, and collation of putative sulfur oxidation genes is a critical first step in assessing the feasibility of sulfur oxidation in these bacteria. Moreover, even though the presence/absence of core TOMES genes has been described for *Methylococcales*, there are currently no published data illustrating the genomic organization, operonic conservation, or presence of co-conserved genes¹³⁵.

To begin addressing this knowledge gap, TOMES-possessing *Methylococcales* strains were identified and found to have conserved, discrete *sox* operons dispersed across their respective genomes (Fig. 4.2). Localization of *sox* genes consisted of separate, genomically distant operons, analogous to some SOB. For example, *Acidithiobacillus caldus* possesses six

distinct operons involved in sulfur oxidation, although these operons correspond to discrete segments of the overall sulfur oxidation pathway, for example the *hqr* and *sox* clusters²⁰². Similar system-specific genomic localization has also been observed within green sulfur bacteria (GSB), such as in *Chlorobaculum tepidum*, which possesses separate *sox*, APSR, and *hdr* operons²⁰³. Separation of TOMES genes has been observed in *Allochromatium vinosum*, with *soxYZ* encoded separately from the remaining genes, and *soxXA* and *soxB* encoded in divergent operons within the same locus¹²³. However, these observations contrast with the genomic organization of complete TOMES genomic inventories observed in alphaproteobacterial facultative SOB. Prominent examples include *S. novella* and *P. pantotrophus*, in which *sox* genes are localized within a single locus alongside regulatory and accessory components, while the core TOMES genes are encoded within a single operon^{126,168}. While the separation of the *Methylococcales* TOMES loci is not unprecedented, this organization is reminiscent of rDSR SOB as opposed to SoxCD-possessing species like *P. pantotrophus* and *Starkeya novella*^{195,204,205}.

During the initial *sox* protein alignment of *Mt. buryatense* 5BG1C to *Methylococcales*, the majority of TOMES genes identified displayed unique conservation patterns owing to well-described phylogenies which dismissed known orthologs¹⁸⁸. Recent work on alpha-MOB sulfur oxidation has also featured validated identities of *Methylococcales* TOMES genes through more sophisticated bioinformatic methods²³. However, there was ambiguity regarding SDH identities, as there were three variations within the NCBI annotations: “sulfite dehydrogenase,” “molybdopterin-dependent oxidoreductase,” and “sulfite oxidase.” These labels are interchangeable to a degree and could describe any SDH isoform, while specific labels including “sulfane dehydrogenase” are absent from the annotations. Aligning *Methylococcales* SDH subunit A protein sequences into a phylogeny illustrated that annotation classifications were reflected in distinct clusters (Fig. 4.1B). Sequences designated as “sulfite dehydrogenase” clustered with

SoxC, while “molybdopterin-dependent oxidoreductases” clustered with SorA. “Sulfite oxidases” formed a separate cluster more closely associated with the SorA group and predominantly comprised of *Methylobacter* SO sequences (Fig 3B). *Methylococcales* strains were shown to possess SDH subunit A homologs of significant similarity to either SoxC or SorA, but no single *Methylococcales* SDH simultaneously corresponds to both (as observed by the clear differentiation in functions in Fig. 4.1A). Indeed, genomes of strains like *Methylotetracoccus oryzae* and *Methylocaldum szegediense* encode genes for both SoxCD and SorAB-like SDHs, a trait shared by *S. novella* and other thiosulfate-oxidizing bacteria. SorAB-like enzymes are believed to be predominantly involved in sulfite detoxification, with a minor contribution towards energy conservation. These data indicate that the combination and differentiation of SorA/SoxC in *S. novella* may be a useful tool to distinguish SorAB versus SoxCD-type SDHs, but this would require further experimental validation beyond protein alignments to confirm functionality.

While the presence of SoxCD-like SDH across gamma-MOB genomes may be indicative of either a complete or vestigial TOMES, SorAB-like SDHs represent a more singular adaptation. Sulfite is disadvantageous for bacteria, as it exhibits toxicity due to its reactivity and is a poor electron donor relative to other RISCs. As a result, SorAB SDHs of the bacterial periplasm are regarded primarily as sulfite detoxification enzymes, although have also been shown to participate in the complete oxidation of more reduced sulfur compounds²⁰⁶. As MOB from both *Alphaproteobacteria* and *Gammaproteobacteria* also encode sulfide:quinone reductases (*sqr*), the involvement of SorAB is consistent with the notion that MOB are subject to selection pressure from toxic sulfur compounds, as are other bacteria which exist near anaerobic clines¹⁷¹.

The analysis of TOMES genes highlights a number of other peculiarities, such as the co-conserved genes predicted within the *sox* loci deviated from expectations when comparing genomic organization of the *Methylococcales* TOMES genes to validated SOB (Fig. 4.1A). These

genes are broadly grouped based on their putative function, as co-factor biosynthesis, response regulation, membrane transport, and hypothetical/unknown function. Intriguingly, in strains which possess the complete TOMES genomic inventory, i.e., *soxBXYZCD*, a subset of these genes is universally conserved within discrete *sox* operons (Fig. 4.1B).

Molybdopterin molybdotransferase (*MoeA*) is one such enzyme universally co-conserved with TOMES in gamma-MOB, responsible for the final biosynthetic step of molybdopterin production through introduction of a molybdate ion to the pterin cofactor precursor. The molybdopterin co-factor (MoCo) is an integral component of various types of enzymes, including nitrogenases, nitrate reductases, formate dehydrogenases, and sulfite oxidases (SO)^{167,207-209}. In the context of the TOMES system, the MoCo is utilized by the SoxC active site to oxidize SoxY-S-sulfane to SoxY-S-sulfone, yielding six electrons per sulfane group oxidized¹¹⁴. The inclusion of the *moeA* on the 3'-end of the *soxYZA* transcriptional unit is a curious placement, as it could be reasonably assumed that a gene encoding for the final step of MoCo synthesis would be associated with the *soxCD* operon. Complex regulation of sulfur oxidizing systems separated between multiple operons has been observed in other sulfur oxidizers including *A. vinosum* and *Acidithiobacillus* spp., however the inclusion of dedicated cofactor biosynthesis genes has not been previously observed. In the context of methanotrophs, the requirement for an additional copy of *moeA* may be related to balancing pterin flux. Pterin is also a precursor for tungstopterin required for tungsten-dependent formate dehydrogenases utilized by many gamma- and alpha-MOB, including *Mt. buryatense* 5GB1^{81,96,170}. MoCo is also required for nitrogenase clusters, with many *Methylococcales* strains possessing the requisite *nif* genes capable of diazotrophic growth^{210,211}. Taking these factors in combination, it can be hypothesized that the *Methylococcales* *moeA/sox* association could be necessary to ensure adequate MoCo production when precursor pools are subject to competition by parallel biosynthetic pathways.

Homologs of *thiDE* thiamine biosynthesis genes, predicted as 4-amino-5-hydroxymethyl-2-methylpyrimidine (HMP) kinase and thiamine phosphate synthase (TPS), were found universally conserved upstream of *soxX* in the strains surveyed. HMP kinase catalyzes the two-stage phosphorylation of HMP to HMP-pyrophosphate (HMP-PP), which is ligated to 4-methyl-5-thiazoleethanol phosphate (THZ-P) by TPS, yielding thiamine monophosphate (TMP)^{212,213}. TMP must then be converted into the active co-factor thiamine pyrophosphate (TPP), commonly known as vitamin B1. TPP is an essential cofactor for enzymes participating in carbohydrate metabolic pathways, some notable examples being pyruvate dehydrogenase (PDH), 2-oxoglutarate dehydrogenase, branched-chained-2-oxoacid dehydrogenase, and transketolase (TK)²¹². PDH and TK are of particular interest in relation to Gamma-MOB metabolism given their respective roles in Embden–Meyerhof–Parnas (EMP) glycolysis and the ribulose monophosphate (RuMP) pathway, which serve as critical routes of energy production and formaldehyde assimilation for these methanotrophs^{18,44,61}. The association between *sox* genes and *thiDE* is not discernable without accompanying experimental data. However, based on the initial hypothesis, RISC oxidation could feasibly spare a greater fraction of methane from complete oxidation to carbon dioxide, resulting in increased carbon flux into central metabolic pathways to and from the tricarboxylic acid (TCA) cycle, therefore increasing demand for core carbohydrate-processing enzymes and their respective cofactors.

Other conserved genes of particular interest are the *tlpA* family thioredoxin in combination with the membrane protein *hemJ*-type protoporphyrinogen IX oxidase (PPO). Thioredoxins are commonly involved in the quality control of periplasmic proteins, ensuring proper conformational changes through reduction/oxidation of disulfide bridges in periplasmic proteins, whereas PPOs perform the penultimate step in cytochrome heme biosynthesis²¹⁴. The combination of *tlpA/hemJ* bears some similarity to the SoxSW thioredoxins of *P. pantotrophus*; as previously mentioned,

SoxS is necessary for the viability of the *sox* system *in vivo* to resolve SoxZY-YZ dimers formed through disulfide bridging of the reactive Cys-110 residue^{109,215,216}. As a result, the inclusion of a thioredoxin in proximity to the *sox* genes of *Methylococcales* is an indication of a similar quality-control function, albeit one described within *Alphaproteobacteria* and not *gammaproteobacterial* strains. This is speculative, as the predicted *Methylococcales* *sox* thioredoxin does not bear any significant homology to either SoxS or SoxW, despite the similarity in predicted function.

The conservation of the *hemJ* homolog alongside *sox* genes in multiple *Methylococcales* strains (Fig. 4.1B) is a more cryptic finding. HemJ membrane proteins and PPOs in general are involved in the intermediate conversion of protoporphyrinogen IX to protoporphyrin IX through oxidation, within the protoporphyrin-dependent (PPD) heme biosynthesis pathway²¹⁴. As *hemJ* is predicted to function as a cytochrome heme maturation enzyme, it is tempting to propose a similar role to that of *moeA*, i.e., biosynthesis of co-factor required for upregulated *sox* enzymes, particularly the cytochrome-dependent SoxD and di/tri-heme SoxAX complex. However, previous studies of the *P. pantotrophus* GB17 *sox* locus also identified a gene encoding a putative cytochrome maturation enzyme, previously denoted as *ccdA*, and subsequently reclassified as *soxV*²¹⁷. It has been determined that the that the SoxV protein is required to keep the associated periplasmic thioredoxin SoxW in a reduced state, and is necessary for chemoautotrophic growth of the strain¹²¹. Moreover, *soxV* is unable to restore cytochrome maturation functionality to *P. pantotrophus* Δ *ccdA* mutants, further illustrating the difference between the two enzymes. These results indicate that the target of SoxV is distinct from that of CcdA, and that SoxV activity involves periplasmic reducing potential as opposed to intramembrane electron shuttles.

Genes encoding putative YedE/YeeE family transporters were conserved upstream of *soxCD* operons belonging to *Methylotheobacterium* spp. And *Methylomicrobium* sp. Wino1 (Fig. 4.2A). YedE/YeeE transporters are small sulfur molecule membrane transporters serving as anion

channels through the inner membrane, although the degree of their selectivity is uncertain¹³⁴. Naturally, the inclusion of sulfur transport proteins within a conserved *Methylococcales* *sox* operon suggests their involvement in the transport of sulfur anions across the cellular membranes. However, whether this function involves substrate acquisition or end-product removal is not clear, nor is it evident whether the inner or outer membrane is the functional site.

Of the remaining genes co-conserved within *Methylococcales* TOMES operons, a putative response regulator observed in *Mp. Oleiharenae* XLMV4 and *Methylotheobacterium* spp., ~100 base pairs downstream of *soxCD*, which contains a C-terminal phosphoacceptor receiver domain, is of note. The presence of this response regulator is encouraging for future research, as its conservation and proximity to *soxCD* implicate it as a potential regulator of TOMES for *Methylococcales*. This would be analogous to a two-component signaling system (TspSR) in *Acidithiobacillus caldus*, which facilitated σ^{54} -dependent transcription of the *sox-I* island in the presence of RISCs; although candidates for the respective sensor kinase for *Methylococcales* are not immediately apparent¹²⁵.

5.2. Effects of thiosulfate on the physiology of *Mt. buryatense* 5GB1C and *Mp. oleiharenae* XLMV4.

Confirmation of a complete thiosulfate oxidizing system encoded across a subset of *Methylococcales* genomes raised the possibility of mixotrophy in this MOB taxon, analogous to the sulfur oxidation capabilities of the facultative *Beijerinckiaceae* MOB *Mv. thiovorans* HY1 (Fig. 4.2, Fig. 4.3)²³. Mixotrophic catabolism has also been observed among other alpha-MOB capable of growing solely on small multi-carbon compounds, and hydrogen oxidation is believed to be a key component of verrucomicrobial MOB energy conservation^{97,218–220}. However, utilization of alternative electron donors by *Methylococcales* has eluded observation. It was hypothesized that

thiosulfate oxidation would contribute to energy conservation, resulting in higher growth yields and improved carbon conversion efficiency (CCE) when oxygen was non-limiting. Moreover, sulfur oxidation by *Methylococcales* could hypothetically supplement MOB in methane-limiting conditions, allowing for assimilation of limited carbon and continued energy production without competing for molecular oxygen. However, *Mt. buryatense* 5GB1C did not exhibit significant differences for any monitored parameters in the presence of thiosulfate and necessary co-factors (Fig. 4.5A-E, Table 1). The uniformity of response between experimental groups, including under carbon and oxygen limitations, indicates that *Mt. buryatense* 5GB1C is incapable of sulfur/methane mixotrophy under these conditions.

Explanation for lack of sulfur oxidation activity by *Mt. buryatense* 5GB1C can be derived through comparison with *Mv. thiovorans* HY1, especially via carbon assimilation strategies. Sulfur oxidation is a critical component of ecological primary production, particularly in dark environments with insufficient light to support photosynthesis³⁸. In environments where light is non-limiting, there exists a diversity of non-oxygenic phototrophic bacteria which require RISCs to replenish electrons lost to non-cyclic electron flow out of major photosystem routes. In both cases the reducing potential necessary to reduce carbon dioxide is sourced from RISCs, and are utilized via well-described autotrophic pathways, including the CBB cycle^{221,222}. The link between carbon fixation and sulfur oxidation is also apparent within facultative SOB, for example *P. pantotrophus* and *Mv. thiovorans* HY1, which transition between chemoautotrophy and their respective heterotrophic and methanotrophic modes based on the availability of carbon dioxide and RISCs^{23,126}. The majority of *Methylococcales* species are incapable of autotrophy, with exceptions including *Mc. capsulatus* Bath which perform CO₂-fixation via ribulose-1,5-bisphosphate carboxylase/oxygenase (RuBisCo), now known to be essential for growth⁹⁵. Notably, *Methylococcales* are distinct in this regard, as CO₂-fixation is widespread and essential in the

majority of methanotrophic taxa including *Verrucomicrobia*, Phylum NC-10, and *Alphaproteobacteria*^{20,23,78,223}. As the *Methylococcales* species which possess complete genomic inventories for TOMES are not known to be capable of autotrophy, this deficiency may be the most important factor contributing to the lack of observable catabolic benefits of sulfur/methane mixotrophy in the taxon.

The specific SoxD isoform may be another complicating factor for thiosulfate oxidation by *Methylococcales*. For TOMES-utilizing SOB, SoxD possesses two heme-binding motifs localized towards the N- and C-termini, which co-ordinate two separate hemes, facilitating SoxC re-oxidation and electron transfer to accessory cytochromes^{224,225}. Gwak and colleagues produced SoxD protein alignments from well-described SOB and *Methylococcales*, which demonstrated a C-terminal truncation resulting in the absence of the second heme-binding motif of SoxD sequences in the latter²³. The authors postulate that the missing SoxD heme-2 could explain the lack of observed thiosulfate activity in *Methylococcales*, as this motif is universally conserved among SOB with experimentally validated TOMES. Indeed, this singular heme setup is analogous to sulfite dehydrogenase SorB subunits and correlated to the $\alpha 1\beta 1$ quaternary structure of SorAB SDHs^{114,163}. This contrasts with the $\alpha 2\beta 2$ structure observed for SoxCD sulfane dehydrogenases, where the sequestered SoxC active site is re-oxidized by the proximal SoxD heme, with the distal heme completing the intra-enzyme redox chain from a more favorable position for interaction with accessory cytochromes¹¹⁴.

However, *P. pantotrophus* SoxD C-terminal deletion mutants (SoxD₁) present a challenge to this hypothesis²²⁵. When the TOMES system was reconstituted *in vitro*, the SoxCD₁ variant exhibited a cytochrome *c* reduction rate and electron yield comparable to the wild-type system, indicating that the second SoxD heme is dispensable for catalytic activity. *In vivo*, *P. pantotrophus* with SoxD₁ had ~2.5-fold lower specific activity, whereas molar oxygen consumption and electron

yields were comparable to the wild-type enzyme. These data indicate that, *in vivo*, the loss of the SoxD heme-2 has an adverse effect on SoxCD kinetics, but that the holoenzyme can still function with roughly equivalent reaction stoichiometries. While the truncated SoxD of *Methylococcales* may not be as deleterious to overall TOMES functionality as proposed, the reduced efficiency of TOMES featuring SoxD₁ complicates the potential of sulfur oxidation in *Methylococcales*. In general, *Methylococcales* are regarded as *r*-strategists among methanotrophs, where intermittent periods of increased methane availability result in rapid growth and substrate utilization, after which they transition to low-activity stationary phase¹⁹. Therefore, it is possible that a high-efficiency TOMES system would be disadvantageous under the conditions tested, as the increased demand for oxidizing species during mixotrophic methane and sulfur oxidation may result in a redox disbalance and interruption of essential catabolic processes. This would be especially true if the reducing potential from methane and sulfur oxidation were fed into the same energy conservation system, i.e., ATP production via inner membrane electron transport. For *Mv. thiovorans* HY1 there was a clear relationship between CBB cycle and sulfur oxidation regulation in the presence of RISCs, providing an outlet for RISC reducing potential through carbon fixation²³.

Given the difficulties in demonstrating methane/sulfur mixotrophy in *Methylococcales*, the initial hypothesis that catabolic sulfur oxidation may increase CCE under conditions of methane limitation is increasingly implausible, at least under the conditions tested. An alternative hypothesis regarding the presence of TOMES among *Methylococcales* strains is now required, given the degree of conservation of the *sox* operons across multiple gamma-MOB genera. Inspiration was derived from the *Betaproteobacterium Advenella kashmirensis*, which employs a novel tetrathionate intermediate (S4I) pathway variant in which a lanthanide-dependent MDH (XoxF) homolog was shown to be essential for thiosulfate oxidation¹⁸². This XoxF homolog was dubbed thiol dehydrotransferase (ThdT), and it was shown that ThdT expression correlated with

thiosulfate concentration and $\Delta thdT$ mutants were unable to completely oxidize thiosulfate to sulfate, producing tetrathionate as the terminal product. In this model, ThdT plausibly conducts a two-step reaction initiated by PQQ-dependent oxidative coupling of two thiosulfate molecules to produce tetrathionate¹⁸². In the second step ThdT ligates tetrathionate to a small molecule sulfur carrier (e.g., glutathione) for complete oxidation via SoxB and SoxCD. Notably, ThdT can only convert ~50% of supplied thiosulfate to tetrathionate and operates in tandem with the well-studied S4I pathway enzyme thiosulfate dehydrogenase (TsdA), which enables the complete conversion of supplied thiosulfate²²⁶.

As a result of these findings, lanthanum was included in the *Mp. oleiharenae* XLMV4 thiosulfate-oxidation assays (Fig. 4.8). *Mc. oleiharenae* XLMV4 is an alkaliphilic methanotroph closely related to *Methylobacter* and *Methylomicrobium* genera isolated from oil sands-associated tailings sediment in the Athabaskan region of Alberta, Canada²⁴. The strain possesses an XoxF-type MDH which could feasibly conduct a similar reaction to ThdT. This notion was reinforced by the high levels of conservation between *A. kashmirensis* ThdT and *Methylococcales* XoxF amino acid sequences (Fig. 4.10). Initial experimentation with thiosulfate-grown *Mp. oleiharenae* XLMV4 cultures yielded promising results including increased growth rate, shortened lag period, and improved CCE, seeming to support the initial hypothesis that methane/sulfur mixotrophy could increase the rate of carbon assimilation (Fig. 4.6, Table 1). However, the phenotype could not be replicated in following experiments utilizing revived *Mp. oleiharenae* XLMV4 cultures; potentially, the strain used in previous experiments may have adapted to oxidize RISCs in culture conditions following multiple passages, or the result of experimental error. Therefore, the sulfur oxidation capability of *Mp. oleiharenae* XLMV4 as it relates to energy conservation remains uncertain.

Intriguingly, the addition of lanthanum and thiosulfate in combination negatively impacted the growth of XLMV4, resulting in lower final OD measurements and lowered headspace gas

depletion rates (Fig. 4.8, Fig. 4.9, Table 1). This result was replicable between *Mp. oleiharenae* XLMV4 both well-attenuated to laboratory conditions and revived archival cultures, indicating a consistent interaction in contrast to the increased growth rates observed in the initial experiment (Fig. 4.8, Table 1). The significant homology between ThdT and XoxF combined with the inhibitory effects of the lanthanum/thiosulfate condition implicates thiosulfate as a competitive inhibitor of XoxF (Fig. 4.10). Indeed, current models of XoxF-type MDH function indicate that coordination of the alcohol substrate occurs through hydrogen bonding between the lanthanide cation and alcohol hydroxyl group²²⁷. This mechanism may be indicative of thiosulfate oxidation via ThdT, as the overall charge of -1 for the thiosulfate sulfone group, with the oxygen groups therefore capable of similar coordination with the metal cofactor; however, the structure and exact mechanism of ThdT have not been determined. While this interaction remains to be validated, these findings may become the basis for a new hypothesis, that TOMES in *Methylococcales* may function to relieve the inhibition of XoxF by thiosulfate. This would explain both the lack of a sulfur/methane mixotrophic phenotype reported in the literature and the widespread presence and apparent conservation of TOMES among the gamma-MOB.

6. Conclusion

In summary, despite the broad conservation of TOMES across *Methylococcales* genera, growth benefit reflective of dissimilatory sulfur oxidation was not observed in the assayed strains under the conditions tested. Recent research points to the lack of autotrophic carbon fixation ability of TOMES-possessing gamma-MOB strains as the primary reason for the lack of growth benefit by RISCs, which is reinforced in contrast to the alpha-MOB *Mv. thiovorans* HY1 which utilizes reducing potential from sulfur compounds to fix carbon dioxide via the CBB cycle²²⁸.

Despite initial physiological data indicating a pronounced thiosulfate-dependent growth rate increase in *Mc. oleiharenae* XLMV4, this was later contradicted in replicate experiments (Figs. 4.8, 4.9). However, lanthanide/thiosulfate-dependent growth rate decrease was shown to be replicable in *Mc. oleiharenae* XLMV4, indicating a hitherto unreported mechanism of growth inhibition. The direct causal relationship of this growth inhibition remains to be elucidated. The current hypothesis holds that thiosulfate may be a competitive inhibitor of the lanthanide-dependent MDH XoxF, given that the highly similar XoxF homolog ThdT has been revealed as a novel thiosulfate-oxidizing enzyme indispensable for thiosulfate oxidation in *A. kashmirensis*¹⁸². Therefore, a plausible function of TOMES in gamma-MOB may be to alleviate competitive inhibition of thiosulfate on XoxF through conversion to sulfate, as illustrated in Fig. 4.11. Going forward, it is recommended that future research focus on the impacts of thiosulfate and lanthanum on XoxF-utilizing gamma-MOB, with reduced emphasis on eliciting growth improvements via sulfur catabolism.

Regarding further research on the functionality of TOMES within *Methylococcales*, physiological research on the growth impacts of thiosulfate and lanthanum in combination should be performed across a range of gamma-MOB species. These strains would include those TOMES-possessing *Methylococcales* species identified herein, and those which possess XoxF but lack TOMES, for example *Methylomicrobium album* BG8. As is standard practice, knockout and complementation assays targeting *sox* genes utilizing strains with validated genetic manipulation techniques, such as *Mt. buryatense* 5GB1C, would be essential. Complementing this work, consumption/production curves of sulfur species in media over time should be performed via existing HPLC methods to better elucidate thiosulfate oxidation and sulphate production beyond the simple barium precipitation assay²²⁹. Kinetic assays on purified XoxF enzyme would also be required to directly test inhibition of methanol oxidation by thiosulfate, which are feasible owing to validated purification methods for the XoxF enzyme¹⁸⁵. Another line of investigation would involve

transcriptomic assays focusing on the regulation of TOMES and co-conserved coding sequences in *Methylococcales* strains, and to determine whether thiosulfate, lanthanum, or their combination, elicits upregulation of the identified TOMES operons. Finally, it would be beneficial to assess metabolic flux and assimilatory rates of methane carbon in cultures inhibited by lanthanum/thiosulfate, including comparisons to TOMES knockout strains, to assess the metabolic costs associated with XoxF inhibition and independently confirm the decreased growth rate observed in *Mp. oleiharenae* XLMV4.

7. Bibliography

1. Santos, A. A. *et al.* A protein trisulfide couples dissimilatory sulfate reduction to energy conservation. *Science* (80-.). **350**, 1541–1545 (2015).
2. Christensen, T. R. R. *et al.* Tracing the climate signal: mitigation of anthropogenic methane emissions can outweigh a large Arctic natural emission increase. *Sci. Rep.* **9**, 1–8 (2019).
3. Saunio, M. *et al.* The global methane budget 2000-2012. *Earth Syst. Sci. Data* **8**, 697–751 (2016).
4. Ciais, P. *et al.* Carbon and other biogeochemical cycles. *Clim. Chang. 2013 Phys. Sci. Basis Work. Gr. I Contrib. to Fifth Assess. Rep. Intergov. Panel Clim. Chang.* **9781107057**, 465–570 (2013).
5. Wise, M. G., McArthur, J. V. & Shimkets, L. J. Methanotroph diversity in landfill soil: Isolation of novel type I and type II methanotrophs whose presence was suggested by culture-independent 16S ribosomal DNA analysis. *Appl. Environ. Microbiol.* **65**, 4887–4897 (1999).
6. Prather, M. J., Holmes, C. D. & Hsu, J. Reactive greenhouse gas scenarios: Systematic exploration of uncertainties and the role of atmospheric chemistry. *Geophys. Res. Lett.* **39**, 6–10 (2012).
7. Lassey, K. R. Livestock methane emission: From the individual grazing animal through national inventories to the global methane cycle. *Agric. For. Meteorol.* **142**, 120–132 (2007).
8. Kirschke, S. *et al.* Three decades of global methane sources and sinks. *Nat. Geosci.* **6**, 813–823 (2013).
9. IPCC. *Climate Change 2007 The Physical Science Basis. Working Group I Contribution to the Fourth Assessment Report of the Intergovernmental Panel on Climate Change.*

- (Cambridge University Press, 2007). doi:10.1256/wea.58.04.
10. Walter, K. M., Zimov, S. A., Chanton, J. P., Verbyla, D. & Chapin, F. S. Methane bubbling from Siberian thaw lakes as a positive feedback to climate warming. *Nature* **443**, 71–75 (2006).
 11. Zimov, S. A., Schuur, E. A. G. & Stuart Chapin, F. Permafrost and the global carbon budget. *Science (80-.)*. **312**, 1612–1613 (2006).
 12. Tveit, A., Schwacke, R., Svenning, M. M. & Urich, T. Organic carbon transformations in high-Arctic peat soils: Key functions and microorganisms. *ISME J.* **7**, 299–311 (2013).
 13. MacKelprang, R. *et al.* Metagenomic analysis of a permafrost microbial community reveals a rapid response to thaw. *Nature* **480**, 368–371 (2011).
 14. Schuur, E. A. G. *et al.* Vulnerability of permafrost carbon to climate change: Implications for the global carbon cycle. *Bioscience* **58**, 701–714 (2008).
 15. Tamocai, C. *et al.* Soil organic carbon pools in the northern circumpolar permafrost region. *Global Biogeochem. Cycles* **23**, 1–11 (2009).
 16. Bulygina, E. S. *et al.* Taxonomic studies on methylotrophic bacteria by 5S ribosomal RNA sequencing. *J. Gen. Microbiol.* **136**, 441–446 (1990).
 17. Chistoserdova, L., Laukel, M., Portais, J. C., Vorholt, J. A. & Lidstrom, M. E. Multiple Formate Dehydrogenase Enzymes in the Facultative Methylotroph *Methylobacterium extorquens* AM1 Are Dispensable for Growth on Methanol. *J. Bacteriol.* **186**, 22–28 (2004).
 18. Khmelenina, V. N., Colin Murrell, J., Smith, T. J. & Trotsenko, Y. A. Physiology and Biochemistry of the Aerobic Methanotrophs. *Aerob. Util. Hydrocarb. Oils, Lipids* 73–97 (2019) doi:10.1007/978-3-319-50418-6_4.

19. Knief, C. Diversity and habitat preferences of cultivated and uncultivated aerobic methanotrophic bacteria evaluated based on pmoA as molecular marker. *Front. Microbiol.* **6**, (2015).
20. Khadem, A. F. *et al.* Autotrophic methanotrophy in verrucomicrobia: *Methylacidiphilum fumarolicum* solv uses the Calvin-Benson-Bassham cycle for Carbon Dioxide Fixation. *J. Bacteriol.* **193**, 4438–4446 (2011).
21. Kalyuzhnaya, M. G., Puri, A. W. & Lidstrom, M. E. Metabolic engineering in methanotrophic bacteria. *Metab. Eng.* **29**, 142–152 (2015).
22. Gilman, A. *et al.* Bioreactor performance parameters for an industrially-promising methanotroph *Methylomicrobium buryatense* 5GB1. *Microb. Cell Fact.* **14**, 1–8 (2015).
23. Gwak, J. H. *et al.* Sulfur and methane oxidation by a single microorganism. *Proc. Natl. Acad. Sci. U. S. A.* **119**, 1–12 (2022).
24. Saidi-Mehrabad, A. *et al.* *Methyllicorpusculum oleiharenae* gen. Nov., sp. nov., an aerobic methanotroph isolated from an oil sands tailings pond. *Int. J. Syst. Evol. Microbiol.* **70**, 2499–2508 (2020).
25. Ghashghavi, M. *et al.* *Methylotetracoccus oryzae* Strain C50C1 Is a Novel Type Ib Gammaproteobacterial Methanotroph Adapted to Freshwater Environments. *mSphere* **4**, 1–15 (2019).
26. Ghosh, W. & Dam, B. Biochemistry and molecular biology of lithotrophic sulfur oxidation by taxonomically and ecologically diverse bacteria and archaea. *FEMS Microbiol. Rev.* **33**, 999–1043 (2009).
27. Dahl, C. & Friedrich, C. G. *Microbial Sulfur Metabolism. Microbial Sulfur Metabolism* vol. 1 (2008).

28. Dahl, C. *Chapter 3 A biochemical view on the biological sulfur cycle*. (2019).
29. Dahl, C. *et al.* Structural and Molecular Genetic Insight into a Widespread Sulfur Oxidation Pathway. *J. Mol. Biol.* **384**, 1287–1300 (2008).
30. Pokorna, D. & Zabranska, J. Sulfur-oxidizing bacteria in environmental technology. *Biotechnol. Adv.* **33**, 1246–1259 (2015).
31. Reeburgh, W. S. Oceanic Methane Biogeochemistry. *ChemInform* **38**, 486–513 (2007).
32. Conrad, R. The global methane cycle: Recent advances in understanding the microbial processes involved. *Environ. Microbiol. Rep.* **1**, 285–292 (2009).
33. Kallistova, A. Y., Merkel, A. Y., Tarnovetskii, I. Y. & Pimenov, N. V. Methane formation and oxidation by prokaryotes. *Microbiol. (Russian Fed.)* **86**, 671–691 (2017).
34. Cedervall, P. E., Dey, M., Pearson, A. R., Ragsdale, S. W. & Wilmot, C. M. Structural insight into methyl-coenzyme M reductase chemistry using coenzyme B analogues. *Biochemistry* **49**, 7683–7693 (2010).
35. Bethke, C. M., Sanford, R. A., Kirk, M. F., Jin, Q. & Flynn, T. M. The thermodynamic ladder in geomicrobiology. *Am. J. Sci.* **311**, 183–210 (2011).
36. Op den Camp, H. J. M. *et al.* Environmental, genomic and taxonomic perspectives on methanotrophic Verrucomicrobia. *Environ. Microbiol. Rep.* **1**, 293–306 (2009).
37. Colin Murrell, J. & Jetten, M. S. M. The microbial methane cycle. *Environ. Microbiol. Rep.* **1**, 279–284 (2009).
38. Chen, Y. *et al.* Life without light: Microbial diversity and evidence of sulfur- and ammonium-based chemolithotrophy in Movile Cave. *ISME J.* **3**, 1093–1104 (2009).
39. Hutchens, E., Radajewski, S., Dumont, M. G., McDonald, I. R. & Murrell, J. C. Analysis of

- methanotrophic bacteria in Movile Cave by stable isotope probing. *Environ. Microbiol.* **6**, 111–120 (2004).
40. Van Duinen, G. A. *et al.* Methane as a carbon source for the food web in raised bog pools. *Freshw. Sci.* **32**, 1260–1272 (2013).
 41. Agasild, H. *et al.* Biogenic methane contributes to the food web of a large, shallow lake. *Freshw. Biol.* **59**, 272–285 (2014).
 42. Iguchi, H., Yurimoto, H. & Sakai, Y. Stimulation of methanotrophic growth in cocultures by cobalamin excreted by rhizobia. *Appl. Environ. Microbiol.* **77**, 8509–8515 (2011).
 43. Ho, A. *et al.* The more, the merrier: Heterotroph richness stimulates methanotrophic activity. *ISME J.* **8**, 1945–1948 (2014).
 44. Kalyuzhnaya, M. G. *et al.* Highly efficient methane biocatalysis revealed in a methanotrophic bacterium. *Nat. Commun.* **4**, 1–7 (2013).
 45. Szafranski, K. M., Piquet, B., Shillito, B., Lallier, F. H. & Duperron, S. Relative abundances of methane- and sulfur-oxidizing symbionts in gills of the deep-sea hydrothermal vent mussel *Bathymodiolus azoricus* under pressure. *Deep. Res. Part I Oceanogr. Res. Pap.* **101**, 7–13 (2015).
 46. Whittenbury, R., Phillips, K. C. & Wilkinson, J. F. Enrichment, isolation and some properties of methane-utilizing bacteria. *J. Gen. Microbiol.* **61**, 205–218 (1970).
 47. Bowman, J. P., Sly, L. I. & Stackebrandt, E. The phylogenetic position of the family Methylococcaceae. *Int. J. Syst. Bacteriol.* **45**, 182–185 (1995).
 48. Bowman, J. P., Skerratt, J. H., Nichols, P. D. & Sly, L. I. Phospholipid fatty acid and lipopolysaccharide fatty acid signature lipids in methane-utilizing bacteria. *FEMS Microbiol.*

- Lett.* **85**, 15–22 (1991).
49. Bowman, J. P., Sly, L. I., Nichols, P. D. & Hayward, A. C. Revised taxonomy of the methanotrophs: Description of *Methylobacter* gen. nov., emendation of *Methylococcus*, validation of *Methylosinus* and *Methylocystis* species, and a proposal that the family Methylococcaceae includes only the group I methanotrophs. *Int. J. Syst. Bacteriol.* **43**, 735–753 (1993).
 50. Bratina, B. J., Brusseau, G. A. & Hanson, R. S. Use of 16S rRNA analysis to investigate phylogeny of methylotrophic bacteria. *Int. J. Syst. Bacteriol.* **42**, 645–648 (1992).
 51. Hanson, R. S. & Hanson, T. E. Methanotrophic bacteria. *Microbiol. Rev.* **60**, 439–471 (1996).
 52. Semrau, J. D., Dispirito, A. A. & Yoon, S. Methanotrophs and copper. *FEMS Microbiol. Rev.* **34**, 496–531 (2010).
 53. But, S. Y., Egorova, S. V., Khmelenina, V. N. & Trotsenko, Y. A. Serine-glyoxylate aminotranferases from methanotrophs using different C1-assimilation pathways. *Antonie van Leeuwenhoek, Int. J. Gen. Mol. Microbiol.* **112**, 741–751 (2019).
 54. Sugden, S., Lazic, M., Sauvageau, D. & Stein, L. Y. Transcriptomic and Metabolomic Responses to Carbon and Nitrogen Sources in *Methylobacterium album* BG8. *Appl. Environ. Microbiol.* **87**, (2021).
 55. Balasubramanian, R. *et al.* Oxidation of methane by a biological dicopper centre. *Nature* **465**, 115–119 (2010).
 56. Ross, M. O. & Rosenzweig, A. C. A tale of two methane monooxygenases. *J. Biol. Inorg. Chem.* **22**, 307–319 (2017).
 57. Orata, F. D., Meier-Kolthoff, J. P., Sauvageau, D. & Stein, L. Y. Phylogenomic analysis of

- the gammaproteobacterial methanotrophs (order methylococcales) calls for the reclassification of members at the genus and species levels. *Front. Microbiol.* **9**, 1–17 (2018).
58. Murreil, J. C., Gilbert, B. & McDonald, I. R. Molecular biology and regulation of methane monooxygenase. *Arch. Microbiol.* **173**, 325–332 (2000).
 59. Semrau, J. D. Bioremediation via methanotrophy: Overview of recent findings and suggestions for future research. *Front. Microbiol.* **2**, 1–7 (2011).
 60. Semrau, J. D. *et al.* Methanobactin and MmoD work in concert to act as the ‘copper-switch’ in methanotrophs. *Environ. Microbiol.* **15**, 3077–3086 (2013).
 61. Akberdin, I. R. *et al.* Methane utilization in *Methylobacterium alcaliphilum* 20ZR: A systems approach. *Sci. Rep.* **8**, 1–13 (2018).
 62. Bordel, S. *et al.* Genome scale metabolic modeling reveals the metabolic potential of three Type II methanotrophs of the genus *Methylocystis*. *Metab. Eng.* **54**, 191–199 (2019).
 63. Stone, K. *et al.* Comparative study of oxygen-limited and methane-limited growth phenotypes of *Methylobacterium buryatense* 5GB1. *Biochem. Eng. J.* **161**, 107707 (2020).
 64. Gu, W. & Semrau, J. D. Copper and cerium-regulated gene expression in *Methylosinus trichosporium* OB3b. *Appl. Microbiol. Biotechnol.* **101**, 8499–8516 (2017).
 65. Brantner, C. A. *et al.* Intracytoplasmic membrane formation in *Methylobacterium album* BG8 is stimulated by copper in the growth medium. *Can. J. Microbiol.* **43**, 672–676 (1997).
 66. Pesch, M. L., Christl, I., Barmettler, K., Kraemer, S. M. & Kretzschmar, R. Isolation and purification of Cu-free methanobactin from *Methylosinus trichosporium* OB3b. *Geochem. Trans.* **12**, 1–9 (2011).

67. Semrau, J. D., DiSpirito, A. A., Gu, W. & Yoon, S. Metals and methanotrophy. *Appl. Environ. Microbiol.* **84**, 7–14 (2018).
68. Bandow, N. *et al.* Spectral and copper binding properties of methanobactin from the facultative methanotroph *Methylocystis* strain SB2. *J. Inorg. Biochem.* **110**, 72–82 (2012).
69. Kenney, G. E. & Rosenzweig, A. C. Methanobactins: Maintaining copper homeostasis in methanotrophs and beyond. *J. Biol. Chem.* **293**, 4606–4615 (2018).
70. Choi, D. W. *et al.* Spectral and thermodynamic properties of methanobactin from γ -proteobacterial methane oxidizing bacteria: A case for copper competition on a molecular level. *Journal of Inorganic Biochemistry* vol. 104 1240–1247 (2010).
71. El Ghazouani, A. *et al.* Variations in methanobactin structure influences copper utilization by methane-oxidizing bacteria. *Proc. Natl. Acad. Sci. U. S. A.* **109**, 8400–8404 (2012).
72. Vorobev, A. *et al.* Detoxification of mercury by methanobactin from *Methylosinus trichosporium* OB3b. *Appl. Environ. Microbiol.* **79**, 5918–5926 (2013).
73. Chang, J. *et al.* Methanobactin from *Methylosinus trichosporium* OB3b inhibits N₂O reduction in denitrifiers. *ISME J.* **12**, 2086–2089 (2018).
74. Anthony, C. The quinoprotein dehydrogenases for methanol and glucose. *Arch. Biochem. Biophys.* **428**, 2–9 (2004).
75. Chu, F. & Lidstrom, M. E. XoxF acts as the predominant methanol dehydrogenase in the type I methanotroph *Methylomicrobium buryatense*. *J. Bacteriol.* **198**, 1317–1325 (2016).
76. Anthony, C. & Williams, P. The structure and mechanism of methanol dehydrogenase. *Biochim. Biophys. Acta - Proteins Proteomics* **1647**, 18–23 (2003).
77. Pol, A. *et al.* Rare earth metals are essential for methanotrophic life in volcanic mudpots.

- Environ. Microbiol.* **16**, 255–264 (2014).
78. Yang, S. *et al.* Global molecular analyses of methane metabolism in methanotrophic alphaproteobacterium, *Methylosinus trichosporium* OB3b. Part II. metabolomics and ¹³C-labeling study. *Front. Microbiol.* **4**, 1–13 (2013).
 79. Wu, M. L. *et al.* XoxF-type methanol dehydrogenase from the anaerobic methanotroph ‘*Candidatus Methyloirabilis oxyfera*’. *Appl. Environ. Microbiol.* **81**, 1442–1451 (2015).
 80. Matsen, J. B., Yang, S., Stein, L. Y., Beck, D. & Kalyuzhnaya, M. G. Global molecular analyses of methane metabolism in Methanotrophic alphaproteobacterium, *Methylosinus trichosporium* OB3b. Part I: Transcriptomic study. *Front. Microbiol.* **4**, 1–16 (2013).
 81. Akberdin, I. R. *et al.* Rare Earth Elements alter redox balance in methylomicrobium *alcaliphilum* 20ZR. *Front. Microbiol.* **9**, 1–12 (2018).
 82. Wehrmann, M., Billard, P., Martin-Meriadec, A., Zegeye, A. & Klebensberger, J. Functional role of lanthanides in enzymatic activity and transcriptional regulation of pyrroloquinoline quinone-dependent alcohol dehydrogenases in *Pseudomonas putida* KT2440. *MBio* **8**, 1–14 (2017).
 83. Taubert, M. *et al.* XoxF encoding an alternative methanol dehydrogenase is widespread in coastal marine environments. *Environ. Microbiol.* **17**, 3937–3948 (2015).
 84. Knief, C. *et al.* Metaproteogenomic analysis of microbial communities in the phyllosphere and rhizosphere of rice. *ISME J.* **6**, 1378–1390 (2012).
 85. Schmidt, S., Christen, P., Kiefer, P. & Vorholt, J. A. Functional investigation of methanol dehydrogenase-like protein XoxF in *Methylobacterium extorquens* AM1. *Microbiology* **156**, 2575–2586 (2010).

86. Maia, L. B., Moura, J. J. G. & Moura, I. Molybdenum and tungsten - dependent formate dehydrogenases. (2014) doi:10.1007/s00775-014-1218-2.
87. Torre, A. *et al.* Genome-scale metabolic reconstructions and theoretical investigation of methane conversion in *Methylobacterium buryatense* strain 5G(B1). *Microb. Cell Fact.* **14**, 1–15 (2015).
88. He, L., Fu, Y. & Lidstrom, M. E. Quantifying Methane and Methanol Metabolism of “*Methylobacterium buryatense*” 5GB1C under Substrate Limitation. *mSystems* **4**, 1–14 (2019).
89. Rozova, O. N., Khmelena, V. N., Bocharova, K. A., Mustakhimov, I. I. & Trotsenko, Y. A. Role of NAD⁺-dependent malate dehydrogenase in the metabolism of *Methylobacterium alcaliphilum* 20Z and *Methylobacterium trichosporium* OB3b. *Microorganisms* **3**, 47–59 (2015).
90. Fu, Y., He, L., Reeve, J., Beck, D. A. C. & Lidstrom, M. E. Core metabolism shifts during growth on methanol versus methane in the methanotroph *Methylobacterium buryatense* 5GB1. *MBio* **10**, 1–14 (2019).
91. Nguyen, A. D., Kim, D. & Lee, E. Y. A comparative transcriptome analysis of the novel obligate methanotroph *Methylobacterium* sp. DH-1 reveals key differences in transcriptional responses in C1 and secondary metabolite pathways during growth on methane and methanol. *BMC Genomics* **20**, 1–16 (2019).
92. He, L., Groom, J. D. & Lidstrom, M. E. The Entner-Doudoroff Pathway Is an Essential Metabolic Route for *Methylobacterium Buryatense* 5GB1C. *Appl. Environ. Microbiol.* **87**, 1–11 (2020).
93. Nguyen, A. D. *et al.* Genome-scale evaluation of core one-carbon metabolism in gammaproteobacterial methanotrophs grown on methane and methanol. *Metab. Eng.* **57**,

- 1–12 (2020).
94. Fu, Y., Li, Y. & Lidstrom, M. The oxidative TCA cycle operates during methanotrophic growth of the Type I methanotroph *Methylomicrobium buryatense* 5GB1. *Metab. Eng.* **42**, 43–51 (2017).
 95. Henard, C. A. *et al.* Ribulose-1,5-Bisphosphate Carboxylase/Oxygenase (RubisCO) Is Essential for Growth of the Methanotroph *Methylococcus capsulatus* Strain Bath. *Appl. Environ. Microbiol.* **87**, 1–13 (2021).
 96. Crowther, G. J., Kosály, G. & Lidstrom, M. E. Formate as the main branch point for methylotrophic metabolism in *Methylobacterium extorquens* AM1. *J. Bacteriol.* **190**, 5057–5062 (2008).
 97. Tamas, I., Smirnova, A. V., He, Z. & Dunfield, P. F. The (d)evolution of methanotrophy in the Beijerinckiaceae—a comparative genomics analysis. *ISME J.* **8**, 369–382 (2014).
 98. Vorholt, J. A., Marx, C. J., Lidstrom, M. E. & Thauer, R. K. Novel formaldehyde-activating enzyme in *Methylobacterium extorquens* AM1 required for growth on methanol. *J. Bacteriol.* **182**, 6645–6650 (2000).
 99. Pomper, B. K., Vorholt, J. A., Chistoserdova, L., Lidstrom, M. E. & Thauer, R. K. A methenyl tetrahydromethanopterin cyclohydrolase and a methenyl tetrahydrofolate cyclohydrolase in *Methylobacterium extorquens* AM1. *Eur. J. Biochem.* **261**, 475–480 (1999).
 100. Ermler, U. *et al.* Structure of methylene-tetrahydromethanopterin dehydrogenase from *Methylobacterium extorquens* AM1. *Structure* **10**, 1127–1137 (2002).
 101. Hagemeyer, C. H., Chistoserdova, L., Lidstrom, M. E., Thauer, R. K. & Vorholt, J. A. Characterization of a second methylene tetrahydromethanopterin dehydrogenase from *Methylobacterium extorquens* AM1. *Eur. J. Biochem.* **267**, 3762–3769 (2000).

102. Cecilia Martinez-Gomez, N., Nguyen, S. & Lidstrom, M. E. Elucidation of the role of the methylene-tetrahydromethanopterin dehydrogenase MtdA in the tetrahydromethanopterin-dependent oxidation pathway in methylobacterium extorquens AM1. *J. Bacteriol.* **195**, 2359–2367 (2013).
103. Marx, C. J. & Lidstrom, M. E. Development of an insertional expression vector system for Methylobacterium extorquens AM1 and generation of null mutants lacking mtdA and/or fch. *Microbiology* **150**, 9–19 (2004).
104. Pomper, B. K., Saurel, O., Milon, A. & Vorholt, J. A. Generation of formate by the formyltransferase/hydrolase complex (Fhc) from Methylobacterium extorquens AM1. *FEBS Lett.* **523**, 133–137 (2002).
105. Pomper, B. K. & Vorholt, J. A. Characterization of the formyltransferase from methylobacterium extorquens AM1. *Eur. J. Biochem.* **268**, 4769–4775 (2001).
106. Marx, C. J., Laukel, M., Vorholt, J. A. & Lidstrom, M. E. Purification of the Formate-Tetrahydrofolate Ligase from Methylobacterium extorquens AM1 and Demonstration of Its Requirement for Methylo-trophic Growth. *J. Bacteriol.* **185**, 7169–7175 (2003).
107. Marx, C. J., Chistoserdova, L. & Lidstrom, M. E. Formaldehyde-Detoxifying Role of the Tetrahydromethanopterin-Linked Pathway in Methylobacterium extorquens AM1. *J. Bacteriol.* **185**, 7160–7168 (2003).
108. Mittenhuber, G., Sonomoto, K., Egert, M. & Friedrich, C. G. G. Identification of the DNA region responsible for sulfur-oxidizing ability of Thiosphaera pantotropha. *J. Bacteriol.* **173**, 7340–7344 (1991).
109. Rother, D., Orawski, G., Bardischewsky, F. & Friedrich, C. G. SoxRS-mediated regulation of chemotrophic sulfur oxidation in Paracoccus pantotrophus. *Microbiology* **151**, 1707–1716

- (2005).
110. Rother, D., Henrich, H. J., Quentmeier, A., Bardischewsky, F. & Friedrich, C. G. Novel genes of the sox gene cluster, mutagenesis of the flavoprotein SoxF, and evidence for a general sulfur-oxidizing system in *Paracoccus pantotrophus* GB17. *J. Bacteriol.* **183**, 4499–4508 (2001).
 111. Dambe, T., Quentmeier, A., Rother, D., Friedrich, C. & Scheidig, A. J. Structure of the cytochrome complex SoxXA of *Paracoccus pantotrophus*, a heme enzyme initiating chemotrophic sulfur oxidation. *J. Struct. Biol.* **152**, 229–234 (2005).
 112. Kappler, U. & Maher, M. J. The bacterial SoxAX cytochromes. *Cell. Mol. Life Sci.* **70**, 977–992 (2013).
 113. Sauvé, V., Bruno, S., Berks, B. C. & Hemmings, A. M. The SoxYZ complex carries sulfur cycle intermediates on a peptide swinging arm. *J. Biol. Chem.* **282**, 23194–23204 (2007).
 114. Zander, U. *et al.* Structural basis for the oxidation of protein-bound sulfur by the sulfur cycle molybdohemo-enzyme sulfane dehydrogenase SoxCD. *J. Biol. Chem.* **286**, 8349–8360 (2011).
 115. Quentmeier, A. & Friedrich, C. G. The cysteine residue of the SoxY protein as the active site of protein-bound sulfur oxidation of *Paracoccus pantotrophus* GB17. *FEBS Lett.* **503**, 168–172 (2001).
 116. Quentmeier, A. *et al.* Sulfur oxidation in *Paracoccus pantotrophus*: Interaction of the sulfur-binding protein SoxYZ with the dimanganese SoxB protein. *Biochem. Biophys. Res. Commun.* **312**, 1011–1018 (2003).
 117. Drew, S. C. *et al.* Spectroscopic characterization of the molybdenum cofactor of the sulfane dehydrogenase SoxCD from *paracoccus pantotrophus*. *Inorg. Chem.* **50**, 409–411 (2011).

118. Quentmeier, A., Janning, P., Hellwig, P. & Friedrich, C. G. Activation of the heterodimeric central complex SoxYZ of chemotrophic sulfur oxidation is linked to a conformational change and SoxY-Y interprotein disulfide formation. *Biochemistry* **46**, 10990–10998 (2007).
119. Carius, Y., Rother, D., Friedrich, C. G. & Scheidig, A. J. The structure of the periplasmic thiol-disulfide oxidoreductase SoxS from *Paracoccus pantotrophus* indicates a triple Trx/Grx/DsbC functionality in chemotrophic sulfur oxidation. *Acta Crystallogr. Sect. D Biol. Crystallogr.* **65**, 229–240 (2009).
120. Rother, D., Ringk, J. & Friedrich, C. G. Sulfur oxidation of *Paracoccus pantotrophus*: The sulfur-binding protein SoxYZ is the target of the periplasmic thiol-disulfide oxidoreductase SoxS. *Microbiology* **154**, 1980–1988 (2008).
121. Bardischewsky, F., Fischer, J., Höller, B. & Friedrich, C. G. SoxV transfers electrons to the periplasm of *Paracoccus pantotrophus* - An essential reaction for chemotrophic sulfur oxidation. *Microbiology* **152**, 465–472 (2006).
122. Welte, C. *et al.* Interaction between Sox proteins of two physiologically distinct bacteria and a new protein involved in thiosulfate oxidation. *FEBS Lett.* **583**, 1281–1286 (2009).
123. Hensen, D., Sperling, D., Trüper, H. G., Brune, D. C. & Dahl, C. Thiosulphate oxidation in the phototrophic sulphur bacterium *Allochromatium vinosum*. *Mol. Microbiol.* **62**, 794–810 (2006).
124. Mandal, S., Chatterjee, S., Dam, B., Roy, P. & Das Gupta, S. K. The dimeric repressor SoxR binds cooperatively to the promoter(s) regulating expression of the sulfur oxidation (sox) operon of *Pseudaminobacter salicylatoxidans* KCT001. *Microbiology* **153**, 80–91 (2007).
125. Li, L. F. *et al.* The σ^{54} -dependent two-component system regulating sulfur oxidization (Sox) system in *Acidithiobacillus caldus* and some chemolithotrophic bacteria. *Appl. Microbiol.*

- Biotechnol.* **101**, 2079–2092 (2017).
126. Friedrich, C. G. *et al.* Novel genes coding for lithotrophic sulfur oxidation of *Paracoccus pantotrophus* GB17. *J. Bacteriol.* **182**, 4677–4687 (2000).
 127. Ghosh, W. & Roy, P. Chemolithoautotrophic oxidation of thiosulfate, tetrathionate and thiocyanate by a novel rhizobacterium belonging to the genus *Paracoccus*. *FEMS Microbiol. Lett.* **270**, 124–131 (2007).
 128. Grimm, F., Franz, B. & Dahl, C. Regulation of dissimilatory sulfur oxidation in the purple sulfur bacterium *Allochromatium vinosum*. *Front. Microbiol.* **2**, 1–11 (2011).
 129. Sander, J., Engels-Schwarzlose, S. & Dahl, C. Importance of the DsrMKJOP complex for sulfur oxidation in *Allochromatium vinosum* and phylogenetic analysis of related complexes in other prokaryotes. *Arch. Microbiol.* **186**, 357–366 (2006).
 130. Thorup, C., Schramm, A., Findlay, A. J., Finster, K. W. & Schreiber, L. Disguised as a sulfate reducer: Growth of the deltaproteobacterium *Desulfurivibrio alkaliphilus* by Sulfide Oxidation with Nitrate. *MBio* **8**, 1–9 (2017).
 131. Löffler, M. *et al.* DsrL mediates electron transfer between NADH and rDsrAB in *Allochromatium vinosum*. *Environ. Microbiol.* **22**, 783–795 (2020).
 132. Møllerup, A., Holkenbrink, C., Oco, S., Otaki, H. & Frigaard, N. Sulfur globule oxidation in green sulfur bacteria is dependent on the dissimilatory sulfite reductase system. *Microbiology* **157**, 1229–1239 (2011).
 133. Maki, J. S. Bacterial intracellular sulfur globules: Structure and function. *J. Mol. Microbiol. Biotechnol.* **23**, 270–280 (2013).
 134. Tanaka, Y. *et al.* Crystal structure of a YeeE/YedE family protein engaged in thiosulfate

- uptake. *Sci. Adv.* **6**, (2020).
135. Gwak, J. *et al.* Sulfur and methane oxidation by a single microorganism. *Proc. Natl. Acad. Sci. U. S. A.* **119**, (2022).
 136. Prange, A. *et al.* Quantitative speciation of sulfur in bacterial sulfur globules: X-ray absorption spectroscopy reveals at least three different species of sulfur. *Microbiology* **148**, 267–276 (2002).
 137. Bartsch, R. G., Newton, G. L., Sherrill, C. & Fahey, R. C. Glutathione amide and its perthiol in anaerobic sulfur bacteria. *J. Bacteriol.* **178**, 4742–4746 (1996).
 138. Stockdreher, Y. *et al.* New Proteins Involved in Sulfur Trafficking in the Cytoplasm of *Allochromatium vinosum*. *J. Biol. Chem.* **289**, 12390–12403 (2014).
 139. Venceslau, S. S., Stockdreher, Y., Dahl, C. & Pereira, I. A. C. The ‘bacterial heterodisulfide’ DsrC is a key protein in dissimilatory sulfur metabolism. *Biochim. Biophys. Acta - Bioenerg.* **1837**, 1148–1164 (2014).
 140. Dahl, C., Franz, B., Hensen, D., Kesselheim, A. & Zigann, R. Sulfite oxidation in the purple sulfur bacterium *Allochromatium vinosum*: Identification of SoeABC as a major player and relevance of SoxYZ in the process. *Microbiol. (United Kingdom)* **159**, 2626–2638 (2013).
 141. Quatrini, R. *et al.* Extending the models for iron and sulfur oxidation in the extreme Acidophile *Acidithiobacillus ferrooxidans*. *BMC Genomics* **10**, 394 (2009).
 142. Stockdreher, Y. *et al.* Cytoplasmic sulfurtransferases in the purple sulfur bacterium *Allochromatium vinosum*: Evidence for sulfur transfer from DsrEFH to DsrC. *PLoS One* **7**, (2012).
 143. Löffler, M., Wallerang, K. B., Venceslau, S. S., Pereira, I. A. C. & Dahl, C. The Iron-Sulfur

- Flavoprotein DsrL as NAD(P)H:Acceptor Oxidoreductase in Oxidative and Reductive Dissimilatory Sulfur Metabolism. *Front. Microbiol.* **11**, 1–15 (2020).
144. Oliveira, T. F. *et al.* The crystal structure of *Desulfovibrio vulgaris* dissimilatory sulfite reductase bound to DsrC provides novel insights into the mechanism of sulfate respiration. *J. Biol. Chem.* **283**, 34141–34149 (2008).
145. Grein, F., Pereira, I. A. C. & Dahl, C. Biochemical characterization of individual components of the *Allochromatium vinosum* DsrMKJOP transmembrane complex aids understanding of complex function in vivo. *J. Bacteriol.* **192**, 6369–6377 (2010).
146. CECIL, R. & WAKE, R. G. The reactions of inter- and intra-chain disulphide bonds in proteins with sulphite. *Biochem. J.* **82**, 401–406 (1962).
147. Tietze, M. *et al.* Redox potentials of methanophenazine and CoB-S-S-CoM, factors involved in electron transport in methanogenic archaea. *ChemBioChem* **4**, 333–335 (2003).
148. Bechtel, T. J. & Weerapana, E. From structure to redox: The diverse functional roles of disulfides and implications in disease. *Proteomics* **17**, 1–49 (2017).
149. Wouters, M. A., Fan, S. W. & Haworth, N. L. Erratum: Disulfides as redox switches: From molecular mechanisms to functional significance (*Antioxidants & Redox Signaling* (2010) 12:1 (53-91)). *Antioxidants Redox Signal.* **12**, 321 (2010).
150. Urban, P. F. & Klingenberg, M. Redox Potentials of Ubiquinone and Cytochrome. *Eur. J. Biochem.* **9**, 519–525 (1969).
151. Ramos, A. R., Keller, K. L., Wall, J. D. & Cardoso Pereira, I. A. The membrane qmoABC complex interacts directly with the dissimilatory adenosine 5'-phosphosulfate reductase in sulfate reducing bacteria. *Front. Microbiol.* **3**, 1–10 (2012).

152. Dahl, C. *Sulfur Metabolism in Phototrophic Bacteria*. (2017). doi:10.1007/978-3-319-51365-2.
153. Grein, F. *et al.* DsrJ, an essential part of the DsrMKJOP transmembrane complex in the purple sulfur bacterium *allochromatium vinosum*, is an unusual triheme cytochrome c. *Biochemistry* **49**, 8290–8299 (2010).
154. Meyer, B. & Kuever, J. Molecular analysis of the distribution and phylogeny of dissimilatory adenosine-5'-phosphosulfate reductase-encoding genes (*aprBA*) among sulfur-oxidizing. *Microbiology* **153**, 3478–3498 (2007).
155. Gregersen, L. H., Bryant, D. A. & Frigaard, N. U. Mechanisms and evolution of oxidative sulfur metabolism in green sulfur bacteria. *Front. Microbiol.* **2**, 1–14 (2011).
156. Pereira, I. A. C. *et al.* A comparative genomic analysis of energy metabolism in sulfate reducing bacteria and archaea. *Front. Microbiol.* **2**, 1–22 (2011).
157. Lampreia, J., Pereira, A. S. & Moura, J. J. G. Adenylylsulfate reductases from sulfate-reducing bacteria. *Methods Enzymol.* **243**, 241–260 (1994).
158. Dahl, C. Insertional gene inactivation in a phototrophic sulphur bacterium : APS-reductase-deficient mutants of *Chromatium vinosum*. *Microbiology* **142**, 3363–3372 (1996).
159. Sánchez, O., Ferrera, I., Dahl, C. & Mas, J. In vivo role of adenosine-5'-phosphosulfate reductase in the purple sulfur bacterium *Allochromatium vinosum*. *Arch. Microbiol.* **176**, 301–305 (2001).
160. Meyer, B. & Kuever, J. Homology modeling of dissimilatory APS reductases (*AprBA*) of sulfur-oxidizing and sulfate-reducing prokaryotes. *PLoS One* **3**, (2008).
161. Parey, K. *et al.* Structural, Biochemical and Genetic Characterization of Dissimilatory ATP

- Sulfurylase from *Allochromatium vinosum*. *PLoS One* **8**, (2013).
162. Weissgerber, T., Watanabe, M., Hoefgen, R. & Dahl, C. Metabolomic profiling of the purple sulfur bacterium *Allochromatium vinosum* during growth on different reduced sulfur compounds and malate. *Metabolomics* **10**, 1094–1112 (2014).
 163. Kappler, U. & Bailey, S. Molecular basis of intramolecular electron transfer in sulfite-oxidizing enzymes is revealed by high resolution structure of a heterodimeric complex of the catalytic molybdopterin subunit and a c-type cytochrome subunit. *J. Biol. Chem.* **280**, 24999–25007 (2005).
 164. Kisker, C. *et al.* Molecular basis of sulfite oxidase deficiency from the structure of sulfite oxidase. *Cell* **91**, 973–983 (1997).
 165. Eilers, T. *et al.* Identification and biochemical characterization of *Arabidopsis thaliana* sulfite oxidase: A new player in plant sulfur metabolism. *J. Biol. Chem.* **276**, 46989–46994 (2001).
 166. Kappler, U., Bennett, B., Deutzmann, R., Mcewan, A. G. & Dahl, C. Sulfite : Cytochrome c Oxidoreductase from *Thiobacillus novellus*. **275**, 13202–13212 (2000).
 167. Kappler, U. Bacterial sulfite-oxidizing enzymes. *Biochim. Biophys. Acta - Bioenerg.* **1807**, 1–10 (2011).
 168. Kappler, U. & Nouwens, A. S. Metabolic adaptation and trophic strategies of soil bacteria- C1-metabolism and sulfur chemolithotrophy in *Starkeya novella*. *Front. Microbiol.* **4**, 1–12 (2013).
 169. Weinitschke, S., Denger, K., Cook, A. M. & Smits, T. H. M. The DUF81 protein TauE in *Cupriavidus necator* H16, a sulfite exporter in the metabolism of C2 sulfonates. *Microbiology* **153**, 3055–3060 (2007).

170. Ghashghavi, M. *et al.* Methylospirillum oryzae Strain C50C1 Is a Novel Type Ib Gammaproteobacterial Methanotroph Adapted to Freshwater Environments. *mSphere* **4**, 1–15 (2019).
171. Marcia, M., Ermler, U., Peng, G. & Michel, H. The structure of Aquifex aeolicus sulfide:quinone oxidoreductase, a basis to understand sulfide detoxification and respiration. *Proc. Natl. Acad. Sci. U. S. A.* **106**, 9625–9630 (2009).
172. Gouet, P., Courcelle, E., Stuart, D. I. & Métoz, F. ESPript: Analysis of multiple sequence alignments in PostScript. *Bioinformatics* **15**, 305–308 (1999).
173. Robert, X. & Gouet, P. Deciphering key features in protein structures with the new ENDscript server. *Nucleic Acids Res.* **42**, 320–324 (2014).
174. Sauvé, V. *et al.* Mechanism for the hydrolysis of a sulfur-sulfur bond based on the crystal structure of the thiosulfohydrolase SoxB. *J. Biol. Chem.* **284**, 21707–21718 (2009).
175. Mount, D. W. Using BLOSUM in sequence alignments. *Cold Spring Harb. Protoc.* **3**, (2008).
176. Camacho, C. *et al.* BLAST+: Architecture and applications. *BMC Bioinformatics* **10**, 1–9 (2009).
177. Altschul, S. F., Gish, W., Miller, W., Myers, E. W. & Lipman, D. J. Basic local alignment search tool. *J. Mol. Biol.* **215**, 403–410 (1990).
178. Gilchrist, C. L. M. & Chooi, Y. H. Clinker & clustermap.js: Automatic generation of gene cluster comparison figures. *Bioinformatics* **37**, 2473–2475 (2021).
179. Pearson, W. R. An introduction to sequence similarity ('homology') searching. *Curr. Protoc. Bioinforma.* **1**, 1286–1292 (2013).
180. Dereeper, A., Audic, S., Claverie, J. M. & Blanc, G. BLAST-EXPLORER helps you building

- datasets for phylogenetic analysis. *BMC Evol. Biol.* **10**, 8–13 (2010).
181. Dereeper, A. *et al.* Phylogeny.fr: robust phylogenetic analysis for the non-specialist. *Nucleic Acids Res.* **36**, 465–469 (2008).
 182. Pyne, P. *et al.* Homologs from sulfur oxidation (Sox) and methanol dehydrogenation (Xox) enzyme systems collaborate to give rise to a novel pathway of chemolithotrophic tetrathionate oxidation. *Mol. Microbiol.* **109**, 169–191 (2018).
 183. Berman, H. M. *et al.* The Protein Data Bank. *Nucleic Acids Res.* **28**, 235–242 (2000).
 184. Berman, H., Henrick, K. & Nakamura, H. Announcing the worldwide Protein Data Bank. *Nat. Struct. Biol.* **10**, 980 (2003).
 185. Deng, Y. W., Ro, S. Y. & Rosenzweig, A. C. Structure and function of the lanthanide-dependent methanol dehydrogenase XoxF from the methanotroph *Methylomicrobium buryatense* 5GB1C. *J. Biol. Inorg. Chem.* **23**, 1037–1047 (2018).
 186. Yan, X., Chu, F., Puri, A. W., Fu, Y. & Lidstrom, M. E. Electroporation-based genetic manipulation in type I methanotrophs. *Appl. Environ. Microbiol.* **82**, 2062–2069 (2016).
 187. Puri, A. W. *et al.* Genetic tools for the industrially promising methanotroph *Methylomicrobium buryatense*. *Appl. Environ. Microbiol.* **81**, 1775–1781 (2015).
 188. Meyer, B., Imhoff, J. F. & Kuever, J. Molecular analysis of the distribution and phylogeny of the soxB gene among sulfur-oxidizing bacteria - Evolution of the Sox sulfur oxidation enzyme system. *Environ. Microbiol.* **9**, 2957–2977 (2007).
 189. Epel, B., Schäfer, K. O., Quentmeier, A., Friedrich, C. & Lubitz, W. Multifrequency EPR analysis of the dimanganese cluster of the putative sulfate thiohydrolase SoxB of *Paracoccus pantotrophus*. *J. Biol. Inorg. Chem.* **10**, 636–642 (2005).

190. Madeira, F. *et al.* The EMBL-EBI search and sequence analysis tools APIs in 2019. *Nucleic Acids Res.* **47**, W636–W641 (2019).
191. Henikoff, S. & Henikoff, J. G. Amino acid substitution matrices from protein blocks. *Proc. Natl. Acad. Sci. U. S. A.* **89**, 10915–10919 (1992).
192. Waterhouse, A. M., Procter, J. B., Martin, D. M. A., Clamp, M. & Barton, G. J. Jalview Version 2-A multiple sequence alignment editor and analysis workbench. *Bioinformatics* **25**, 1189–1191 (2009).
193. Procter, J. B. *et al.* Alignment of Biological Sequences with Jalview. *Methods Mol. Biol.* **2231**, 203–224 (2021).
194. Leimkühler, S., Lemaire, O. N. & Iobbi-Nivol, C. Bacterial Molybdoenzymes: Chaperones, Assembly and Insertion. *RSC Met.* **2017-Janua**, 117–142 (2017).
195. Kappler, U., Friedrich, C. G., Trüper, H. G. & Dahl, C. Evidence for two pathways of thiosulfate oxidation in *Starkeya novella* (formerly *Thiobacillus novellus*). *Arch. Microbiol.* **175**, 102–111 (2001).
196. Kappler, U. & Nouwens, A. S. The molybdoproteome of *Starkeya novella*-insights into the diversity and functions of molybdenum containing proteins in response to changing growth conditions. *Metallomics* **5**, 325–334 (2013).
197. Holt, L. E., Pierce, J. A. & Kajdi, C. N. The solubility of the phosphates of strontium, barium, and magnesium and their relation to the problem of calcification. *J. Colloid Sci.* **9**, 409–426 (1954).
198. Saidi-mehrabad, A. *et al.* Methanotrophic bacteria in oilsands tailings ponds of northern Alberta. *ISME J.* **7**, 908–921 (2013).

199. Stasik, S., Schmidt, J. & Wendt-Potthoff, K. High potential for anaerobic microbial sulfur oxidation in oil sands tailings ponds. *Microorganisms* **9**, (2021).
200. Marchler-Bauer, A. *et al.* CDD/SPARCLE: Functional classification of proteins via subfamily domain architectures. *Nucleic Acids Res.* **45**, D200–D203 (2017).
201. Petri, R., Podgorsek, L. & Imhoff, J. F. Phylogeny and distribution of the soxB gene among thiosulfate-oxidizing bacteria. *FEMS Microbiol. Lett.* **197**, 171–178 (2001).
202. Mangold, S., Valdés, J., Holmes, D. S. & Dopson, M. Sulfur metabolism in the extreme acidophile *Acidithiobacillus caldus*. *Front. Microbiol.* **2**, 1–18 (2011).
203. Frigaard, N.-U. & Bryant, D. A. Genomic Insights into the Sulfur Metabolism of Phototrophic Green Sulfur Bacteria. 337–355 (2008) doi:10.1007/978-1-4020-6863-8_17.
204. Mukhopadhyaya, P. N., Deb, C., Lahiri, C. & Roy, P. A soxA gene, encoding a diheme cytochrome c, and a sox locus, essential for sulfur oxidation in a new sulfur lithotrophic bacterium. *J. Bacteriol.* **182**, 4278–4287 (2000).
205. Weissgerber, T. *et al.* Genome-wide transcriptional profiling of the purple sulfur bacterium *allochromatium vinosum* DSM 180t during growth on different reduced sulfur compounds. *J. Bacteriol.* **195**, 4231–4245 (2013).
206. Kappler, U. & Schwarz, G. Chapter 7: The Sulfite Oxidase Family of Molybdenum Enzymes. in *Molybdenum and Tungsten Enzymes: Biochemistry* vols 2017-Janua 240–273 (The Royal Society of Chemistry, 2017).
207. Boughanemi, S., Infossi, P., Giudici-Orticoni, M. T., Schoepp-Cothenet, B. & Guiral, M. Sulfite oxidation by the quinone-reducing molybdenum sulfite dehydrogenase SoeABC from the bacterium *Aquifex aeolicus*. *Biochim. Biophys. Acta - Bioenerg.* **1861**, 148279 (2020).

208. Maia, L. B., Moura, J. J. G. & Moura, I. Molybdenum and tungsten-dependent formate dehydrogenases. *J. Biol. Inorg. Chem.* **20**, 287–309 (2015).
209. Nichols, J. D. & Rajagopalan, K. V. In vitro molybdenum ligation to molybdopterin using purified components. *J. Biol. Chem.* **280**, 7817–7822 (2005).
210. Auman, A. J., Speake, C. C. & Lidstrom, M. E. nifH Sequences and Nitrogen Fixation in Type I and Type II Methanotrophs. *Appl. Environ. Microbiol.* **67**, 4009–4016 (2001).
211. Buckley, D. H., Huangyutitham, V., Hsu, S. F. & Nelson, T. A. ¹⁵N₂-DNA-stable isotope probing of diazotrophic methanotrophs in soil. *Soil Biol. Biochem.* **40**, 1272–1283 (2008).
212. Pohl, M., Sprenger, G. A. & Müller, M. A new perspective on thiamine catalysis. *Curr. Opin. Biotechnol.* **15**, 335–342 (2004).
213. Dorrestein, Zhai, McLafferty & Begley. The Biosynthesis of the Thiazole Phosphate Moiety of Thiamin: The Sulfur Transfer Mediated by the Sulfur Carrier Protein ThiS. *Artif. Intell. Med.* **11**, ARTMED1118 (2010).
214. Layer, G. Heme biosynthesis in prokaryotes. *Biochimica et Biophysica Acta - Molecular Cell Research* vol. 1868 118861 (2021).
215. Orawski, G. *et al.* The periplasmic thioredoxin SoxS plays a key role in activation in vivo of chemotrophic sulfur oxidation of paracoccus pantotrophus. *Microbiology* **153**, 1081–1086 (2007).
216. Bagchi, A. & Ghosh, T. C. Structural identification of a novel thioredoxin SoxS: Prediction of the function in the process of transport of reductants during sulfur oxidation by the novel global sulfur oxidation reaction cycle. *J. Mol. Struct. THEOCHEM* **758**, 113–118 (2006).
217. Appiaayme, C. & Berks, B. C. SoxV, an orthologue of the CcdA disulfide transporter, is

- involved in thiosulfate oxidation in *Rhodovulum sulfidophilum* and reduces the periplasmic thioredoxin SoxW. *Biochem. Biophys. Res. Commun.* **296**, 737–741 (2002).
218. Dunfield, P. F. & Dedysh, S. N. *Methylocella*: A gourmand among methanotrophs. *Trends Microbiol.* **22**, 368–369 (2014).
219. Carere, C. R. *et al.* Mixotrophy drives niche expansion of verrucomicrobial methanotrophs. *ISME J.* **11**, 2599–2610 (2017).
220. Mohammadi, S. S. *et al.* The acidophilic methanotroph *methylacidimicrobium tartarophylax* 4ac grows as autotroph on h₂ under microoxic conditions. *Front. Microbiol.* **10**, 1–10 (2019).
221. Esparza, M., Crdenas, J. P., Bowien, B., Jedlicki, E. & Holmes, D. S. Genes and pathways for CO₂ fixation in the obligate, chemolithoautotrophic acidophile, *Acidithiobacillus ferrooxidans*, Carbon fixation in *A. ferrooxidans*. *BMC Microbiol.* **10**, (2010).
222. Wang, Y. nan *et al.* Response of *cbb* gene transcription levels of four typical sulfur-oxidizing bacteria to the CO₂ concentration and its effect on their carbon fixation efficiency during sulfur oxidation. *Enzyme Microb. Technol.* **92**, 31–40 (2016).
223. Rasigraf, O., Kool, D. M., Jetten, M. S. M., Sinninghe Damsté, J. S. & Ettwig, K. F. Autotrophic carbon dioxide fixation via the Calvin-Benson-Bassham cycle by the denitrifying methanotroph ‘*Candidatus Methyloirabilis oxyfera*’. *Appl. Environ. Microbiol.* **80**, 2451–2460 (2014).
224. Zander, U. *et al.* Structural basis for the oxidation of protein-bound sulfur by the sulfur cycle molybdohemo-enzyme sulfane dehydrogenase SoxCD. *J. Biol. Chem.* **286**, 8349–8360 (2011).
225. Bardischewsky, F. *et al.* Sulfur dehydrogenase of *Paracoccus pantotrophus*: The heme-2

- domain of the molybdoprotein cytochrome c complex is dispensable for catalytic activity. *Biochemistry* **44**, 7024–7034 (2005).
226. Kikumoto, M., Nogami, S., Kanao, T., Takada, J. & Kamimura, K. Tetrathionate-forming thiosulfate dehydrogenase from the acidophilic, chemolithoautotrophic bacterium *Acidithiobacillus ferrooxidans*. *Appl. Environ. Microbiol.* **79**, 113–120 (2013).
227. Bogart, J. A., Lewis, A. J. & Schelter, E. J. Dft study of the active site of the xoxf-type natural, cerium-dependent methanol dehydrogenase enzyme. *Chem. - A Eur. J.* **21**, 1743–1748 (2015).
228. Gwak, J., Imisi, S., Nguyen, N., Yu, W. & Yang, H. Supplementary Information for Sulfur and methane oxidation by a single microorganism.
229. Rethmeier, J., Rabenstein, A., Langer, M. & Fischer, U. Detection of traces of oxidized and reduced sulfur compounds in small samples by combination of different high-performance liquid chromatography methods. *J. Chromatogr. A* **760**, 295–302 (1997).